

UNIVERSITÉ DE MONTRÉAL

FABRICATION ET CARACTÉRISATION DE DISPOSITIFS PHOTONIQUES  
EN VERRE HYBRIDE SYNTHÉTISÉ PAR VOIE DE SOL-GEL

RAHMANI SARA  
DÉPARTEMENT DE GÉNIE PHYSIQUE ET DE GÉNIE DES MATÉRIAUX  
ÉCOLE POLYTECHNIQUE DE MONTRÉAL

MÉMOIRE PRÉSENTÉ EN VUE DE L'OBTENTION  
DU DIPLÔME DE MAÎTRISE ÈS SCIENCES APPLIQUÉES  
(GÉNIE PHYSIQUE)  
DÉCEMBRE 1998

© Rahmani SARA, 1998.



National Library  
of Canada

Acquisitions and  
Bibliographic Services

395 Wellington Street  
Ottawa ON K1A 0N4  
Canada

Bibliothèque nationale  
du Canada

Acquisitions et  
services bibliographiques

395, rue Wellington  
Ottawa ON K1A 0N4  
Canada

*Your file* *Votre référence*

*Our file* *Notre référence*

The author has granted a non-exclusive licence allowing the National Library of Canada to reproduce, loan, distribute or sell copies of this thesis in microform, paper or electronic formats.

The author retains ownership of the copyright in this thesis. Neither the thesis nor substantial extracts from it may be printed or otherwise reproduced without the author's permission.

L'auteur a accordé une licence non exclusive permettant à la Bibliothèque nationale du Canada de reproduire, prêter, distribuer ou vendre des copies de cette thèse sous la forme de microfiche/film, de reproduction sur papier ou sur format électronique.

L'auteur conserve la propriété du droit d'auteur qui protège cette thèse. Ni la thèse ni des extraits substantiels de celle-ci ne doivent être imprimés ou autrement reproduits sans son autorisation.

0-612-38708-9

**Canada**

UNIVERSITÉ DE MONTRÉAL

ÉCOLE POLYTECHNIQUE DE MONTRÉAL

Ce mémoire intitulé:  
FABRICATION ET CARACTÉRISATION DE DISPOSITIFS PHOTONIQUES  
EN VERRE HYBRIDE SYNTHÉTISÉ PAR VOIE DE SOL-GEL

présenté par: SARA Rahmani

en vue de l'obtention du diplôme de: Maîtrise ès sciences appliquées

a été dûment accepté par le jury d'examen constitué de:

M. AKYEL Cevdet, Ph.D., président

M. NAJAFI S. Iraj, Ph.D., membre et directeur de recherche

M. MACIEJKO Romain, Ph.D., membre

À mes parents pour leur soutien, leurs encouragements et leurs prières,

et à Djamila Kheribi,  
qui m'a enraciné à Lille, où elle a partagé ma souffrance, ma passion et mes rêves,  
et qui, loin de mes yeux, n'est jamais loin de mon coeur.

## REMERCIEMENTS

Je tiens en premier lieu à exprimer mes remerciements les plus vifs à mon directeur, Mr. S. Iraj Najafi, Directeur du Groupe de Recherche en Photonique (GRP), pour le soutien qu'il m'a accordé dans le cadre de cette recherche et pour ses précieux conseils. Il m'a fait découvrir de nombreux aspects du travail scientifique et du travail en équipe.

Je voudrais également exprimer ma reconnaissance à Mr. P. Mark Andrews, Directeur du Groupe de Recherche en Polymère et Photonique (GRPP) au département de chimie de l'université McGill, qui m'a permis de préparer mon sol-gel au sein de son laboratoire et qui a répondu à mes questions avec professionnalisme et amabilité.

Je tiens à exprimer mes remerciements les plus vifs à Messieurs Cevdet Akyel et Romain Maciejko, qui ont bien voulu consacrer quelques heures de leur temps à la lecture et à l'évaluation de ce travail.

Ce mémoire est le fruit d'un travail d'équipe avec Dr. T. Touam, que je dois bien sûr remercier et associer aux résultats obtenus, comme j'y associe tous les membres du laboratoire GPR et ceux du laboratoire GRPP.

Que tous ceux qui m'ont aidé avec gentillesse et efficacité dans la réalisation matérielle de ce mémoire trouvent l'expression de mes sincères remerciements.

## RÉSUMÉ

L'objectif visé par ce travail est la conception et la réalisation de composants en optique intégrée. Le procédé de fabrication adopté à cette fin est le procédé sol-gel, qui consiste en la fabrication d'un guide d'ondes par photopolymérisation aux ultraviolets. Un film de gel d'une seule couche est préparé à basse température puis insolé par une dose donnée d'énergie ultraviolet. Cette dernière doit être ajustée pour pouvoir photoincrire à travers un masque le patron du circuit optique intégré requis. Le circuit obtenu doit avoir des dimensions aussi fidèles que possible aux dimensions du patron sur le masque, et des parois les plus verticales possibles.

Une différence d'indice de réfraction est enregistrée entre la région insolée et la région non insolée. Sa caractérisation est réalisée par le biais des guides plans obtenus par revêtement. Ces derniers ont subi un traitement préalable (pré-recuit) pour sécher le film, un traitement à l'ultraviolet pour induire une augmentation d'indice, et finalement un recuit pour figer et densifier la structure par réticulation des précurseurs minéraux. La méthode de couplage par prisme et l'ellipsométrie sont alors utilisées pour mesurer l'indice de réfraction.

La réalisation de dispositifs optiques intégrés nécessite la maîtrise de la fabrication du composant de base, qui est le guide d'ondes. Il peut être un guide canal, en fouille ou en relief selon l'exigence de la conception optique. Ainsi, la microscopie électronique à balayage et à force atomique est utilisée pour évaluer l'effet des paramètres physique et technologique de la fabrication tels que la dose ultraviolet, le temps de développement, la nature et la dose des précurseurs métalliques et la température de recuit sur la structure et sur la forme du guide.

Une synthèse des conditions favorables de fabrication nous a permis de réaliser des dispositifs photoniques performants tels que des filtres spectraux, des multi/démultiplexeurs de longueur d'ondes pour deux longueurs d'ondes (1.3/1.55  $\mu\text{m}$  et 1.55/0.98  $\mu\text{m}$ ), un réseau de Bragg et un coupleur en étoile.

## ABSTRACT

The aim of this project is to design and produce a wide range of integrated optical devices. As an alternative to high temperature waveguide process, we have been exploring low-temperature Sol-gel process. This wet-process is based on photopolymerisation effect to create the waveguide. The single-layer film is prepared at low temperature and deep UV-light is employed to make the waveguide. By means of well-known photolithography process, it is possible to obtain low-cost waveguide. Like any photo-imaging process, the energy should exceed a threshold energy of chemical bonds in the photo-active components of hybrid glass material to form the expected integrated optic pattern with excellent linewidth control and vertical sidewalls. To achieve optical waveguide a refractive index difference occurred between the insolated and surrounding region. Accordingly, the refractive index emerges as a fundamental device performance material parameter and it is investigated using slab waveguide.

Sol-gel films were coated by spinning or dipping on silicon substrates which had thermally grown SiO<sub>2</sub> layer on their surface. A prebake, UV-light insolation and postbake follow to make slab waveguide. By means of prisme coupling and ellipsometry, the dependence refractive index versus UV-light dose and bake temperature is evaluated. The surface, burried or ridge waveguide fabrication control leads to ensure photonic devices performance. Hence the physical and technical fabrication parameters, chemical composition of sol, colateral densification, UV-light dose, time development and bake temperature, effect on waveguide shape and structure are investigated. Consequently, suited fabrication conditions are synthetised and used to make high compact photonic devices such as Spectral Discrimination Filters, Wavelength Division/Multiplexer, Bragg Grating, and Star Coupler.

## TABLE DES MATIERES

<b>DÉDICACE.....</b>	<b>iv</b>
<b>REMERCIEMENTS .....</b>	<b>v</b>
<b>RÉSUMÉ.....</b>	<b>vi</b>
<b>ABSTRACT .....</b>	<b>vii</b>
<b>TABLE DES MATIERES .....</b>	<b>viii</b>
<b>LISTE DES TABLEAUX.....</b>	<b>xi</b>
<b>LISTE DES FIGURES .....</b>	<b>xii</b>
<b>LISTE DES SIGLES ET ABRÉVIATIONS .....</b>	<b>xvii</b>
<b>INTRODUCTION .....</b>	<b>1</b>
<b>RÉFÉRENCES POUR L'INTRODUCTION.....</b>	<b>5</b>
<b>CHAPITRE I: SOL-GEL POUR LA PHOTONIQUE .....</b>	<b>6</b>
<b>1.1. Historique.....</b>	<b>6</b>
<b>1.2. Synthèse du verre hybride par voie sol-gel (VHSG).....</b>	<b>7</b>
<b>1.3. Caractérisation des guides plans .....</b>	<b>9</b>
1.3.1. Film mince .....	10
1.3.2. Trempage.....	10
1.3.3. Tournette.....	11
1.3.4. Spectre d'absorption UV .....	12
1.3.5. Évolution de l'indice de réfraction.....	13
1.3.6. Couplage par prisme.....	15
1.3.7. Ellipsométrie.....	17
<b>1.4. Références .....</b>	<b>21</b>



<b>CHAPITRE II: FABRICATION DES GUIDES D'ONDES OPTIQUE POLYGLASS.....</b>	<b>25</b>
<b>2.1. Photolithography Fabrication of Sol-Gel Ridge Waveguide .....</b>	<b>25</b>
2.1.1. Abstract.....	25
2.1.2. Introduction.....	25
2.1.3. Experiment.....	26
2.1.4. Results and Discussion.....	26
2.1.5. Acknowledgments.....	33
2.1.6. References.....	33
<b>2.2. SEM and AFM Studies of Polyglass Ridge Waveguides.....</b>	<b>34</b>
2.2.1. Abstract.....	34
2.2.2. Introduction.....	34
2.2.3. Ridge Waveguide Characterization.....	35
2.2.4. Atomic Force Microscopy.....	44
2.2.5. Conclusions.....	46
2.2.6. Acknowledgments.....	47
2.2.7. References.....	47
 <b>CHAPITRE III: COMPOSANT PHOTONIQUE POUR LA TELECOMMUNICATION .....</b>	 <b>50</b>
<b>3.3. Polyglass Integrated Optics Devices for Lightwave Communication.....</b>	<b>50</b>
3.3.1. Abstract.....	50
3.3.2. Introduction.....	50
3.3.3. SDF Design and performance.....	51
3.3.4. 1.55 $\mu\text{m}$ / 1.3 $\mu\text{m}$ and 1.55 $\mu\text{m}$ / 0.98 $\mu\text{m}$ WDM.....	55
3.3.4. Star Coupler.....	56
3.3.5. Acknowledgments.....	57
3.3.6. References.....	58
<b>3.4. Sol-gel glass Waveguide and Grating on Silicon.....</b>	<b>60</b>
3.4.1. Abstract.....	60
3.4.2. Introduction and background.....	60
3.4.3. Hybrid sol-gel glass films.....	62
3.4.3.1. Synthesis and fabrication.....	62
3.4.3.2. Characterization and results.....	63
3.4.4. Channel waveguides.....	68
3.4.4.1. Ridge channel waveguide fabrication.....	70
3.4.5. Ridge waveguide with grating.....	72
3.4.5.1. Grating fabrication.....	72
3.4.5.2. Grating properties.....	74
3.4.6. Conclusion.....	76
3.4.7. Acknowledgment.....	77

3.4.8. References..... 77

**3.3. Sol-gel Integrated Optics Devices: Star Coupler and Dense WDM ..... 79**

    3.3.1. References..... 82

    3.3.2. Acknowledgment ..... 83

**CHAPITRE IV: CONCLUSION ET PERSPECTIVE ..... 84**

**4.1. Conclusion ..... 84**

**4.2. Perspectives ..... 85**

**BIBLIOGRAPHIE..... 87**

**LISTE DES TABLEAUX**

Tableau 1.1	Mesure de l'indice de réfraction d'un film mince de silice d'aluminophosphate en fonction de la dose UV.....	16
Tableau 1.2	Mesure de l'indice de réfraction d'un film épais de silice d'aluminophosphate en fonction de la dose UV.....	16
Tableau 1.3	Comparaison des mesures d'indice de réfraction et d'épaisseur entre le couplage par prisme et l'ellipsométrie.....	20
Table 3.1	Parameters of dual wavelength coupler WDMs.....	56

## LISTE DES FIGURES

Figure 1.1	Synthèse à température ambiante de trois variantes de verre hybride par voie sol-gel.....	9
Figure 1.2	Mesure de la dépendance (épaisseur versus vitesse de trempage).....	11
Figure 1.3	Mesure de la dépendance (épaisseur versus vitesse de tournette).....	12
Figure 1.4	Spectre d'absorption UV relatif aux trois variantes du verre hybride. Aucun traitement de recuit n'est opéré.....	13
Figure 1.5	Comparaison entre le spectre d'absorption UV de la silice aluminophosphate humide et pré-recuite.....	14
Figure 1.6	Évolution de la microstructure de la silice aluminophosphate en fonction de la dose UV, le temps d'exposition est (a) 0 min, (b) 5 min et (c) 30 min.....	18
Figure 1.7	Courbe de dispersion de 2 $\mu\text{m}$ de $\text{SiO}_2$ sur Si mesurée par ellipsométrie.....	19
Figure 1.8	Courbe de dispersion de la silice d'aluminophosphate exposée à 10 min. UV mesurée par ellipsométrie.....	20
Figure 2.1	Viscosity of $(1-x)\text{SiO}_2 - x\text{ZrO}_2$ ( $x = 0, 8.3, 18.8, 22.2$ and $25.0$ ) sol-gel as a function of aging time.....	27
Figure 2.2	Viscosity of $(1-x)\text{SiO}_2 - x\text{ZrO}_2$ ( $x = 18.8$ ) and $(1-y)\text{SiO}_2 - y\text{Al}_2\text{O}_3$ ( $y=15$ ) sol-gel as a function of aging time.....	28

Figure 2.3	Variation of 80SiO <sub>2</sub> -20ZrO <sub>2</sub> sol-gel film thickness as a function of aging time Spin-coating speed are 1000 rpm and 1500 rpm.....	29
Figure 2.4	SEM photographs of 80SiO <sub>2</sub> -20ZrO <sub>2</sub> ridge waveguide. Used film thickness and DUV-light exposure time are: top (left)= 1.25μm and 10 sec.; top(right)= 1.25 μm and 30 sec.; bottom (left)= 3 μm and 10 sec, bottom (right)= 3μm and 60 sec.....	30
Figure 2.5	Variation of $\Delta W$ ( $= W_{\max} - W_0$ ) as a function of mask width. $W_{\max}$ is the maximum width of waveguide cross section and $W_0$ is the width of mask opening. The films are 1.25 μm and 3 μm thick.....	31
Figure 2.6	Variation of $W_{\min}/W_{\max}$ , for 1.25 μm and 3 μm thick waveguides, as a function of DUV-light exposure time. $W_{\max}$ and $W_{\min}$ are maximum and minimum widths of waveguide cross section respectively.....	32
Figure 2.7	SEM photographs of 80SiO <sub>2</sub> -15Al <sub>2</sub> O <sub>3</sub> ridge waveguides. Used film thickness and UV-light exposure time are 4.16μm and 120 sec. Used mask opening was 2 and 10 μm .....	32
Figure 2.8	SEM top view of ridge waveguides created by solvent wet etching for different openings of the photomask.....	36
Figure 2.9	SEM image of ridge waveguides cross section (nominal composition 85 SiO <sub>2</sub> -15 Al <sub>2</sub> O <sub>3</sub> ) as function of exposure time: (a) 5 sec., (b) 10 sec., (c) 30 sec., (d) 120 sec. and (e) 900 sec. Mask opening = 10 μm.....	37
Figure 2.10	SEM image of ridge waveguides cross section (nominal composition 85 SiO <sub>2</sub> -15 Al <sub>2</sub> O <sub>3</sub> ) as function of exposure time: (a) 5 sec., (b) 10 sec., (c) 30 sec., (d) 120 sec. and (e) 900 sec. Mask opening = 6 μm.....	38

Figure 2.11	Characteristic curve for the hybrid organoaluminosilicate section (nominal composition 85 SiO <sub>2</sub> -15 Al <sub>2</sub> O <sub>3</sub> ) showing the ratio H/H <sub>0</sub> as function of exposure time. The exposure dose is plotted on a logarithmic scale.....	39
Figure 2.12	Variation of $W_{\max}/W_{\min}$ as function of exposure dose. $W_{\max}$ and $W_{\min}$ are maximum and minimum width of waveguide cross-section, respectively. ....	41
Figure 2.13	Variation of $\Delta W (=W_{\max}-W_0)$ as function of exposure dose. $W_{\max}$ is the maximum width for waveguides cross section and $W_0$ is the opening mask feature width.....	41
Figure 2.14	SEM image of ridge waveguide cross section (nominal composition 86 SiO <sub>2</sub> -7 Al <sub>2</sub> O <sub>3</sub> -7 P <sub>2</sub> O <sub>5</sub> ) as function of exposure time: (a) 3 sec., (b) 5 sec. and (c) 10 sec. Mask opening = 10 $\mu\text{m}$ .....	42
Figure 2.15	SEM image of ridge waveguide cross section (nominal composition 86 SiO <sub>2</sub> -7 Al <sub>2</sub> O <sub>3</sub> -7 P <sub>2</sub> O <sub>5</sub> ) as function of exposure time: (a) 3 sec., (b) 5 sec. and (c) 10 sec. Mask opening = 6 $\mu\text{m}$ .....	42
Figure 2.16	Characteristic curve for the hybrid aluminophosphate silica, showing the ratio H/H <sub>0</sub> as function of exposure time. The exposure dose is plotted on a logarithmic scale.....	43
Figure 2.17	Variation of $W_{\max}/W_{\min}$ as function of exposure dose. $W_{\max}$ and $W_{\min}$ are maximum and minimum width of waveguide cross-section, respectively. ....	44
Figure 2.18	Variation of $\Delta W (=W_{\max}-W_0)$ as function of exposure dose. $W_{\max}$ is the maximum width for waveguides cross section and $W_0$ is the opening mask feature width.....	44
Figure 2.19	Atomic Force Microscopy (AFM) 3-D view of the surface relief waveguide inscribed an organoaluminophosphate <i>polyglass</i> film. The depressed region distinguishes the densified waveguide structure from the surrounding matrix that has not been exposed to UV light.....	45

Figure 2.20	Variation in organoluminophosphate <i>polyglass</i> film thickness as function of exposure time.....	46
Figure 3.1	Mask pattern of the Mach-Zehnder filter.....	51
Figure 3.2	Cross section of the SDF waveguide structure.....	52
Figure 3.3	Response signal obtained from the four outputs of the MZI filter.....	53
Figure 3.4	Mask pattern of directional coupler filter.....	53
Figure 3.5	Optical micrograph of directional coupler.....	54
Figure 3.6	Output signal obtained from the six outputs of the directional coupler filter.....	55
Figure 3.7	Schematic diagram of the WDM coupler and its waveguide structure.....	55
Figure 3.8	Mask pattern of the star coupler.....	57
Figure 3.9	Star coupler output when light at $\lambda=1.55 \mu\text{m}$ is coupled into the input waveguide number 9.....	57
Figure 3.10	(a) Refractive index of zirconium-doped sol-gel glass films as a function of Zr concentration. Postbake temperature and time are 150 °C and 5 hm respectively. UV-light exposure time is 2 min. (b) Same as (a) for aluminum-doped sol-gel.....	64
Figure 3.11	(a) refractive index of 20 mole% Zr sol-gel films as a function of postbake temperature. The films are exposed to UV-light for 2 min. (b) Similar to (a) for 15 mole% Al solgel films. Postbake time is 1h.....	65
Figure 3.12	(a) Refractive index of 20 mole% Zr-doped sol-gel films as a function of UV-light exposure time for 130 and 150 °C postbake temperatures, and 1, 5 and 10 h postbake times. (b) Refractive index increase, $\Delta n$ , as a function of UV-light exposure time for the same samples.....	67

Figure 3.13	Similar to Fig. 3.12(a), but for 15 mole% Al-doped sol-gel films.....	68
Figure 3.14	Schematic representation of different sol-gel glass channel waveguides on silicon. From top to bottom: surface, ridge and buried waveguides.....	69
Figure 3.15	Measured mode profile of single mode, from top to bottom, surface, ridge and buried sol-gel glass waveguide. $\lambda = 1.55 \mu\text{m}$ .....	70
Figure 3.16	(a) and (b) Optical microscope photograph of Zr-doped ridge waveguides exposed to UV-light for (a) and (c) 4 min and (b) and (d) 1 min. Waveguide widths are, respectively, 8 $\mu\text{m}$ and 6 $\mu\text{m}$ . (c) and (d) Scanning electron micrograph of the waveguides.....	72
Figure 3.17	(a) Optical microscope photograph of a grating imprinted in sol-gel ridge waveguides. Grating period in 0.5025 $\mu\text{m}$ . (b) Atomic force microscope picture grating.....	73
Figure 3.18	Waveguide configuration employed in the analysis of sol-gel ridge waveguides with grating.....	75
Figure 3.19	Calculated and measured response of a 4.5- $\mu\text{m}$ thick, 6- $\mu\text{m}$ wide, sol-gel ridge waveguide with Bragg grating. Grating length = 5 mm.....	75
Figure 3.20	Scanning electron micrograph of sol-gel glass ridge waveguide.....	79
Figure 3.21	Top) Schematic representation and dimensions of 8x31 star coupler. Bottom) Optical micrograph of output side of the coupler.....	80
Figure 3.22	Star coupler output when light at 1.55 $\mu\text{m}$ is coupled into the central waveguide. Inset is a photograph of light from the output ports of the star coupler, at 1.55 $\mu\text{m}$ , focused on a camera.....	81
Figure 3.23	Optical response of 64 channel dense WDM.....	82



**LISTE DES SIGLES ET ABRÉVIATIONS**

a: facteur d'asymétrie

A: angle du prisme adjacent à la surface de contact

AFM: Atomic Force Microscopy

AT&T: American Telephone and Telegraph

b: indice normalisé

BPM: Beam Propagation Method

CVD: Chemical Vapor Deposition

DBR: Distributed Bragg Reflector

DLVO: Deryaguin, Landau, Verwey et Overbeek

DUV: Deep UV-light

DWDM: Dense Wavelength-Division Multiplexing

e: épaisseur du revêtement

E: dose de l'énergie d'exposition à un temps donné

$E_0$ : dose de l'énergie d'exposition à partir de laquelle le film est complètement dissout

EDWA: Erbium Doped Waveguide Amplifier

FHD: Flame Hydrolysis Deposition

g: gravité

h: taux d'évaporation

$H_0$ : épaisseur du film correspondant à  $E_0$

H: épaisseur du film correspondant à E

HSGG: Hybrid Sol-Gel Glasses

I: intensité de la radiation UV

K: constante dépendant des matériaux

m: nombre de modes

MAA: Methacrylic Acid

MAPTMS: Methacryloxypropyltrimethoxysilane

MZI: Mach Zehnder Interferometers

n: indice de réfraction

**N**: indice effectif  
**nc**: indice de réfraction de l'air  
**nf**: indice de réfraction du film  
**ns**: indice de réfraction du substrat  
**NASA**: National Aeronautics and Space Administration  
 **$n_p$** : indice de réfraction du prisme  
**NTT**: Nippon Telegraph and Telephone  
**OSA**: Optical Spectrum Analyzer  
**RPM**: révolution par minute  
**SDF**: Spectral Discrimination Filters  
**SEM**: Scanning Electron Microscope  
**t**: temps d'exposition  
**TE**: Transverse Electric  
**TM**: Transverse Magnetic  
**UV**: radiation ultra-violet  
**v**: la vitesse de retrait  
**V**: fréquence normalisée  
**VHSG**: verre hybride synthétisé par voie de sol-gel  
 **$W_{max}$** : largeur maximale du guide  
 **$W_{min}$** : largeur minimale du guide  
 **$W_0$** : largeur de l'ouverture du photomasque  
**WDM**: Wavelength Division Multiplexing  
 **$\eta$** : viscosité du sol  
 **$\lambda$** : longueur d'ondes de la lumière dans le vide  
 **$\Lambda$** : pas du réseau  
 **$\gamma$** : contraste photolithographique  
 **$\Delta n$** : différence d'indice de réfraction (définie par la différence entre l'indice du film exposé et celui du film non exposé)  
 **$\Delta W$** : différence entre la largeur maximale et la largeur minimale du guide d'ondes

$\mu$ : masse de solvant volatilisée par unité de volume

$\mu_0$ : masse initiale du solvant

$\rho$ : densité du sol

$\theta$ : angle mesuré

$\omega$ : vitesse de rotation

3-D: trois dimensions

## INTRODUCTION

La technologie des semi-conducteurs a connu une évolution progressive mais rapide. À chaque étape de son histoire, une difficulté est surmontée. Souvent, ces difficultés sont d'ordre échelles et dopants mais le choix du matériau de base, qui reste les semi-conducteurs III-V, n'est jamais remis en question. Ainsi, pour passer de l'échelle moyenne d'intégration (*Medium Scale Integration*) à une échelle supérieure (*Very Large Scale Integration*), il a fallu développer des techniques nouvelles au détriment d'autres depuis longtemps maîtrisées. En effet, le procédé par diffusion a fait place à l'implantation ionique<sup>1</sup>, dans laquelle la température n'est plus un paramètre contraignant. Mieux, on y contrôle la concentration et la profondeur de diffusion des dopants ainsi que la diffusion latérale de ces derniers. Toutefois, il y a un prix à cette amélioration substantielle, qui est le coût d'équipement et d'entretien très élevé ainsi que la nécessité d'une main-d'œuvre hautement qualifiée. Ce sort n'est pas exclusif à la technologie des semi-conducteurs: il en va de même pour bien d'autres technologies telles que l'optoélectronique et la photonique. Cette dernière, de plus en plus intégrée et monolithique, fait face à des difficultés de taille. Andrews et Najafi<sup>2</sup> ont revu les plus récentes technologies de fabrication et définissent les perspectives d'application et les limitations d'un circuit photonique. À l'opposé de la technologie des semi-conducteurs, ils proposent une technique facile à coût très faible, celle du procédé humide sol-gel. On y comprend que les procédés "classiques" de fabrication de guide d'ondes tels que l'échange ionique sur verre et la déposition par plasma et hydrolyse à la flamme ne peuvent pas offrir une intégration parfaitement monolithique, à l'image du circuit électronique intégré. Ceci est dû essentiellement à la haute température et aux bombardements très énergétiques susceptibles d'endommager certains composants prédisposés du circuit photonique intégré (CPI). Ce dernier est défini par Kogelnik<sup>3</sup> comme étant une connexion laser-guide d'ondes sur le même substrat (*on-chip*). Ainsi, le guide d'ondes est la pièce maîtresse dans la construction du CPI. Il n'est donc pas surprenant de voir que la recherche scientifique en optique intégrée lui a consacré son attention au cours des vingt dernières années. Les efforts ont pour but de développer un

procédé de fabrication de guide d'ondes à faibles pertes de propagation, indépendant de la polarisation et doué d'une grande capacité de confinement de la lumière.

À notre connaissance, la plupart de ces procédés ont choisi comme matériau constituant le film la silice ( $\text{SiO}_2$ ), l'oxynitride de silicium ( $\text{SiON}$ ) et la nitrure de silicium ( $\text{Si}_3\text{N}_4$ ). Le guide inorganique qui en résulte présente une différence d'indice de réfraction très faible entre le cœur et la région limitrophe ( $\Delta n = 10^{-3}$ - $10^{-2}$ ). Cette faible différence a pour conséquence un manque de confinement des modes, et de là des dispositifs de dimensions considérables. En effet, cette contrainte vient éclipser les qualités du guide  $\text{SiO}_2/\text{Si}$ . Verbeek et al.<sup>4</sup> ont ainsi utilisé un guide de silice sur du silicium dopé au phosphore caractérisé par des pertes de propagation inférieures à 0.05 dB/cm. En revanche, le dispositif réalisé est de l'ordre du centimètre de long. Pour contourner cette difficulté, une nouvelle approche a été entreprise en choisissant les polymères comme matériau de base. Le guide organique obtenu souffre d'une déficience marquée par des pertes de propagation très élevées aux longueurs d'ondes utilisées en télécommunication. Cependant, les qualités intrinsèques du guide et les avantages de la méthode de fabrication tels que la basse température, la compatibilité avec tout genre de substrat et surtout le coefficient thermo-optique dix fois supérieur à celui de la silice, incitent des laboratoires de renommée internationale comme AT&T (*American Telephone & Telegraph*) et NTT<sup>5</sup> (*Nippon Telegraph & Telephone*) à travailler sur le problème des pertes.

Il est donc raisonnable de chercher un moyen de combiner les caractères bénéfiques du guide organique et ceux du guide inorganique. Najafi et al. (par. 2.2.7 et 3.1.6) ont prouvé la faisabilité d'une telle combinaison en choisissant un verre hybride organique-inorganique préparé par voie sol-gel. En effet, la capacité à manipuler la structure et les propriétés du guide d'ondes au niveau moléculaire engendre un potentiel d'intégration et de monolithisme énorme. Notre mémoire s'inscrit dans la perspective ouverte par ces recherches. Il a pour but de donner une meilleure compréhension du phénomène sous l'influence d'interactions compétitives intermoléculaire, molécule-substrat et molécule-solvant (chapitre 1) et de proposer des moyens de contrôler la structure et les propriétés

du guide d'ondes (chapitre 2). On synthétise ensuite les conditions favorables à la fabrication des composants photoniques performants (chapitre 3). Ces derniers ont été conçus et réalisés non seulement pour prouver la reproductibilité, l'efficacité et la facilité du procédé mais aussi pour servir de composants essentiels au système optique de communication. Ce dernier n'est plus une technologie du futur, mais au contraire un service déjà opérationnel qui possède actuellement une capacité de transmission de l'ordre du gigabit/seconde<sup>6</sup>. Ceci est rendu possible par l'utilisation de la fibre monomode, par le développement de l'amplificateur optique, qui a remplacé l'amplificateur électrique, et par le multiplexage dense par répartition en longueur d'onde (DWDM, *Dense Wavelength-Division Multiplexing*). En effet, grâce à la capacité de l'amplificateur optique à produire les longueurs d'ondes multiples par émission spontanée et à l'aide du réseau de guides du DWDM, rend possible de multiplexer/démultiplexer les longueurs d'ondes d'une fibre en longueurs d'ondes séparées par canal.

Le déploiement du système DWDM en télécommunications n'est qu'un premier pas vers un réseau de télécommunications tout-optique où le canal de longueur d'ondes optiques peut être connecté, déconnecté et transféré à travers le réseau. Pour ce faire, il faut développer optiquement l'équivalent du filtre insertion/extraction, répartiteur et commutateur électrique. On montre qu'il est possible d'obtenir optiquement ces composants. En effet, les composants réalisés lors de ce projet par voie sol-gel tels que:

- le filtre spectral (par. 3.1.3), qui manifeste une fine sélectivité spectrale, peut jouer le rôle de filtre insertion/extraction (*Add/drop Filter*).
- le multiplexeur à deux longueurs d'ondes ( $1.55/1.3 \mu\text{m}$  et  $1.55/0.98 \mu\text{m}$ ) (par.3.1.4) peut être utilisé comme répartiteur (*Cross-connect System*).
- le réseau de Bragg (par. 3.2.5), dont la réflectivité atteint presque 100%, peut servir aussi de filtre insertion/extraction; connecté à une fibre, il permet d'éliminer la dispersion de cette dernière.

- le coupleur en étoile (*Star Coupler*) (par. 3.3) a pour rôle de diviser la puissance optique entre 31 portes. Il constitue l'élément de base du DWDM. Ce dernier joue le rôle d'une matrice (NxN) de commutation optique (*Optical Switch Matrix*)<sup>7</sup>.

Tout au long de ce mémoire, le lecteur constatera sans doute les capacités du verre hybride organique-inorganique à satisfaire les exigences de la photonique. Cependant, beaucoup reste à faire pour comprendre la structure des gels organiques-inorganiques (qu'elle soit dense ou ouverte) et la cinétique de polymérisation, de même que pour améliorer les performances optiques. Finalement, des suggestions et une conclusion termineront ce travail (chapitre 4).

## RÉFÉRENCES POUR L'INTRODUCTION

1. S. M. Sze, "Semiconductor Devices Physics and Technology", Murray Hill, New Jersey, (1985), 382-427.
2. Mark P. Andrews, S. Iraj Najafi, "Passive and Active Sol-Gel Materials and Devices", Critical Review Conference Sol-gel Polymer Photonic Devices, SPIE, San Diego, Vol. CR68, (1997), 253-285.
3. H. Kogelnik, "Glass Integrated Optics, OIECs or PICs?", Academic Press, ed J. W. Goodman, New York, (1991).
4. B. H. Verbeek, C. H. Henry, N. A. Olson, K. J. Orlowski, R. R. Kazainov and B. H. Johnson, "Integrated Four-Chanel Mach-Zehnder Multi/Demultiplexer Fabricated with Phosphorous Doped SiO<sub>2</sub> Waveguide on Si", Journal of Lightwave Technology, Vol. 6, No. 6, (1988), 1011-1015.
5. T. Watanabe, N. Ooba, S. Hayashida, T. Kurihara and S. Imamura, "Polymeric Optical Waveguide Circuits Formed Using Silicon Resin", Journal of Lightwave Technology, Vol. 16, No. 6, (1998), 1049-1055.
6. C. R. Giles, "Lightwave Application of Fiber Bragg Grating", Journal of Lightwave Technology, Vol. 15, No. 8, (1997), 1391-1404.
7. C. Dragone, "An NxN Optical Multiplexer Using Planar Arrangement of Two Star Couplers", IEEE Photonics Technology Letters, Vol. 3, No. 9, (1991), 812-814.



## CHAPITRE I: SOL-GEL POUR LA PHOTONIQUE

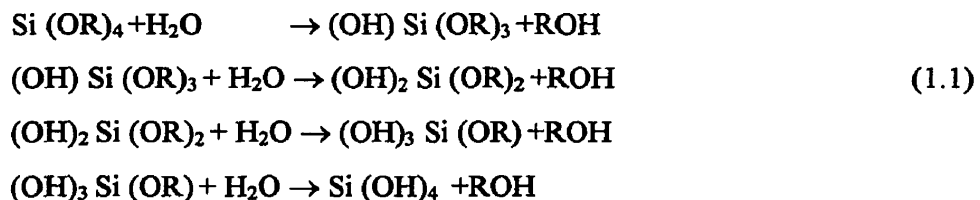
### 1.1. Historique

Sol-gel est un mot composé de sol et de gel, termes qui identifient deux états de matière<sup>1</sup> aussi utilisés depuis les premières civilisations que le sont le lait, l'argile et l'encre. Mais c'est seulement au 19<sup>ème</sup> siècle que l'on a commencé à s'intéresser à ces deux états de matière et que la science des colloïdes a été mise au point par Graham (1861). En effet, le premier sol réalisé en laboratoire est celui de l'or, qui a été obtenu par Faraday en 1853, et le premier sol de silice synthétisé est celui de Feidel et Crafts en 1863<sup>2</sup>. Cependant, la maîtrise de la taille des particules à partir des précurseurs organiques ou inorganiques est récente<sup>3-5</sup>. Elle a nécessité le concours de plusieurs disciplines scientifiques telles que la thermodynamique, l'électrostatique ou la théorie DLVO (d'après les initiales des inventeurs: Deryaguin, Landau, Verwey et Overbeek) et l'optique, entre autres, pour en arriver à une profonde compréhension et à une grande fiabilité. Ainsi, Flory<sup>6</sup> a mis au point une théorie expliquant la structure du réseau d'un gel et sa formation ou gélification. Hammersley<sup>7</sup> a élaboré la théorie de la percolation qui a servi de base pour élucider les critères de transfert sol/gel; le phénomène de gélification n'est donc plus seulement considéré comme une réaction chimique, mais aussi comme un phénomène critique en physique. Toutefois, le procédé sol-gel n'a pas quitté les tables de laboratoire avant 1960, quand la NASA a effectué une première application industrielle à l'état sol pour contrôler l'écoulement des carburants d'engins spatiaux en apesanteur<sup>8</sup>. Ce premier pas a ouvert la voie à une croissance exponentielle de l'application du procédé, notamment dans les technologies avancées telles que la photonique. Les besoins du marché en photonique, en optoélectronique ou simplement en télécommunications nécessitent le développement de nouveaux matériaux, ou du moins l'amélioration de ceux déjà existants. Le procédé a montré son aptitude à satisfaire cette demande. Des poudres submicroniques de haute pureté, des particules cristallines<sup>9</sup> et des films d'oxydes pour des applications optiques et électriques<sup>10-14</sup> ont ainsi été réalisés avec succès.

## 1.2. Synthèse du verre hybride par voie sol-gel (VHSG)

Nombreuses sont les applications qui nécessitent une structure vitreuse de silice incorporée de métaux<sup>15-18</sup> pour améliorer la réflexion, l'absorption et la transmission à certaines longueurs d'ondes ou simplement pour accroître la résistance aux alcalins en ajoutant du zirconium. Certains types de verres ne sont pas réalisables par le procédé de trempe conventionnel à cause de l'existence d'une lacune de miscibilité empêchant l'obtention d'un verre homogène avec certaines compositions ou parce que les différentes composantes, telles que les métaux de Zr, Ti et Al, sont difficiles à fondre. Si, en plus, il faut intégrer ces verres à une structure existante et endommageable à haute température, le procédé sol-gel constitue alors la seule alternative. En effet, la préparation des verres par le procédé sol-gel à des températures beaucoup plus basses que par le procédé conventionnel est possible si une chaîne polymérique comprenant les différents éléments répartis d'une manière homogène se forme par polycondensation. Ceci est possible en utilisant des alkoxydes métalliques. Ces précurseurs photosensibles résultent d'une réaction directe entre un métal M et un alcool ROH, et sont symbolisés par  $M(OR)_n$ <sup>5</sup>. Ils se prêtent à des ruptures nettes de la liaison M-OR ou MO-R, par hydrolyse, entre le métal M, qui peut être Si, Ti ou Zr, par exemple, et le groupe alkyl (OR) généralement de la forme  $OC_nH_{2n-1}$

Fort heureusement, la chimie des alkoxydes métalliques fait l'objet d'une étude approfondie et exhaustive prenant comme modèle le silicium, qui, selon le protocole chimique suivi, conduit soit à des sols polymériques, soit à des colloïdaux de la silice. Néanmoins, les réactions d'hydrolyse (1.1) et de polycondensation par déshydratation (1.2) ou dé-alcoolisation (1.3) sont essentielles à l'obtention d'un sol<sup>19</sup>.





L'ensemble de ces réactions a souvent lieu dans un solvant qui est l'alcool correspondant. Selon la cinétique relative des réactions de condensation et d'hydrolyse où le PH est l'un des paramètres-clés, il est possible d'obtenir soit des polymères linéaires, soit des particules colloïdales. Plusieurs techniques existent pour identifier le produit résultant: la diffraction des rayons X, les analyses optiques et les mesures de viscosité<sup>20</sup> (par. 2.1.4) en sont quelques-unes.

Moyennant les réactions (1.1), (1.2) et (1.3), trois types de verres hybrides sont synthétisés avec succès au sein du groupe *Photonics Research Group*, et sont résumés en figure 1.1.

L'alkoxyde source de silice est le MAPTMS<sup>21</sup>, acronyme de methacryloxypropyltriméthoxysilane, et de formule  $\text{H}_2\text{C}=\text{C}(\text{CH}_3)\text{CO}_2(\text{CH}_2)_3\text{Si}(\text{OCH}_3)_3$ . D'autres alkoxydes tels que le triméthylphosphate<sup>21</sup>  $(\text{O})\text{P}(\text{OCH}_3)_3$  et l'isobutoxyaluminoxytriéthoxysilane<sup>22</sup>  $\text{C}_{14}\text{H}_{33}\text{AlO}_6\text{Si}$  viennent s'ajouter au MAPTMS. Le premier a pour rôle d'améliorer l'épaisseur et le second de modifier l'indice de réfraction<sup>12</sup>. Le verre obtenu est un système ternaire  $\text{SiO}_2\text{-Al}_2\text{O}_3\text{-P}_2\text{O}_5$ , et est appelé silice d'aluminophosphate. La deuxième variante est obtenue en ajoutant le zirconium-n-propoxide<sup>23</sup>  $\text{Zr}(\text{OC}_3\text{H}_7)_4$  dans le but de modifier l'indice de réfraction et d'améliorer la stabilité mécanique<sup>24</sup>. Le système binaire  $\text{SiO}_2\text{-ZrO}_2$  obtenu est connu sous le nom de silice de zircon. Finalement, la troisième variante consiste en l'ajout d'isobutoxyaluminoxytriéthoxysilane  $\text{C}_{14}\text{H}_{33}\text{AlO}_6\text{Si}$  comme modificateur d'indice<sup>24</sup>; le système binaire résultant  $\text{SiO}_2\text{-Al}_2\text{O}_3$  est dit silice d'alumine ou aluminosilicate.

À cette variabilité de précurseurs modificateurs correspond une large variation des propriétés optiques<sup>12,24</sup>. Toutefois, l'hydrolyse de ces précurseurs dépend des mêmes facteurs, à savoir:

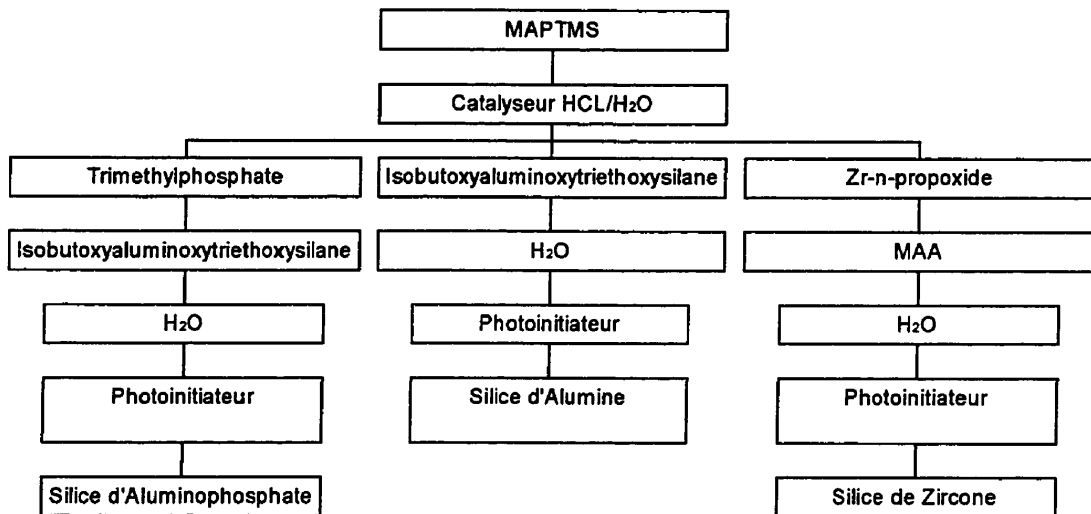


Figure 1.1 Synthèse à température ambiante de trois variantes de verre hybride par voie sol-gel.

- le groupement alkyl  $R^{25,26}$ , puisqu'un groupe alkyl plus gros ralentit l'hydrolyse et la cinétique de diffusion, ce qui a pour effet de produire par condensation des polymères de taille faible. À cet effet, lors de la préparation des trois sols, il a été décidé d'ajouter de l'acide HCl en faible proportion ( $[acide]/[alkyl] < 0.3$ ) pour favoriser la formation d'une chaîne linéaire et pour obtenir une solution claire.
- la proportion d'eau d'hydrolyse<sup>27</sup>, dont l'augmentation affecte le contenu en oxyde du produit.
- l'augmentation de la température d'hydrolyse, dont la conséquence est l'augmentation de la vitesse d'hydrolyse et de cristallisation, qui à son tour privilégie une structure finale cristalline plutôt qu'amorphe.

### 1.3. Caractérisation des guides plans

Les sols obtenus précédemment doivent subir une transformation (gélification) pour former un gel. C'est l'étape où les oligomères<sup>28</sup> établissent des liaisons entre eux de façon à former un réseau solide tridimensionnel. Cette transition peut être dirigée de

façon à produire des fibres continues, des poudres de tailles données ou des films minces. La gélification en film vitreux mince à partir de ces sols est obtenue soit par traitement thermique, soit par exposition à des radiations UV (ultraviolet).

### 1.3.1. Film mince

Un film mince est obtenu par revêtement, ce qui est rendu possible par trempage (*deep-coating*) ou tournette (*spin-coating*). Le séchage suit: son but est d'évaporer le solvant pour favoriser le rapprochement et la liaison entre les chaînes polymériques et aussi d'éliminer les stress induits lors du revêtement.

### 1.3.2. Trempage

Un substrat de silicium muni d'une couche de 2  $\mu\text{m}$  de silice oxydée thermiquement est plongé dans un sol de silice d'aluminophosphate, puis retiré. L'opération est réalisée à l'aide d'un moteur pas-à-pas contrôlé par ordinateur. Dans ce cas, l'épaisseur du revêtement est contrôlée par<sup>15</sup>:

$$e = K * \left( \frac{\eta V}{\rho g} \right) \quad (1.4)$$

où  $\eta$  est la viscosité du sol,  $\rho$  sa densité,  $V$  la vitesse de retrait,  $g$  la gravité et  $K$  une constante dépendant des matériaux. Pour avoir la même viscosité, un ensemble d'échantillons est trempé successivement à différentes vitesses et l'ensemble subit instantanément un traitement thermique. Ce dernier consiste à placer pendant une heure les échantillons dans un four à circulation d'air où la température est de 100 °C. À l'aide d'un profilomètre Sloan DekTak et par couplage par prisme<sup>12</sup>, l'épaisseur correspondante est mesurée (figure 1.2). Un accord parfait existe entre la théorie (formule 1.4) et l'expérience. En effet, pour une viscosité fixe et faible, il est possible de déduire linéairement l'épaisseur correspondante à une vitesse donnée.

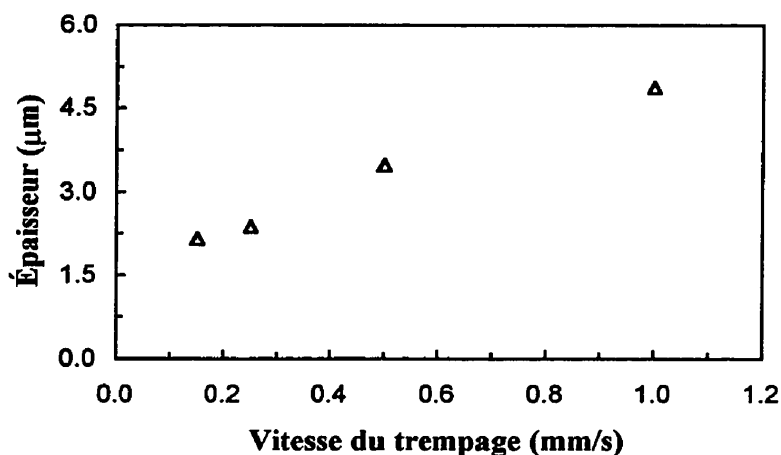


Figure 1.2 Mesure de la dépendance (épaisseur versus vitesse de trempage).

### 1.3.3. Tournette

Le substrat décrit ci-dessus est maintenu par le vide sur l'arbre d'une tournette, et le sol est dispersé dessus en quantité suffisante pour prévenir des bosses sur les bords du substrat en cas d'excès et des creux en cas de carence. Par rotation, le sol s'étale en un film mince. L'épaisseur du film résultant est difficilement contrôlable. Ceci est compliqué par l'interaction entre plusieurs phénomènes physiques, dont l'évaporation du solvant, la dynamique du fluide et la viscosité du sol sont les plus influents.

Des études menées dans le but de bâtir un modèle relatif à la formation des films de sols minces par tournette arrivent à prédire l'épaisseur du film en considérant la fluidité du sol en régime Newtonien<sup>20,28</sup>.

$$e = \left(1 - \frac{\mu_0}{\mu}\right) * \left(\frac{3\eta h}{2\mu_0 \omega^2}\right)^{1/3} \quad (1.5)$$

où  $\mu$  est défini comme la masse de solvant volatilisée par unité de volume,  $\mu_0$  sa valeur initiale,  $h$  le taux d'évaporation et  $\omega$  la vitesse de rotation. Pour les trois variantes de sol, cette relation se trouve vérifiée à condition que les sols soient frais. Un ensemble d'échantillons soumis à un revêtement par tournette à différentes vitesses puis à un

traitement thermique identique à celui du trempage a permis de vérifier la relation (1.5) comme indiqué en figure 1.3.

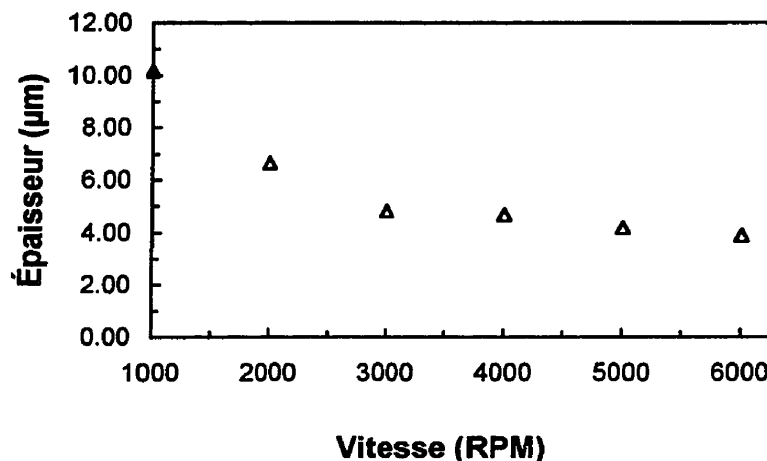


Figure 1.3 Mesure de la dépendance (épaisseur versus vitesse de tournette).

#### 1.3.4. Spectre d'absorption UV

Il est prouvé que la densification du verre hybride organique-inorganique est possible si celui-ci est sujet à une interaction photonique. L'énergie du photon ne peut pas excéder une certaine limite sous peine de perturber la fonctionnalité du composant organique et de causer une déshydratation du composant inorganique<sup>29</sup>.

Une étude axée sur la photochimie menée au sein du groupe révèle que la densification et la relaxation d'un film mince de sol-gel est possible pour une énergie photonique n'excédant pas 6.42 eV<sup>30</sup>. Ainsi, il est jugé raisonnable de connaître le spectre d'absorption UV des trois sols pour une densification optimale. Sur substrat de quartz de chez Chemglass Inc., des films de 1 µm sont obtenus par tournette et immédiatement placés sous le faisceau du spectrophotomètre Hawlett Packard 8452 A. Les spectres obtenus (figure 1.4) révèlent que pour une densification optimale, l'énergie photonique doit être comprise entre 7.29 et 4.77 eV, correspondant à 170 et 260 nm de longueur d'ondes.

Il n'y a pas de changement notable ni de décalage spectral lorsque le film subit un traitement thermique préalable (figure 1.5). En effet, le traitement thermique à 100°C pendant 45 minutes du film pré-recuit ne fait que diminuer l'absorption. Ainsi, il est recommandé de sécher le film à de faibles températures (inférieures à la température d'ébullition du solvant) pendant un court laps de temps, une heure au maximum, pour obtenir la flexibilité requise lors du traitement UV.

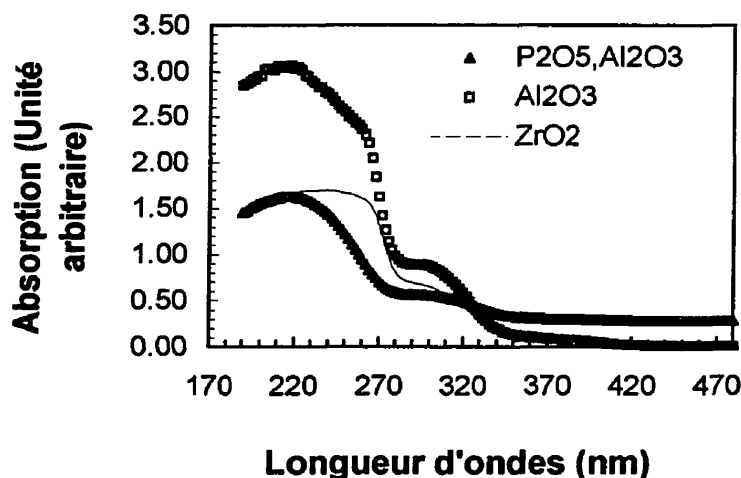


Figure 1.4 Spectre d'absorption UV relatif aux trois variantes du verre hybride. Aucun traitement de recuit n'est opéré.

### 1.3.5. Évolution de l'indice de réfraction

Les gels obtenus précédemment sont des systèmes mixtes comprenant  $\text{SiO}_2$  en tant que composant majoritaire; les dimensions des particules de ce composant n'excèdent pas  $15 \text{ \AA}$  et peuvent atteindre quelques dizaines de nanomètres lorsque les liaisons métalloxanes doubles Si-O-M se forment.<sup>31</sup> Ainsi, la transparence optique du matériau se trouve garantie. Il est observé que cette transparence est perturbée par les pores qui résultent de la formation tridimensionnelle du réseau. Le volume occupé par ces pores peut être extrêmement élevé, spécialement si le gel est séché dans des conditions hypercritiques et hydrolysé dans un excès de solvant.<sup>32</sup>



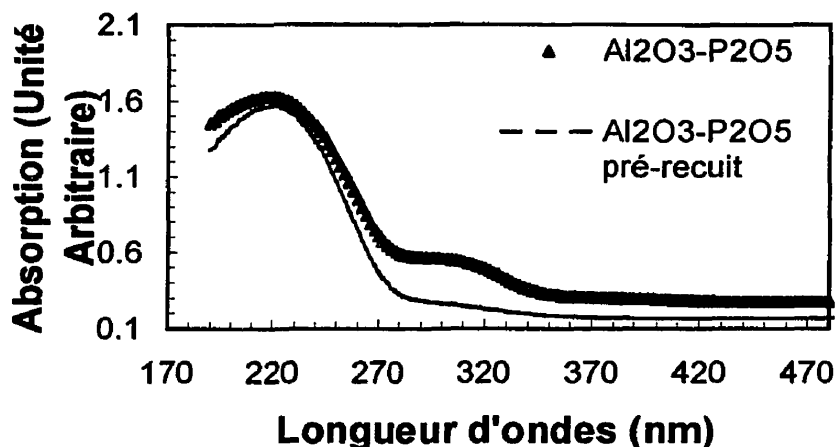


Figure 1.5 Comparaison entre le spectre d'absorption UV de la silice aluminophosphate humide et pré-recuite.

L'obtention d'une structure poreuse du gel dépend de la méthode de préparation du sol. Il est observé que la porosité de la silice de zircone est supérieure à celle de la silice d'aluminophosphate, elle-même supérieure à celle de la silice d'alumine (par. 2.2.4). La taille de ces pores ne dépend pas seulement de la taille des particules, mais aussi du rapport longueur/épaisseur entre deux ponts du réseau solide<sup>33</sup>. Le volume des pores peut être réduit en soumettant le gel à un traitement par UV. En effet, l'UV déclenche une polymérisation des radicaux libres du monomère et une densification collatérale. Une corrélation existe alors entre l'indice de réfraction et la densification. Ainsi, l'évaluation de cet effet est obtenue en mesurant l'indice de réfraction et l'épaisseur d'un guide plan traité par UV. Pour avoir une épaisseur uniforme, on revêt par tournette un large substrat de silice sur silicium d'un film mince de sol (silice aluminophosphate). L'épaisseur du film est de 2.2  $\mu\text{m}$ , mesurée par DekTak. Le film subit immédiatement un pré-recuit à 100 °C pendant une heure. Il est clivé en un ensemble d'échantillons, et chaque échantillon est insolé à l'UV séparément pendant un temps différent. La densité spectrale de la source (para. 2.1.3) est de 28  $\text{mw}/\text{cm}^2$  au niveau du plan du substrat et émet entre 240 nm et 260 nm. Après exposition à l'UV,

l'ensemble des échantillons est soumis à un recuit à 130 °C pendant une heure. Deux méthodes sont utilisées pour mesurer l'indice de réfraction.

### 1.3.6. Couplage par prisme

La méthode consiste à mesurer des angles grâce auxquels les différents modes du guide plan sont excités<sup>34</sup>. L'indice effectif correspondant,  $N$ , est donné par:

$$N = N_p \left( A + \sin \left( \frac{\sin \theta}{N_p} \right) \right) \quad (1.6)$$

où  $N_p$  est l'indice de réfraction du prisme, 1.71653 donné à 632.8 nm,  $A$  est l'angle du prisme adjacent à la surface de contact, et  $\theta$  est l'angle mesuré. Une fois l'indice effectif mesuré, on fait appel à l'équation de dispersion<sup>35</sup> d'un guide plan en polarisation transverse électrique, TE. Les normalisations suivantes sont introduites pour universaliser le calcul.

- Fréquence normalisée  $V$ .

$$V = \frac{2\pi}{\lambda} * d * \sqrt{(nf^2 - ns^2)} \quad (1.7)$$

- Indice normalisé  $b$ .

$$b = \frac{N^2 - ns^2}{nf^2 - ns^2} \quad (1.8)$$

- Facteur d'asymétrie  $a$ .

$$a = \frac{ns^2 - nc^2}{nf^2 - ns^2} \quad (1.9)$$

où  $nc$ ,  $nf$  et  $ns$  sont respectivement les indices de réfraction de l'air, du film et du substrat. La longueur d'ondes correspondant à toutes les mesures est 632,8 nm. Pour un mode quelconque  $m$ , l'équation de dispersion est

$$V * \sqrt{1-b} = (m+1) * \pi - a \tan \sqrt{\frac{1-b}{b}} - a \tan \sqrt{\frac{1-b}{a+b}} \quad (1.10)$$

Pour le mode fondamental ( $m=0$ ) et le second mode ( $m=1$ ) l'équation (1.10) engendre le système d'équations suivant:

$$\left. \begin{aligned} V * \sqrt{1-b_0} &= 1 * \pi - a \tan \sqrt{\frac{1-b_0}{b_0}} - a \tan \sqrt{\frac{1-b_0}{a+b_0}} \\ V * \sqrt{1-b_1} &= 2 * \pi - a \tan \sqrt{\frac{1-b_1}{b_1}} - a \tan \sqrt{\frac{1-b_1}{a+b_1}} \end{aligned} \right\} \quad (1.11)$$

Pour résoudre ce système d'équations, un calcul numérique est nécessaire. Deux modes (indices effectifs) sont suffisants pour calculer l'indice du film  $n_f$ . Toutefois, en utiliser davantage permet une plus grande précision grâce à un calcul effectué par combinaison de deux. Ainsi, il est très important de pouvoir distinguer et identifier les modes. Le tableau 1.1 résume les résultats obtenus par ce calcul.

Tableau 1.1 Mesure de l'indice de réfraction d'un film mince de silice d'aluminophosphate en fonction de la dose UV

Temps d'exposition UV (min.)	Indice de réfraction	Épaisseur ( $\mu\text{m}$ )
0	1.4898	2.116
5	1.494243	2.312
10	1.498236	2.248
15	1.498511	2.211
30	1.498076	2.119
60	1.497928	2.155

Un deuxième ensemble d'échantillons est réalisé dans le but d'évaluer l'effet de l'épaisseur en gardant constants tous les paramètres de fabrication. L'épaisseur mesurée par DekTak est de  $5.1 \mu\text{m}$  et les résultats du calcul sont résumés dans le tableau 1.2.

Tableau 1.2 Mesure de l'indice de réfraction d'un film épais de silice d'aluminophosphate en fonction de la dose UV

Temps d'exposition UV (min.)	Indice de réfraction	Épaisseur ( $\mu\text{m}$ )
0	1.489	5.7
5	1.493	5.3
15	1.493	4.7
60	1.496	5.04

La différence d'indice de réfraction  $\Delta n$  est définie par la différence entre l'indice du film exposé et celui du film non exposé. Le premier ensemble montre que cette différence est stable à partir de 10 min. d'exposition (qui correspondent à une saturation du matériau) et est évaluée à 0,008. En revanche, pour le deuxième ensemble, beaucoup plus épais, cette saturation n'a pas lieu même si l'exposition est relativement longue (60 min). Toutefois la tendance à l'augmentation d'indice est similaire à celle du premier ensemble et à celle mesurée dans un travail antérieur<sup>12</sup>.

Ce résultat vient confirmer l'effet de la densification sur l'indice de réfraction. Ainsi, plus le film est épais, plus la proportion de volume occupée par les pores est élevée et plus la quantité d'énergie photonique, évaluée en temps d'exposition, est importante. En effet, l'observation de ces films par microscope électronique à balayage (*SEM scanning electron microscope*) montre une évolution en fonction du temps d'exposition au point de vue de la microstructure (figure 1.6).

Si la méthode du couplage par prisme est précise, elle est cependant incomplète puisqu'elle ne donne pas l'indice de réfraction correspondant aux longueurs d'ondes 1550 et 1300 nm, très utilisées en télécommunications. Néanmoins, les mesures d'indices et d'épaisseurs à 632,8 nm ont servi de critère pour valider les mesures par ellipsométrie.

### 1.3.7. Ellipsométrie

Comme pour les mesures par prisme, un film mince est obtenu par tournette. Après un pré-recuit, il est insolé pendant 10 min. et subit un recuit défini ci-dessus. Ce dernier est rendu nécessaire pour prévenir d'éventuelles polymérisations dues au fait que le faisceau de l'ellipsomètre en question couvre un large spectre, soit 300-2000 nm. Le modèle utilisé pour le calcul d'indice est celui de Cauchy:  $n^2=A+B/\lambda^2+ C/\lambda^4+\dots$

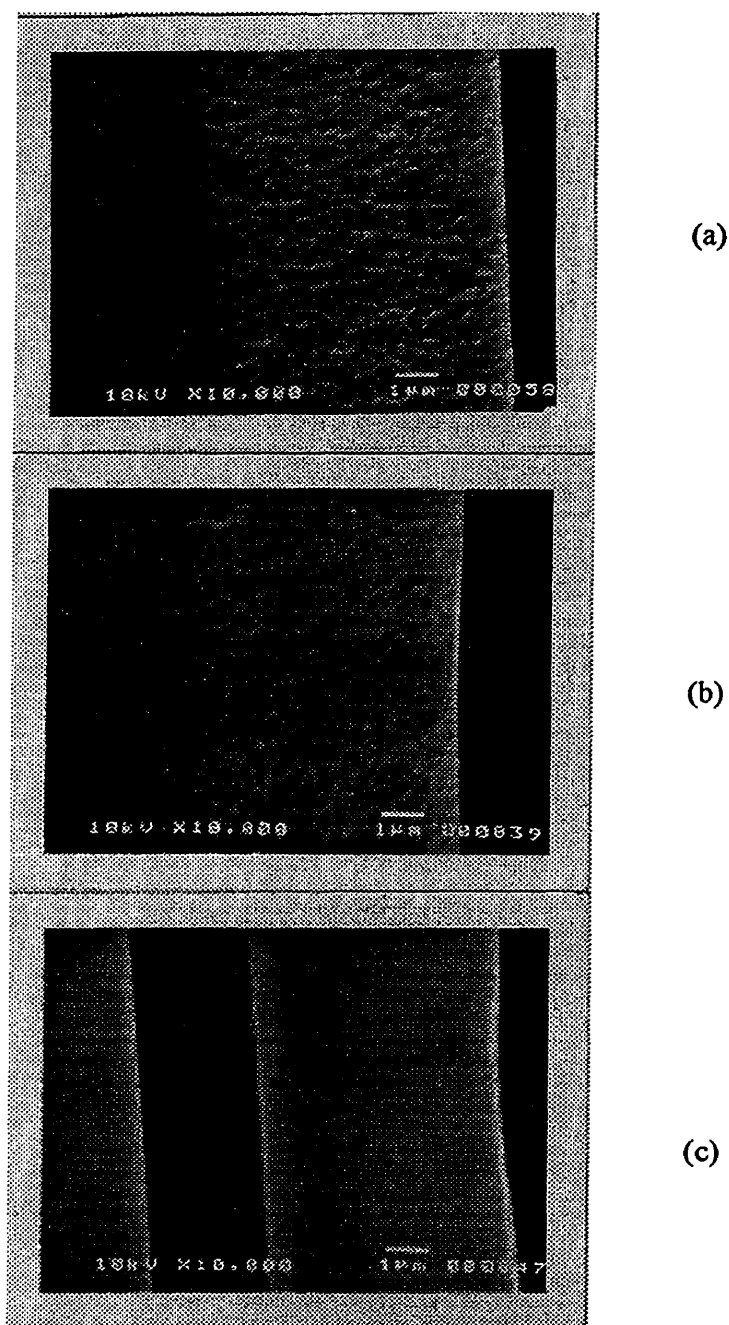


Figure 1.6 Évolution de la microstructure de la silice aluminophosphate en fonction de la dose UV, le temps d'exposition est (a) 0 min, (b) 5 min et (c) 30 min.

Ce modèle est appliqué à la structure du guide plan qui est multicouche (VHSG/SiO<sub>2</sub>/Si). La courbe de dispersion utilisée lors du calcul est obtenue en mesurant le substrat de chez Nova Electronic Materials Inc., qui consiste en un film de 2 μm de silice thermiquement oxydée sur du silicium (figure 1.7).

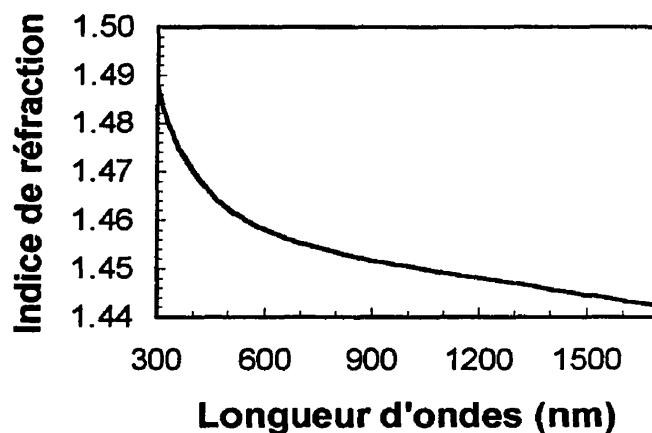


Figure 1.7 Courbe de dispersion de 2 μm de SiO<sub>2</sub> sur Si mesurée par ellipsométrie.

La courbe de dispersion de la silice d'aluminophosphate (figure 1.8) est identique en allure à celle de la silice pure présentée ci-dessus. Désormais, il est facile de connaître l'indice de réfraction du verre hybride (silice d'aluminophosphate) à la longueur d'ondes concernée. De plus, connaissant la différence d'indice  $\Delta n$  obtenue par couplage par prisme, il est possible d'extrapoler l'indice de réfraction du verre hybride insolé à n'importe quelle longueur d'ondes.

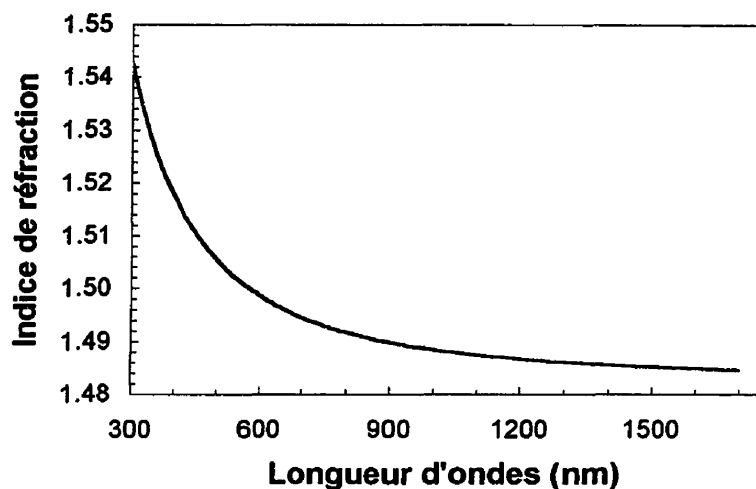


Figure 1.8 Courbe de dispersion de la silice d'aluminophosphate exposée à 10 min. UV mesurée par ellipsométrie.

Pour valider ces mesures, ce même échantillon est mesuré à l'aide du couplage par prisme. Les résultats obtenus permettent de considérer les mesures par ellipsométrie comme exactes.

Tableau 1.3 Comparaison des mesures d'indice de réfraction et d'épaisseur entre le couplage par prisme et l'ellipsométrie.

	Prisme	Ellipsomètre
nf	1.49708	1.498236
Épaisseur ( $\mu\text{m}$ )	2.248	2.2493

#### 1.4. Références

1. J. Robert Hunter, "Introduction to Modern Colloid Science", Oxford University Press, New York, (1993), 1-93.
2. C. Freidel, J. M. Crafts, "Synthesis of Tetraethylsilane from Diethylzinc and Silicon Tetrachloride", *Ann.*, 1865, 136-203.
3. E. Matijevic, "The Role of Chemical Complexing in the Formation and Stability of Colloidal Dispersion", Academic Press, New York, Edt. M. Kerker, A. C. Zettlemayer, R. L. Rowell, Vol. I, (1977), 397-412.
4. R. Roy, "Aids in Hydrothermal Experimentation Methods of Making Mixtures for both 'Dry' and 'Wet' Phase Equilibrium Studies", *Journal of Am. Ceramic Society* 39, (1956), 145-148.
5. K. S. Maddiyasni, C. I. Lynch, J. S. Smith, "Preparation of Ultra-high-purity Submicron Reflectory Oxides", *Journal of Am. Ceramic Society* 48, (1965), 372-375.
6. P. J. Flory, "Molecular Size Distribution in Three-Dimensional Polymers", *Journal of Am. Chemi. Society* 63, (1941), 3083-3100.
7. J. M. Hammersley, "Percolation Theory: II The Connective Constant", *Proceeding Cambridge Philosophia Society* 53, (1957), 642-645.
8. W. C. Elmor, "Ferromagnetic Colloid for Studying Magnetic Structures", *Physic Revue* 54, (1938), 309-310.
9. G. Raman, F. D. Gnamam, P. Ramasamy, "The Growth of SbSBr, SbSCL, and SbSF Single Crystals in Gels", *Journal of Crystal Growth* 75, (1986), 466-470.
10. H. Schroeder, "Oxide Layers Deposited from Organic Solutions", *Physics of Thin Films*, Academic Press, New York, Edt. G. Hass, R. E. Thun, Vol. 5, (1969), 87-141.



11. H. Dislich, P. Hinz, "History and Principles of the Sol-gel Process and Some New Multicomponent Oxide Coatings", *Journal of Non-crystalline Solids* 48, (1982), 11-16.
12. T. Touam, G. Milova, Z. Saddiki, M. A. Fardad, M. P. Andrews, J. Chrostowski, S. I. Najafi, "Organoaluminophosphate Sol-gel Silica Glass Thin Films for Integrated Optics", *Thin Solids Films* 307, (1997), 203-207.
13. C.-Y. Li, M. P. Andrews, S. I. Najafi, J. D. Mackenzie, N. Peyghambarian, "Sol-gel Integrated Optics Coupler by Ultraviolet Light Imprinting", *Electronics Letters* 31, (1995), 271-272.
14. L. Murawski, C. H. Chung, J. D. Mackenzie, "Electrical Properties of Semiconducting Oxide Glasses", *Journal of Non-crystal. Solid.* 32, (1979), 91-104.
15. C. J. Brinker, M. S. Harrington, "Sol-gel Derived Antireflective Coating for Silicon", *Solar Energy Mat.* 5, (1981), 159-172.
16. H. Dislich, "Glassy and Crystalline Systems from Gel: Chemical Basis and Technical Application", *Journal of Non-crystal. Solid.* 57, (1983), 371-388.
17. M. J. Bennett, M. Houlton, J. B. Price, "New Ceramic Coatings for High Temperature Gas-cooled Reactor Materials Protection", *Oesterr. Forschungszt. Seibersdorf. Number OEFZS BER 4086*, (1981), N1-N14.
18. K. Hellmut Schmidt, "Chances and Limitations of Sol-gel Derived Metal Oxide and Chalcogenide Nanocomposites for Optic and Photonic Application", *Proceedings of SPIE*, Vol. 2288, (1994).
19. D. C. Bradley, R. C. Mehrotra, P. D. Gaur, "Metal Alkoxides", Academic Press, London, (1978), 150-160.
20. T. G. M. Van De Ven, "Colloidal Hydrodynamics", Academic Press, *Colloid Science*, Edit. R. H. Ottewil, and R. L. Rowell, (1989), 563-579.
21. Aldrich Chemical & Co. *Catalogue Handbook of Fine Chemicals*, 1996-97.
22. United Chemical Technologies, *Silicon Compounds Register and Review*, 5<sup>th</sup> Edition, (1997).

23. Alfa Aesar, Johnson Matthey Catalogue Company, 1995-96.
24. X. M. Du, T. Touam, L. Degachi, J. L. Guibault, M. P. Andrews, and S. I. Najafi, "Sol-gel Waveguid Fabrication Parameters: An Experimental Investigation", *Optical Engineering* 37, (1998), 1101-1104.
25. J. J. Lanutti, D. E. Clark, "(a) Sol-gel Derived Ceramic-ceramic Composites using Short Fibers, (b) Long Fiber Reinforced Sol-gel Al<sub>2</sub>O<sub>3</sub> Composites", *Mat. Res. Soc. Sympo. Proceeding* 32, (1984), 369-381.
26. D. C. Bradey, D. G. Carter, "Metaloxide Polymers. I Hydrolysis of Some Primary Alkoxides of Zr", *Canadian Journal of Chemistry* 39, (1961), 1434-1443.
27. B. E. Yoldas, "Introduction and Effect of Structural Variation in Inorganic Polymers and Glass Network ", *Journal of Non-crystal. Solid.* 51, (1982), 105-121.
28. C. Jeffrey Brinker, G. W. Sherer, "Sol-gel Science", Academic Press, San Diego, (1990), 113.
29. H. Imai, H. Hiroshima, K. Awazu, and H. Onuki, "Structural Change in Sol-Gel Derived SiO<sub>2</sub> Films Using Ultraviolet Irradiation", *Proc. SPIE*, Vol. 2288, (1994), 71-76.
30. M. P. Andrews, K. Saravanamuttu, T. Touam, R. Sara, X. M. Du, S. I. Najafi, "Collateral Densification Associated with the Photoresponse of Hybrid Sol-gel Glasses for Depositing Bragg Gratings on Ridge Waveguide", *Proc. SPIE*, Vol. 3290, (1998).
31. R. K. Iler, "The Chemistry of Silice", Wiley, New-York, (1979).
32. T. Waignier, J. Phalippon, J. Zarzycki, "Monolithic Aerogels in the Systems SiO<sub>2</sub>-B<sub>2</sub>O<sub>3</sub>, SiO<sub>2</sub>-P<sub>2</sub>O<sub>5</sub> and SiO<sub>2</sub>-B<sub>2</sub>O<sub>3</sub>-P<sub>2</sub>O<sub>5</sub>", *Journal of Non-crystall. Solid.* 63, (1984), 117-130.
33. B. E. Yoldas, "Zirconium Oxides Formed by Hydrolytic Condensation of Alkoxides and Parameters that Affect their Morphology", *Journal of Mat. Sciences* 21, (1986), 1080-1086.

34. S. I. Najafi, "Introduction to Glass Integrated Optics", Artech House Inc., (1992), 108-109.
35. D. Marcuse, "Theory of Dielectric Optical Waveguide", Academic Press, (1974), 7-11.

Ayant défini le protocole chimique qui a permis l'obtention des trois variantes de verre hybride et obtenu les abaques des indices de réfraction en fonction de la dose UV et de la température de recuit, il est désormais possible d'obtenir un guide d'ondes surface, en fouille ou en relief. L'étude d'un guide en relief par microscopie à balayage électronique et à force atomique a pour but d'évaluer l'aptitude de la composante photoactive du verre hybride à s'adapter à la photolithographie optique et de la composante minérale à la condensation par UV. La transparence de ces verres aux longueurs d'ondes d'intérêt en télécommunication est étudiée par mesure de transmission d'un signal large-bande. Cette étude fait l'objet du chapitre suivant, qui réunit deux articles dont le texte est en anglais:

- *Photolithography Fabrication of Sol-Gel Ridge Waveguide* est publié dans le Proceedings of SPIE, *Conference on Organic-Inorganic Hybrid Materials for Photonics*, volume 3469, Juillet 1998, 118-123. Les auteurs sont R. Sara, T. Touam, C. Blanchetiere, Z. Saddiki, K. Saravanamuttu, X. M. Du, T. Chrostowski, M. P. Andrews et S. I. Najafi.
- *SEM and AFM Studies of Polyglass Ridge Waveguides* paraîtra dans le Proceedings of SPIE, *Conference on Integrated Optics Devices III*, Vol. 3620, San Jose, Janvier 1999, Les auteurs sont R. Sara, Z. Saddiki, T. Touam, T. Chrostowski, M. P. Andrews et S. I. Najafi.

## **CHAPITRE II: FABRICATION DES GUIDES D'ONDES OPTIQUE POLYGLASS**

### **2.1. Photolithography Fabrication of Sol-Gel Ridge Waveguide**

#### **2.1.1. Abstract**

We report on fabrication of ridge waveguides in UV-light sensitive glass sol-gel thin films, deposited on silicon substrate, using a simple photolithography process. The single-layer films are prepared at low temperature and deep UV-light (DUV) is employed to make the waveguides. The effect of fabrication parameters on waveguide shape is investigated.

**Keywords:** Integrated optics, Sol-Gel waveguide.

#### **2.1.2. Introduction**

Sol-Gel photolithography process is a cost effective route for integrated optical devices manufacturing on silicon.<sup>1-2</sup> This process can facilitate fiber connection and packaging and allows mass production.

In a previous publication we have discussed the effect of process parameters on the refractive index of sol-gel thin films.<sup>3</sup> Another important issue in production of sol-gel waveguides is controlling the dimension (width and depth) and shape of the waveguide. High-aspect-ratio photolithography (thickness/resolution) is required to provide waveguides with excellent dimensional control and vertical sidewalls.

In this paper, we report on the effect of the fabrication parameters on the size and shape of ridge waveguides.

### 2.1.3. Experiment

Hybrid  $(1 - x)\text{SiO}_2 - x\text{ZrO}_2$  and  $(1 - y)\text{SiO}_2 - y\text{Al}_2\text{O}_3$  sol-gel solutions are prepared as described previously.<sup>3-4</sup> Methacryloxypropyltrioxysilane (MAPTMS), hydrolyzed with 1.5 equivalents of  $\text{H}_2\text{O}$ . 0.1 M HCl, acts as catalyst.  $\text{Zr}(\text{OC}_3\text{H}_7)_4$ , employed as refractive index modifier, is dissolved in isopropanol (1:1 volume ratio) and is added dropwise to the stirred solution of the partially hydrolyzed MAPTMS. After adding water to complete the hydrolyzation of alkoxide substituents, Irgacure 184 (CIBA) is introduced as photoinitiator.

Pinhole and crack-free photosensitive sol-gel films are deposited on  $\text{SiO}_2/\text{Si}$  substrates, which have a 2  $\mu\text{m}$  thick thermally grown  $\text{SiO}_2$  layer, by spin-coating. The sol is aged for up to 30 days prior to deposition. The time elapsed since adding the last fraction of water until coating is called *aging time*. Various spin speeds from 1000 rpm to 2500 rpm, for 30 s, are used in order to obtain different film thicknesses. The resultant samples are pre-baked in an oven at  $110^\circ\text{C}$  for 30 min. Pre-baked samples are exposed to DUV light through 4  $\mu\text{m}$  or 5  $\mu\text{m}$  openings in a dark-field contact mask, using an Oriel filtered DUV-light illumination source. Samples are subsequently developed by isopropanol for a few minutes to remove the unexposed region. Post-bake is performed in a vacuum furnace at  $150^\circ\text{C}$  for 5h. Sols with zirconium concentrations of up to 25% are prepared simultaneously. Viscosity measurements of the sols are made with a Brookfield DV-I+ viscometer. All sols are stored in sealed glass vials. Scanning electron microscopy (SEM) is used for ridge waveguide profile observation.

### 2.1.4. Results and Discussion

The deposition mechanism of spin coating is based on viscose flow under centrifugal force and rapid solvent evaporation from sol layer during spinning. The film thickness may be controlled by spinning speed, sol viscosity and solvent evaporation rate. As spin speed and environment of spinner can be easily controlled, a simplification is that the thickness of a spin-coated film is inversely proportional to the square root of

the spinning speed. This simplification holds as long as the viscosity and concentration of the coating solution remain relatively constant.<sup>5</sup> However, controlling sol viscosity is more difficult because, in general, the viscosity of a given sol-gel increases with aging time due to continuous condensation or cross linking of organic chains in the sol even at room temperature.

Figure 2.1 shows viscosity of  $(1-x)\text{SiO}_2 - x\text{ZrO}_2$  sol-gel solutions, with  $x = 0, 8.3, 18.8, 22.2$  and  $25.0$ , as a function of aging time at room temperature. During the first 3 days, the condensation between Si-OH groups and co-condensation between Si-OH and Zr-OH groups are intense and the viscosity of sols increases rapidly. The viscosity increasing rate slows down afterwards in particular for the sols with zirconium concentrations less than 20%, implying that most of condensation takes place during the first few days. The sols with higher  $\text{ZrO}_2$  concentration have higher initial viscosity and higher viscosity increase rate.

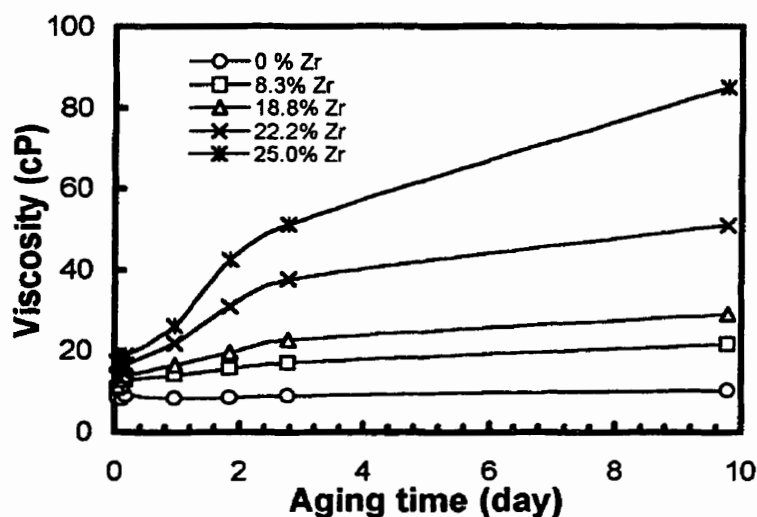


Figure 2.1 Viscosity of  $(1-x)\text{SiO}_2 - x\text{ZrO}_2$  ( $x = 0, 8.3, 18.8, 22.2$  and  $25.0$ ) sol-gel as a function of aging time.

Figure 2.2 shows viscosity of  $(1-x)\text{SiO}_2 - x\text{ZrO}_2$  and  $(1-y)\text{SiO}_2 - y\text{Al}_2\text{O}_3$  sol-gel solutions, with  $x = 18.8$  and  $y = 15$ , as a function of aging time at room temperature. It can be seen that for the sol with  $\text{Al}_2\text{O}_3$  as refractive index modifier most of the

condensation takes place during the first two days. This implies that it is more stable than those with  $ZrO_2$ .

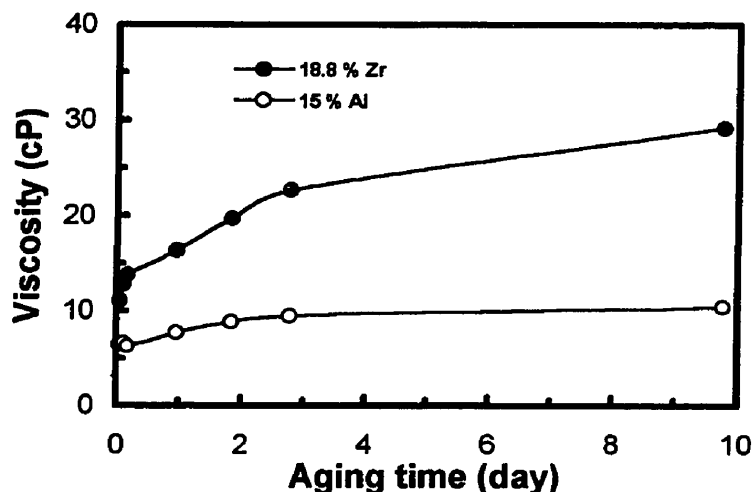


Figure 2.2 Viscosity of  $(1-x)SiO_2 - xZrO_2$  ( $x = 18.8$ ) and  $(1-y)SiO_2 - y Al_2O_3$  ( $y=15$ ) sol-gel as a function of aging time.

For integrated optics applications the geometry of channel waveguide should be well controlled. Therefore, film thickness that directly leads to the height of channel waveguide becomes one of the key dimensional parameters. A Sloan DekTak auto-levelling profilometer was used to measure the thickness of the different layers. The variation of film thickness as a function of aging time is shown in Fig. 2.3.  $80SiO_2-20ZrO_2$  sol is aged from 6 hours to 25 days and then deposited on silicon substrates by spin-coating at 1000 rpm and 1500 rpm. The film thickness increases during the period that follows immediately the sol-gel synthesis. Then, the thickness converges towards a constant value after  $\sim 5$  days aging. The shape of the sol-gel channel waveguide depends on the fabrication parameters and in particular on the chemical compositions of sol, photo-initiator, aging time, gap between mask and sol-gel film, as well as DUV-light dose.

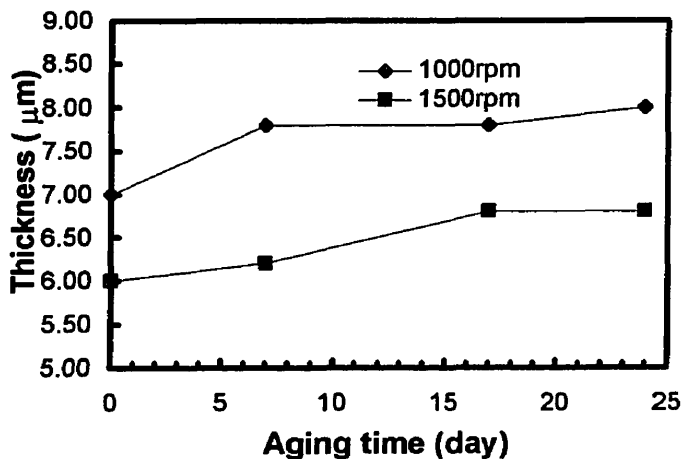


Figure 2.3 Variation of  $80\text{SiO}_2\text{-}20\text{ZrO}_2$  sol-gel film thickness as a function of aging time Spin-coating speed are 1000 rpm and 1500 rpm.

Figure 2.4 shows scanning electron microscope (SEM) photographs of  $80\text{SiO}_2\text{-}20\text{ZrO}_2$  sol-gel ridge waveguide. The waveguide made using thicker film and shorter DUV-light exposure time has a mushroom-like profile. The width of waveguide increases by increasing DUV-light exposure. The waveguide width made using  $1.5\ \mu\text{m}$  thick film may be smaller than the width of the photomask opening when the DUV-light exposure time is less than 10 sec. For  $3\ \mu\text{m}$  thick films, the resultant waveguide width is smaller than the mask width even after 60 sec. exposure to DUV-light.



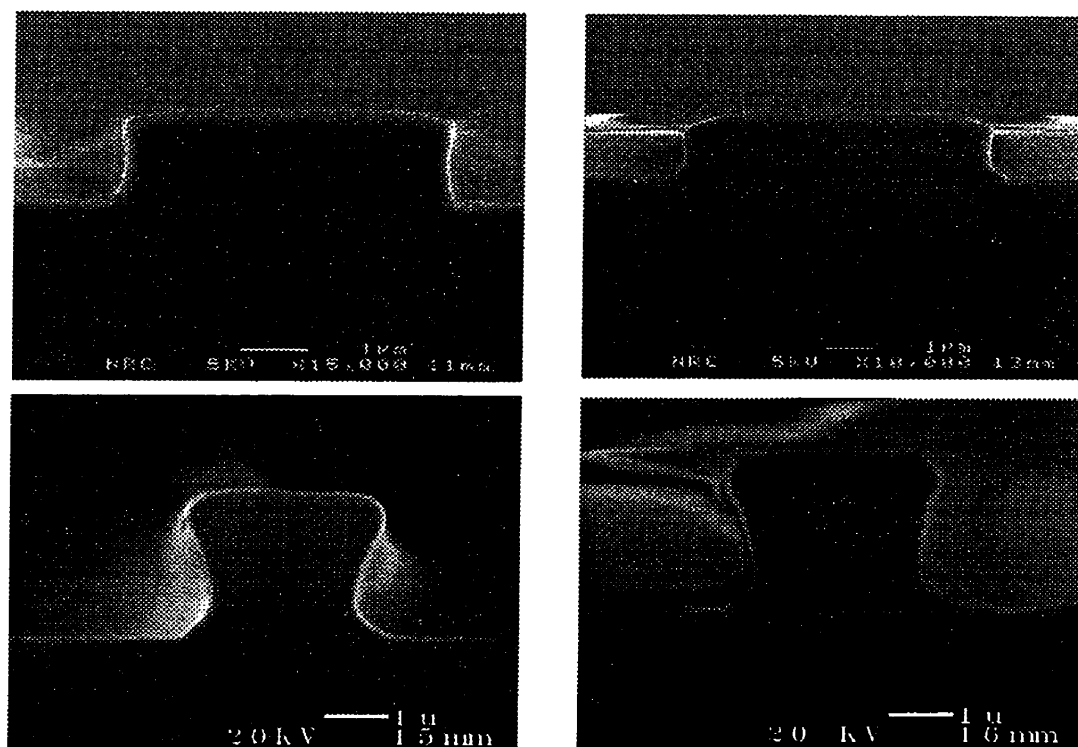


Figure 2.4 SEM photographs of  $80\text{SiO}_2\text{-}20\text{ZrO}_2$  ridge waveguide. Used film thickness and DUV-light exposure time are: top (left)=  $1.25\mu\text{m}$  and 10 sec.; top(right)=  $1.25\mu\text{m}$  and 30 sec.; bottom (left)=  $3\mu\text{m}$  and 10 sec, bottom (right)=  $3\mu\text{m}$  and 60 sec.

Fig. 2.5 depicts the variation of waveguide width broadening,  $\Delta W$ , with UV-light exposure time.  $\Delta W$  is the difference between maximum width of waveguide,  $W_{\text{max}}$ , and the width of photomask opening,  $W_0$ . The degree of polymerization of the vinyl monomer, due to exposure to UV-light, throughout the full thickness of the gel layer depends on the total thickness of the exposed film. For a thicker sol-gel film longer UV-light exposure time is necessary in order to have waveguides with the same width as the used mask.

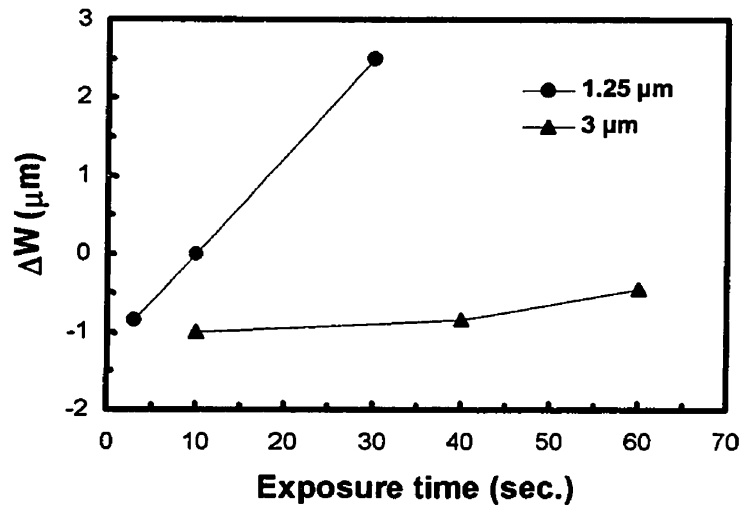


Figure 2.5 Variation of  $\Delta W (= W_{\max} - W_0)$  as a function of mask width.  $W_{\max}$  is the maximum width of waveguide cross section and  $W_0$  is the width of mask opening. The films are 1.25  $\mu\text{m}$  and 3  $\mu\text{m}$  thick.

The mushroom shape of the fabricated waveguide is quantitatively expressed as the ratio of minimum and maximum widths of the cross section,  $W_{\min}/W_{\max}$ . Fig.2.6 shows that  $W_{\min}/W_{\max}$  reaches unity (rectangular shape) after UV-light exposure for  $\sim 10$  sec. in 1.25  $\mu\text{m}$  thick waveguide. However, with the same UV-light dose, a smaller  $W_{\min}/W_{\max}$  ratio is obtained for the thicker film. The incident collimated UV-light passes through the opening of photomask initiating polymeric cross-linking in sol layer and leading to an insoluble gel layer with high-molecular-weight at the top of film. If sol-gel film absorbs small dose of UV-light, i.e. short UV-light exposure time is used, the exposure dose is greater at the surface than at the sol/substrate interface and hence the development rate of the system is not same. Therefore, the intended waveguide will be obtained by opposite undercutting etching when the sample is developed in solvent. The gel occurs in full thickness and adhesion to the substrate only when top of the film absorbs enough radiation which results in a mushroom shape cross section. The main factor to broaden line width is DUV-light scattering.

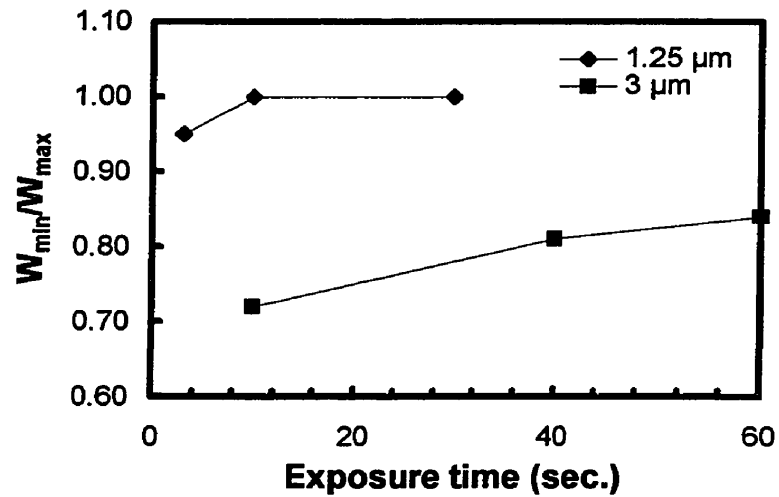


Figure 2.6 Variation of  $W_{\min}/W_{\max}$ , for 1.25  $\mu\text{m}$  and 3  $\mu\text{m}$  thick waveguides, as a function of DUV-light exposure time.  $W_{\max}$  and  $W_{\min}$  are maximum and minimum widths of waveguide cross section respectively.

The broadening,  $\Delta W$ , depends on the mask opening (see Fig. 2.7).  $\Delta W$  for the waveguide made using 2  $\mu\text{m}$  mask opening is much larger (4.34  $\mu\text{m}$ ) than that made using 10  $\mu\text{m}$  mask opening (3.16  $\mu\text{m}$ ).

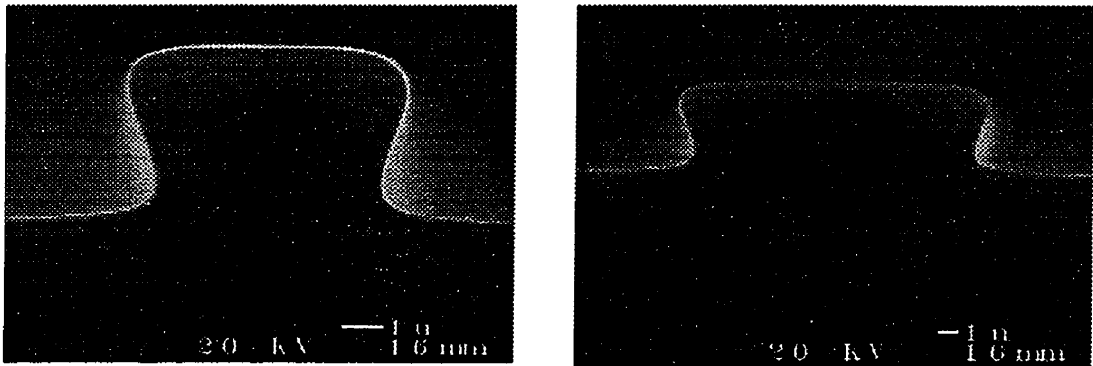


Figure 2.7 SEM photographs of 80SiO<sub>2</sub>-15Al<sub>2</sub>O<sub>3</sub> ridge waveguides. Used film thickness and UV-light exposure time are 4.16 $\mu\text{m}$  and 120 sec. Used mask opening was 2 and 10  $\mu\text{m}$ .

### **2.1.5. Acknowledgments**

This work was funded in part by research grants from NSERC and NRC .

### **2.1.6. References**

1. M.A. Fardad, T. Touam, P. Meshkinfam, R. Sara, X.M. Du, M.P. Andrews and S.I. Najafi, "UV-light imprinted Bragg grating in sol-gel ridge glass waveguide with almost 100% reflectivity", *Electronics Letters* 33, 12 (1997) 1069-1070.
2. Najafi, S. I., Andrews, M. P., Fardad, M. A., Milova, G. Touam, T., and Coudray, P., "UV-light imprinted surface, ridge and buried sol-gel glass waveguide and devices on silicon", *Conf. Integrated Optics for Signal Processing*, Berlin, October 1996, pp. 10 - 15 ( Invited paper).
3. X.M. Du, T. Touam, L. Degachi, J.L. Guilbault, M. P. Andrews, and S.I. Najafi, "Sol-gel waveguide fabrication parameters: an experimental investigation", *Optical Engineering*, Vol. 37 No. 4, April 1998.
4. Fardad, M.A., Andrews, M.P., and Najafi, S.I., "Novel sol-gel fabrication of integrated optical waveguides", *Conf. Integrated Optics Devices: Potential for Commercialization*, SPIE, San Jose, February 1997, Vol.2997, pp.7278.
5. L.F. Thompson and M. T. Bowden in *Introduction to Microlithography*, edited by L.F. Thompson , C.G. Wilson and M. T. Bowden (ACS Symposium 219, Seattle, WA 1983), 161-214.

## 2.2. SEM and AFM Studies of *Polyglass* Ridge Waveguides

### 2.2.1. Abstract

By means of straightforward photolithography, low-cost *polyglass* ridge waveguides can be produced that are suitable for integrated optics. The *polyglass* process uses a hybrid organic-inorganic sol-gel glass, which is attractive for monolithic integration. As in any photo-imaging process, three-dimensional patterning of device features depends on a number of interacting process parameters. Some of these are discussed for several families of hybrid glasses.

**Keywords:** Integrated optics, photolithography, wet etching, linewidth, hybrid glasses, aspect ratio.

### 2.2.2. Introduction

*Polyglass* is a generic term for an extensive family of hybrid glasses that can be deposited in thin film form by solution sol-gel polycondensation reactions. Invariably the glasses contain an organic monomer component, covalently attached to a main group alkoxide. In the presence of a photoinitiator, the monomer can be polymerized after partial inorganic network development in the gel phase. The organic polymer appears to be intimately dispersed within the main group oxide glassy lattice, hence the term *polyglass*. The quality of *polyglass* waveguides depends on the physics and chemistry of film formation and the details of material processing. Waveguides can be made directly by resist-free by photolithography, but to date information has been lacking on the effects of various processing conditions. In a previous paper, we have reported on how several fabrication parameters affect the three-dimensional structure of ridge waveguides<sup>1</sup>. A mushroom-like structure was observed in cross-section, whose dimensions were found to depend on solvent wet-etch fabrication conditions and hybrid

glass chemical composition. Recently, improvements to the process have been made. Some of the results of our findings are reported below.

The process of creating ridge waveguides (and complex optical circuits) from hybrid glasses typically involves the following steps: (i) application of the hybrid glass film by spin-coating onto a silicon substrate; (ii) soft-baking for contact mask photolithography; (iii) brief exposure to UV light to capture a projected image of the optical device as a latent image; (iv) relief development by organic solvent wet-etching; (v) post-baking to densify and harden the device. Good contrast is necessary in photomicroolithography to provide waveguides with vertical wall profiles in relief images, and the highest quality pattern transfer. Dimensional stability (resistance to deformation) is crucial for two reasons: the latent image must not be attacked by the solvent etch; and the waveguide that is produced must have a glass transition, decomposition or softening temperature that meets or exceeds device performance criteria under defined conditions of thermal stress. For integrated optics, the materials must of course meet standards for optical quality, including transparency/loss. To investigate some of the ways in which various processing parameters might affect the quality of ridge waveguides, characteristic curves of various *polyglass* formulations were drawn up as described below. Over a large data set, such curves can be useful in identifying materials and processing conditions suitable for low-cost and high performance integrated optics devices<sup>2-4</sup>.

### 2.2.3. Ridge Waveguide Characterization

*Polyglass* compositions were prepared by sol-gel polycondensation to fabricate ridge waveguides as described elsewhere<sup>5-7</sup>. An aluminosilicate was prepared by acid catalyzed hydrolysis of isobutoxyaluminumoxytriethoxysilane and methacryloxypropyl-trimethoxysilane (MAPTMS). The MAPTMS component was kept fixed for all samples. Irgacure-184 (CIBA) was used as the photoinitiator. The resultant *polyglass*,

nominally 85 SiO<sub>2</sub>-15 Al<sub>2</sub>O<sub>3</sub>, was filtered through a 0.2 μm filter and dispensed uniformly on silicon substrates. Precision spin coating followed at 2000 rpm for 30 sec. The resultant pinhole and crack-free photosensitive film was prebaked at 90°C for 60 minute in order to dry and anneal the film prior to UV exposure. The film/substrate was then cleaved to give a set of samples. Each sample was exposed to deep-UV light for different times through the openings of a dark-field contact mask (chromium on fused silica). Exposure parameters such UV intensity, mask-sample gap, and maskholder-lamp distance were kept constant. Propanol solvent wet-etching for fixed development time, was used to obtain ridge waveguides. These ridges were then subjected to a 150 °C postbake step, performed for 5 h in a vacuum furnace. Samples were cleaved and studied by scanning electron microscopy (SEM), as shown in Figure 2.8. The waveguide lateral dimensions can be seen to increase from left to right, apparently replicating the lateral dimensions of the mask openings. In general, the valleys between the ridge guides were found to be free of debris, while the edges (viewed from the top) appear smooth and parallel.

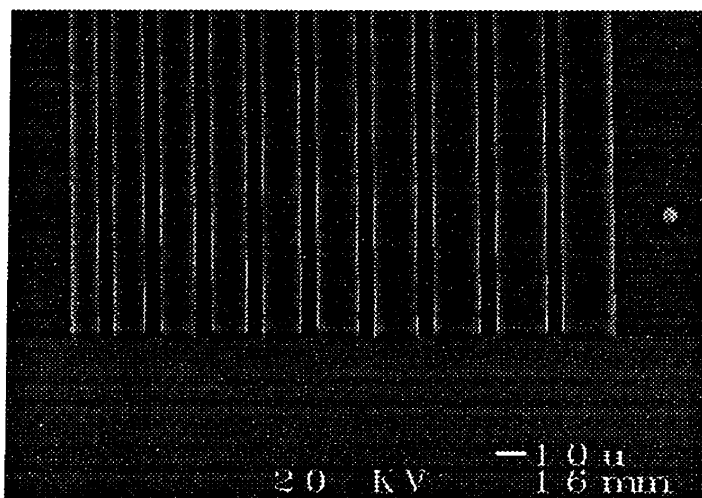


Figure 2.8 SEM top view of ridge waveguides created by solvent wet etching for different openings of the photomask.

The UV exposure time was then varied from sample to sample, with all other process conditions, including the mask opening  $10\ \mu\text{m}$ , held fixed. Figure 2.9 (a)-(e) shows how the waveguide shape and sidewall evolve as a function of UV exposure time. Observe that waveguides made at shorter UV-light exposure times have a mushroom-like cross-section profile. Moreover, the width of the waveguide at early times (as in Figure 2.9 (a)) appears to be smaller than the photomask opening, though the walls are vertical. With increasing UV-light exposure time (Figure 2.9 (d) and (e)), the width of a given waveguide increases. There is loss of edge definition, and slight undercutting of the guide in some cases. These features are given more quantitative explanation later.

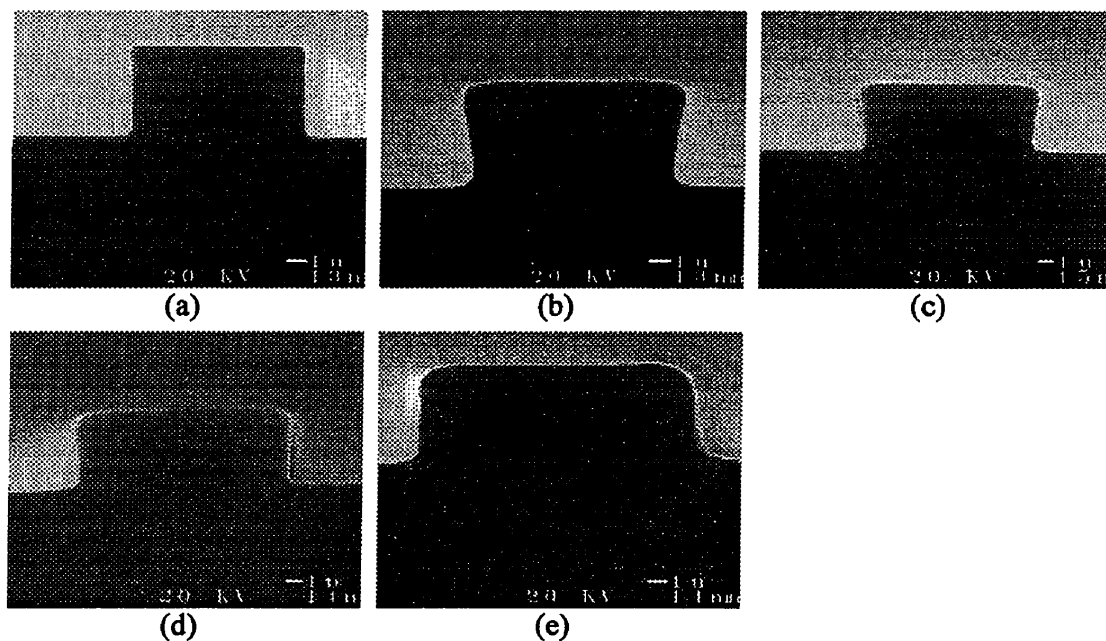


Figure 2.9 SEM image of ridge waveguide cross section (nominal composition  $85\ \text{SiO}_2\text{-}15\ \text{Al}_2\text{O}_3$ ) as function of exposure time: (a) 5 sec., (b) 10 sec., (c) 30 sec., (d) 120 sec. and (e) 900 sec. Mask opening =  $10\ \mu\text{m}$ .

As the size of a line pattern decreases, the central intensity of the image increases. Consequently, the contrast of the image will usually deteriorate, as the line pattern becomes finer. The experiment was repeated for a mask opening of  $6\ \mu\text{m}$ . The results



depicted in Figure 2.10 (a)-(e) are similar to those obtained for the 10  $\mu\text{m}$  opening. The profile of the ridge waveguide in cross-section evidently depends on the exposure time and not on the lateral dimensions of the mask opening at this scale of line.

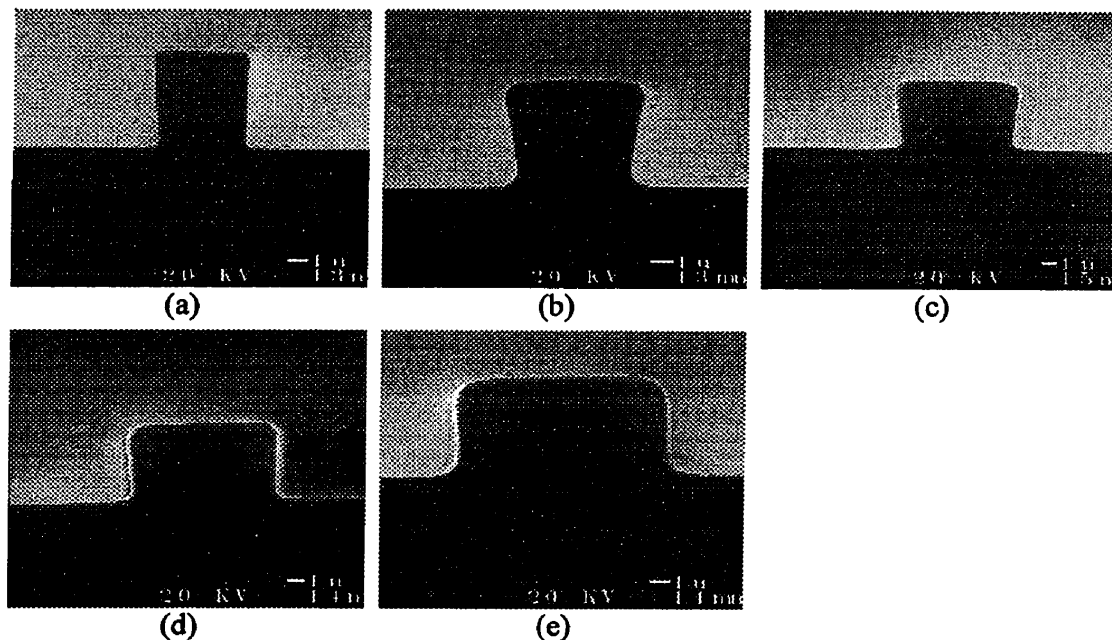


Figure 2.10 SEM image of ridge waveguide cross section (nominal composition 85  $\text{SiO}_2$ -15  $\text{Al}_2\text{O}_3$ ) as function of exposure time: (a) 5 sec., (b) 10 sec., (c) 30 sec., (d) 120 sec. and (e) 900 sec. Mask opening = 6  $\mu\text{m}$ .

To obtain characteristic curves of the organoaluminosilicate, we determined the thickness after development for given exposure and contrast,<sup>8-11</sup>  $\gamma$ , as follows:

$$H = H_0 - \gamma \cdot \ln(E_0 / E) \quad (2.1)$$

In this equation,  $E$  is the exposure energy at given time, as defined by  $E=I \cdot t$ , where  $t$  is the exposure time and  $I$  is the UV-light intensity at the wafer plane surface.  $E_0$  is the energy above which the *polyglass* photosensitive film is completely removed, and  $H_0$  is the thickness of the film belonging to  $E_0$ . Figure 2.11 was obtained by fixing the UV-

light intensity,  $I$ , throughout the process. After a given time, the latent image was exposed by propanol wet-etching, and the thickness of the relief structure defined as  $H/H_0$  was quantified by SEM. For the organoaluminosilicate, the corresponding contrast factor is  $\gamma = 0.11$ .

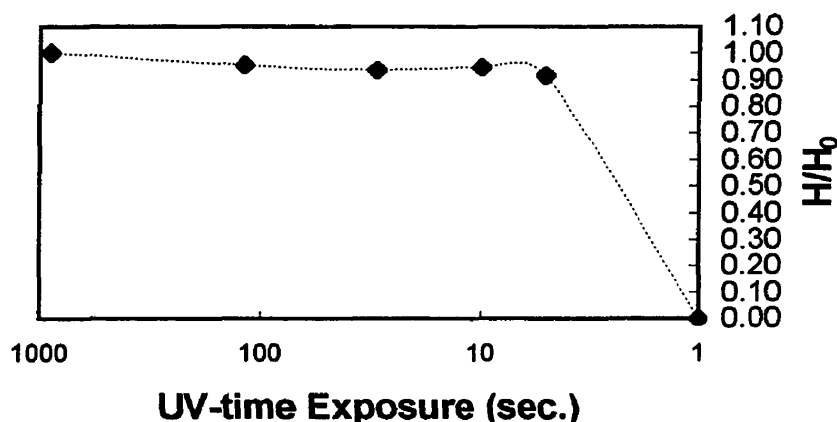


Figure 2.11 Characteristic curve for the hybrid organoaluminosilicate section (nominal composition 85 SiO<sub>2</sub>-15 Al<sub>2</sub>O<sub>3</sub>) showing the ratio  $H/H_0$  as function of exposure time. The exposure time is plotted on a logarithmic scale.

When the mushroom-like shape of a *polyglass* ridge waveguide is expressed as the ratio of maximum and minimum width of the cross section,  $W_{\max}/W_{\min}$ , we observe two conditions under which a rectangular shaped waveguide appears. Figure 2.12 shows that the ratio reaches unity (rectangular shape) after 5 seconds and then again after 100 sec. of UV-light exposure. At 10 seconds, waveguides from the 6 and 10  $\mu\text{m}$  feature mask openings show an increase in  $W_{\max}/W_{\min}$ . The curves in each case track one another. Referring back to Figs. 2.9 and 2.10, we observe that the greatest undercutting occurs as shown in Figure (b) for a 10 sec. exposure time. Afterwards, both the top and bottom dimensions increase, until (Fig. 2.12) roughly vertical sidewalls are obtained again after about 120 seconds. However, Fig. 2.12 says nothing about the quality of the waveguide sidewalls, edges, or the degree to which the relief structure conforms to the

dimensions of the mask openings. We surmise that the ridge waveguides may evolve as follows. When nominally collimated UV-light passes through the opening mask it initiates crosslinking by polymerizing organic monomer in the gel layer. UV light is attenuated roughly exponentially away from the surface. This is due to light absorption by the photoinitiator and the monomer. Therefore, the highest degree of polymerization will occur near the top surface of the film. Figures 2.9(a) and 2.10(a) suggest that crosslinking is sufficient (not necessarily complete) from top to bottom within 5 seconds of exposure, despite partial attenuation of the light. However, proximity effects (diffraction) do not permit the lateral dimension of the mask opening to be faithfully reproduced. As time progresses (Figures 2.9(b) and 2.10(b)), the top surface of the film grows laterally, approaching the mask opening dimensions. This occurs because polymerization of the acrylate monomer attached to silicon in MAPTMS is not spatially confined – diffracted and scattered light and structural relaxations caused by the reduction in non-bonded to covalent C-C bond linkages, all contribute to delocalizing the polymerization process that increases the crosslink density and reduces solubility. If most of the intensity is located in the center of the mask line and at the top of the film, a wedge shape or mushroom-like profile can result. With time, rays diffracted from the edge openings and passing through to the bottom of the film will convert unreacted monomer to crosslinked species. Accordingly, the bottom dimension will gradually evolve to match the top dimension as the source of polymerizable monomer is exhausted.

The extent of acrylate monomer polymerization in the film thickness depends on the total thickness of the film. Hence it is necessary to induce the right dose of UV-light to polymerize the film from top to bottom. The broadening of the waveguide is defined as  $\Delta W = W_{\max} - W_0$ , where  $W_{\max}$  is maximum waveguide width and  $W_0$  is the mask opening width. It is a measure of the linewidth control, which is key to reproducible device fabrication. Figure 2.13 shows that there is no broadening at 10 sec. UV-light exposure, regardless of the width of the opening of the mask feature.

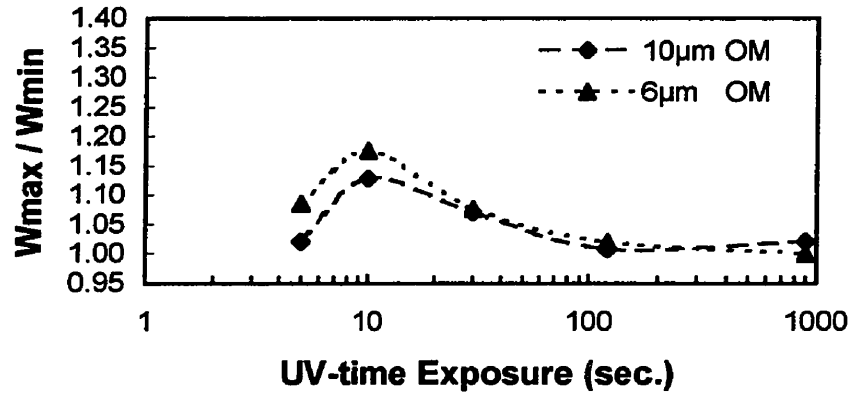


Figure 2.12 variation of  $W_{\max}/W_{\min}$  as function of exposure dose.  $W_{\max}$  and  $W_{\min}$  are the maximum and minimum width of waveguide cross-section, respectively.

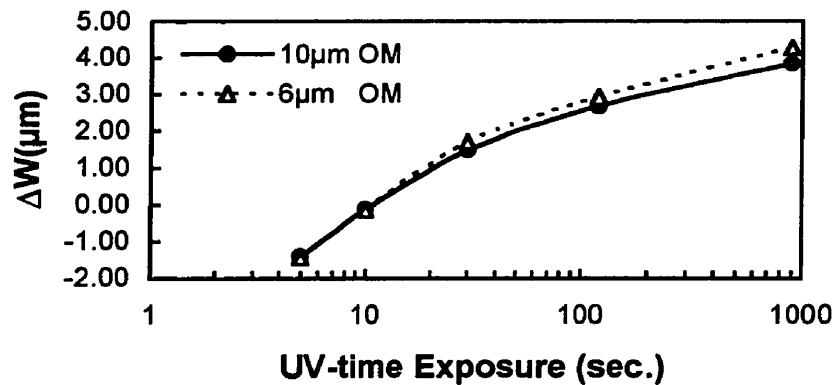


Figure 2.13 Variation of  $\Delta W (=W_{\max}-W_0)$  as function of exposure dose.  $W_{\max}$  is the maximum width for waveguides cross-section and  $W_0$  is the opening mask feature width.

A second variant of *polyglass* was made by condensing isobutoxyaluminoxytriethoxylane and trimethyl-phosphate ( $O=P(CH_3)_3$ ). MAPTMS was included as the photoactive ingredient. Trimethylphosphate gives excellent film-forming properties, and the product is highly soluble in organic solvents. Ridge waveguides were obtained in the same manner as described above. This composition

was found to be more sensitive to UV-light (minimal radiation dose to change film solubility) for the same quantity of photoinitiator and MAPTMS. The results of a study of the effects of varying the exposure time under fixed conditions of UV intensity and identical mask openings are collected in Figures 2.14 and 2.15.

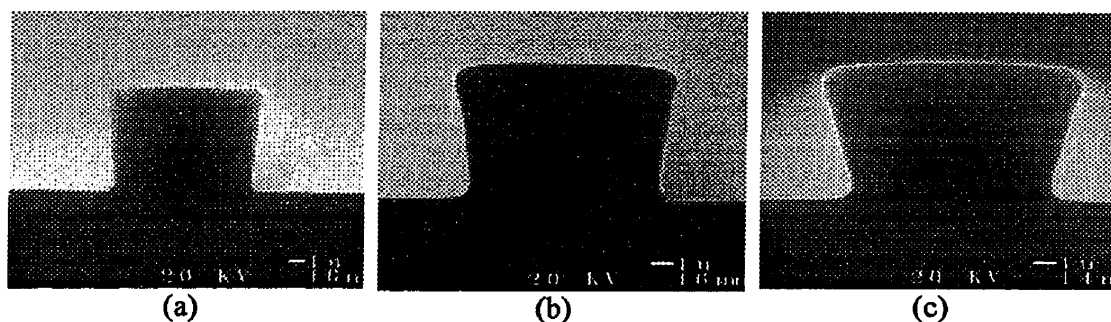


Figure 2.14 SEM image of ridge waveguide cross section (nominal composition 86  $\text{SiO}_2$ -7  $\text{Al}_2\text{O}_3$ -7  $\text{P}_2\text{O}_5$ ) as function of exposure time: (a) 3 sec., (b) 5 sec., and (c) 10 sec. Mask opening = 10  $\mu\text{m}$ .

Figure 2.15 (a)-(c) shows the same effect for the same exposure time when the opening mask is 6  $\mu\text{m}$  wide. Again we note the appearance of the undercutting of the waveguide relief.

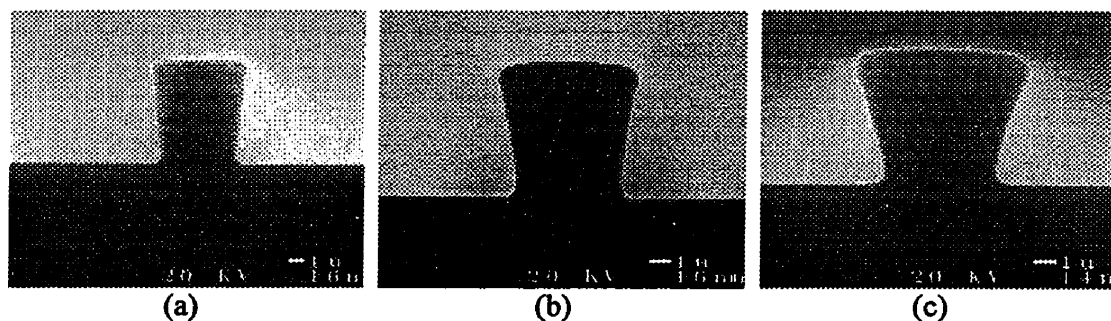


Figure 2.15 SEM image of ridge waveguide cross section (nominal composition 86  $\text{SiO}_2$ -7  $\text{Al}_2\text{O}_3$ -7  $\text{P}_2\text{O}_5$ ) as function of exposure time: (a) 3 sec., (b) 5 sec., and (c) 10 sec. Mask opening = 6  $\mu\text{m}$ .

As depicted in the characteristic curve for this sample in Figure 2.16, the slope at early time rises more steeply than that of the aluminosilicate without the phosphate. The contrast higher at  $\gamma = 0.23$ , and the film is qualitatively more sensitive to radiation crosslinking.

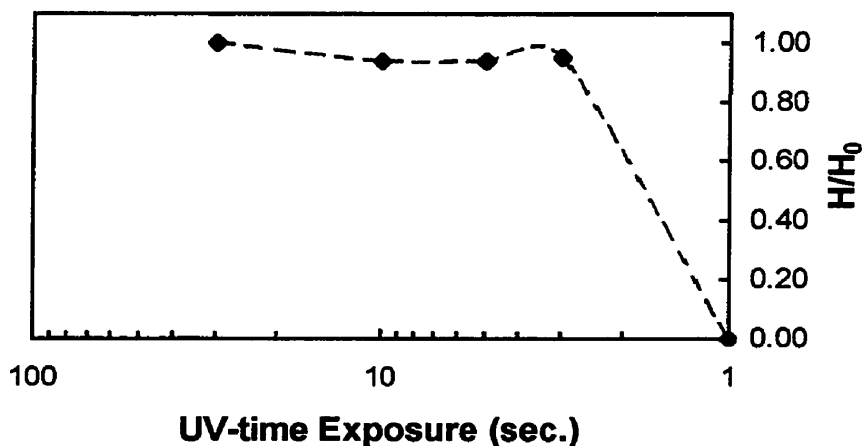


Figure 2.16 Characteristic curve for aluminophosphate silica, showing the ratio  $H/H_0$  as function of exposure time. The exposure time is plotted on a logarithmic scale.

Figure 2.17 shows that the variation in the ratio,  $W_{\max}/W_{\min}$ , qualitatively mirrors that of hybrid glasses that do not contain phosphate (compare Figure 2.12). The difference between the mask opening dimension and the lateral dimension of the ridge waveguide is plotted in Figure 2.18. We observe that for 5 sec exposure, one can replicate the mask opening; however, this occurs with loss of control over the vertical profile of the sidewalls (cf. undercutting in Figures 2.14(b) and 2.15(b)).

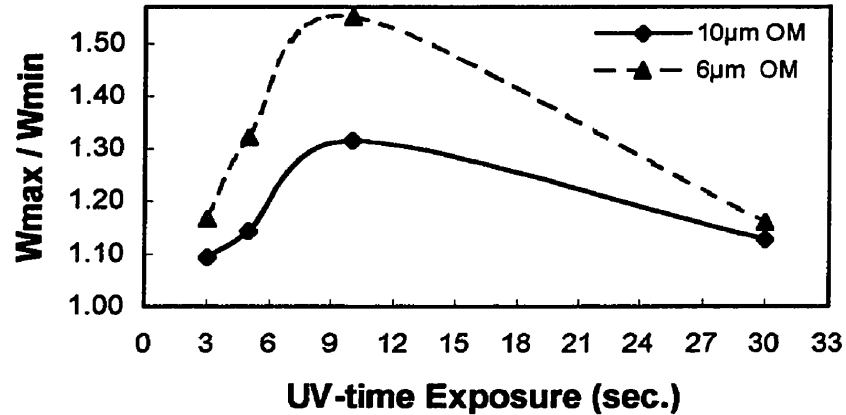


Figure 2.17 Variation of  $W_{\max}/W_{\min}$  as function of exposure dose.  $W_{\max}$  and  $W_{\min}$  are maximum and minimum width of waveguide cross-section, respectively.

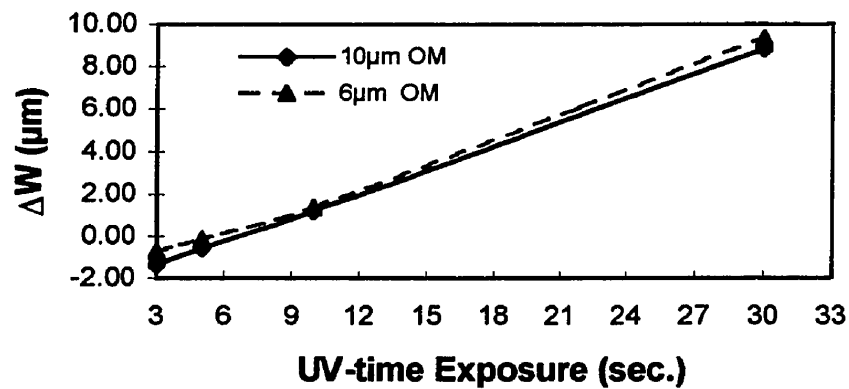


Figure 2.18 Variation of  $\Delta W (=W_{\max}-W_0)$  as function of exposure dose.  $W_{\max}$  is the maximum width for waveguides cross-section and  $W_0$  is the mask width opening.

#### 2.2.4. Atomic Force Microscopy

Polycondensation of the main group alkoxide is accompanied by shrinkage of the gel as the network densifies. Shrinkage and densification continue with postbaking, and upon photopolymerization of the acrylate monomer. The latter effect shows up

dramatically in atomic force microscopy images of the two hybrid glasses discussed in this paper. Figure 2.19 for the organoaluminophosphate glass, shows that the region exposed to UV light through the mask is depressed relative to the surrounding matrix of glass that had not been exposed. A balance between stress and strain fields in the matrix likely causes this. As we have discussed elsewhere<sup>12</sup>, polymerization of the acrylate moieties in the network gel phase film causes a cascade of reactions. The overall effect is to “photo-sinter” the matrix. This phenomenon raises the refractive index of the material by densification. We can offer a simple picture of constrained densification that might account for the depression observed by AFM in the film surface. When a densified region of glass flanked by undensified glass is allowed to relax, the densified region develops tensile stress. This region is bounded by compressive stress in the undensified region. Densification should be greatest nearest the surface of the glass where there is least constraint, with the result that the bounding glass should pull outward on the densified glass, and a depression should appear where the sample has been irradiated through the mask. Figure 2.20 shows how film shrinkage evolves with UV exposure time

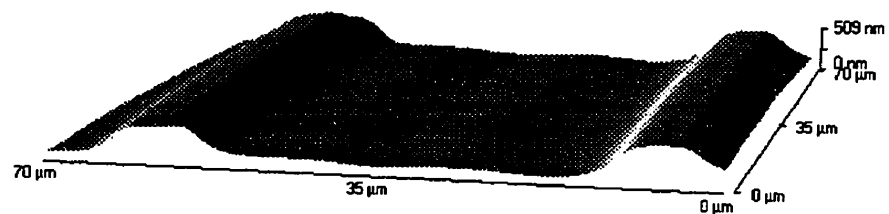


Figure 2.19 Atomic Force Microscopy (AFM) 3-D view of the surface relief waveguide inscribed in an organoaluminophosphate *polyglass* film. The depressed region distinguishes the densified waveguide structure from the surrounding matrix that has not been exposed to UV light.



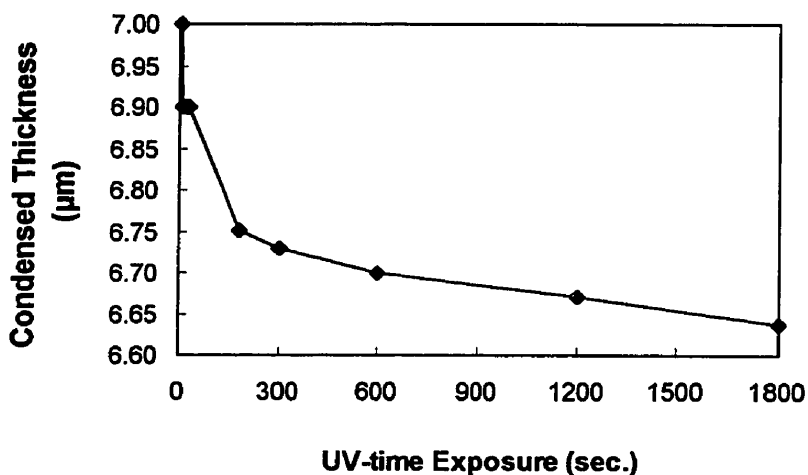


Figure 2.20 Variation in organoaluminophosphate *polyglass* film thickness as function of exposure time.

### 2.2.5. Conclusions

Specific hybrid organic-inorganic glasses were examined for their potential for making planar lightwave circuits by direct photolithography. These initial studies focused on the quality of ridge waveguides produced by combinations of UV light exposure time and solvent wet etching. Characteristic curves were developed to draw relationships between UV exposure time and the ability of the photolithography process to replicate mask dimensions. These early results suggest a complex relationship between the photopolymerization event, structural relaxations in the matrix, and the relief features obtained after wet etching. These effects are compounded with the usual effects (proximity effects) introduced by photolithography through a mask. Photoinduced polymerization is accompanied by shrinkage in the plane of the film. This effect is imaged by proximal probe microscopy. A balance of stress and strain fields is suggested as the source of the surface topography.

### 2.2.6. Acknowledgments

This work was funded in part by research grants from Natural Sciences and Engineering Research Council of Canada and the National Research Council, Ottawa, Canada.

### 2.2.7. References

1. R. Sara, T. Touam, C. Blanchetiere, Z. Saddiki, K. Saravanamuttu, X. M. Du, J. Chrostowski, M. P. Andrews and S. Iraj Najafi, "Photolithography fabrication of Sol-Gel Ridge Waveguide", Proceedings of SPIE, *Conference on Organic-Inorganic Hybrid Materials for Photonics*, Vol. 3469, Sans Diego, July 1998, 118-123.
2. S. I. Najafi, T. Touam, R. Sara, M. P. Andrews and M. A. Farded, "Sol-gel glass waveguide, and grating on silicon", *Journal of Lightwave Technology*, Vol. 16, No. 9, September 1998, 1640-1646.
3. R. Sara, T. Touam, M. P. Andrews and S. Iraj Najafi, " Polyglass Integrated Photonics Devices", Proceedings of SPIE, *Conference on Organic-Inorganic Hybrid Materials for Photonics*, Vol. 3469, Sans Diego, July 1998, 51-53.
4. R. Sara, T. Touam, P. Coudray, M. P. Andrews, S. Iraj Najafi, "*Polyglass* Integrated Optics Devices for Lightwave Communication", Proceedings of SPIE, *Conference on Organic-Inorganic Hybrid Materials for Photonics*, Vol. 3469, Sans Diego, July 1998, 44-50.
5. X. M. Du, T. Touam, L. Degachi, J. L. Guilbault, M. P. Andrews, and S. I. Najafi, "Sol-gel Waveguide Fabrication Parameters: An Experimental Investigation", *Optical Engineering*, Vol. 37, No. 4, April 1998, 1101-1104.
6. T. Touam, G. Milova, Z. Saddiki, M. A. Fardad, M. P. Andrews, J. Chrostowski, and S. Iraj Najafi, " Organoaluminophosphate Sol-gel Silica Glass Thin Films for Integrated Optics", *Thin Solid Films* 307, (1997), 203-207

7. C. Y. Li, J. Chicham, M. P. Andrews, S. I. Najafi, J. D. Mackenzie, N. Peyghambarian, "Sol-Gel Integrated Optics Coupler by Ultra-Violet Light Imprinting", *Electronics Let.*, Vol. 31, 271, February 1995.
8. P. Rai-Choudhury, Handbook of Microlithography, Micromachining, and Microfabrication, vol. 1: Microlithography, *SPIE Optical Engineering Press*, 1997, 17-45.
9. Wehrmann and G. Goodwin, "Photoresist Process Optimization and Control Using Image Contrast", *KTI microelectronics seminar*, 1989, 279-292.
10. S. V. Babv and S Srinivasan, "Optical Density and Contrast of Positive Resist", *Spie Vol. 539*, 1985, 36-46.
11. P. Spragg, R. Hurditch, M. Toukhy, J. Helbert and S. Malhotra, "The Reliability of Contrast and Dissolution Rate-derived Parameters as Predictors of Photoresist Performance", *Spie vol. 1466*, 283-289.
12. M. P. Andrews, K. Saravanamuttu, T. Touam, R. Sara, X. M. Du, S. I. Najafi, "Collateral Densification Associated with the Photoresponse of Hybrid Sol-gel Glasses for Depositing Bragg Grating on Ridge Waveguide", *Proc. SPIE*, Vol. 3290, 1998.

Suite à cette étude (chap. II) et moyennant les abaques d'indice et d'épaisseur, des composants photoniques pour la télécommunication ont été conçus et réalisés. La conception des filtres spectraux et du multi/démultiplexeur de longueurs d'ondes est basée sur la théorie scalaire des modes couplées.

Tout les paramètres de la structure du guide d'ondes (indices de réfractions et dimensions du coeur) ont été déduits des abaques. Ces paramètres ont servi ensuite de données à la simulation par BPM (*Beam Propagation Method*) pour optimiser la longueur et la séparation du coupleur et la différence de phases pour les filtres (interféromètre de Mach-Zehnder). Aussi, ces paramètres ont servi à optimiser la réflectivité, la longueur et le pas d'un réseau de Bragg en se basant sur la théorie vectorielle des modes couplées. Finalement, la théorie de la diffraction

bidimensionnelle a servi à optimiser la cercle de Rowland, la longueur du guide d'ondes à raccord progressif (*Taper Waveguide*), la séparation entre les portes et le nombre de portes d'un coupleur en étoile (*Star Coupler*). Les résultats sont rapportés dans le chapitre III sous forme d'articles, dont le texte est en anglais:

- *Polyglass Integrated Optics Devices for Lightwave Communication* est publié dans le Proceedings of SPIE, *Conference on Organic-Inorganic Hybrid Materials for Photonics*, vol. 3469, Juillet 1998, 44-50. Les auteurs sont R. Sara, T. Touam, P. Coudray, M. P. Andrews et S. I. Najafi.
- *Sol-Gel Glass Waveguide and Grating on Silicon* est publié dans le *Journal of Lightwave Technology*, vol. 16, no.9, septembre 1998, 1640-1646. Les auteurs sont S. I. Najafi, T. Touam, R. Sara, M. P. Andrews, et M. A. Fardad.
- *Sol-gel Integrated Optics Devices: Star Coupler and Dense WDM*, est à paraître dans le *International Conference on Integrated Optics & Optical Fiber Communications*, February 1999, San Diego. Les auteurs sont R. Sara, T. Touam, M. P. Andrews et S. I. Najafi.

## CHAPITRE III: COMPOSANT PHOTONIQUE POUR LA TELECOMMUNICATION

### 3.3. *Polyglass* Integrated Optics Devices for Lightwave Communication

#### 3.3.1. Abstract

The lightwave communication technology is experiencing tremendous growth in the volume and flow of information. Spectral discrimination filtering, wavelength division multiplexing and dense wavelength division multiplexing are making it possible. The high refractive index modulation and design flexibility of *Polyglass* material makes it very attractive to produce such devices.

**Keywords:** Integrated optics, spectral discrimination filter, wavelength division multiplexer, dense wavelength division multiplexer, star coupler, lightwave communication, data communication, computer network.

#### 3.3.2. Introduction

Some signal analysis require spectral discrimination filters (SDF). For instance, the filters that treat discretely a particular wavelength are of great importance in lightwave communication. Other links use wavelength division technology (WDM) where information is transmitted over multiple channels.

The demand for higher transmission rate and volume may be ensured by increasing the volume of information and by using dense wavelength division multiplexing (DWDM) where each wavelength carries its bundle of information. The large bandwidth of erbium doped waveguide amplifier (EDWA) enables integration with DWDM for higher integrated transmission systems.<sup>1</sup> This paper describes a method of fabrication and characterization of high performance spectral filters, WDMs and star couplers. Pinhole and crack free long devices are obtained using *polyglass* technology.<sup>2-5</sup>

### 3.3.3. SDF Design and performance

The SDF diagnostic is based on signal discrimination using wavelength pattern analysis. The larger the finesse of the filter, calculated as the ratio of the separation between the spectral peaks of the filter to the bandwidth of the peaks, the narrower and more widely separated are the spectral peaks. Two approaches are used to design SDF for 1.55  $\mu\text{m}$  wavelength applications.

*Non-symmetric Mach Zehnder Interferometers (MZI)*-The signal to be filtered is split equally between the two interferometer arms (see Fig. 3.1.). The path length difference of the interferometer arms,  $\Delta L$ , induces phase shift between the propagated light in the two arms.<sup>6,7</sup> The output signal spectrum depends on this path difference.

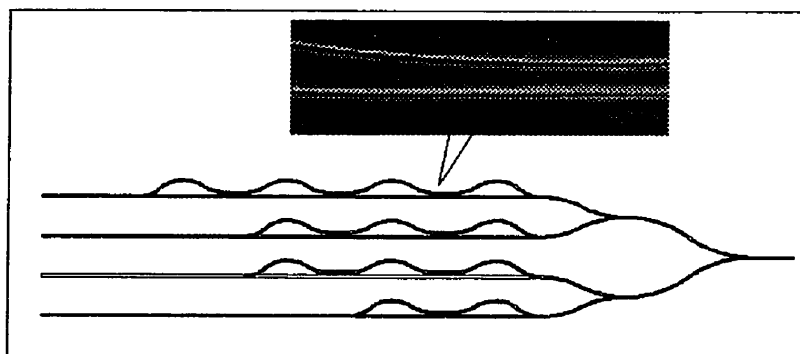


Figure 3.1 Mask pattern of the Mach-Zehnder filter.

The chosen waveguide structure (see Fig. 3.2) manifests low propagation losses.<sup>8</sup> The photosensitive layer is buried between buffer and cladding layers. After pre-bake, this structure is exposed to UV-light through an opening pattern in dark-field contact mask.<sup>5</sup> After 5 min exposure the refractive index increase with respect to the unexposed region is approximately  $\Delta n = 0.015$ . The post-bake at 120  $^{\circ}\text{C}$  during 30 minute densifies and stabilizes the structure.

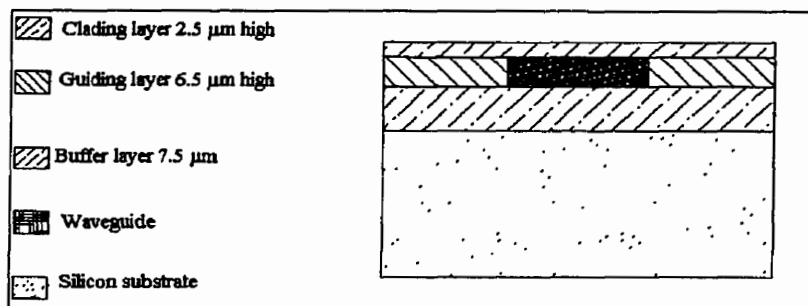


Figure 3.2 Cross section of the SDF waveguide structure.

Signal from a tunable Er-doped fiber laser operating at 1.55  $\mu\text{m}$  is coupled, by a single mode fiber, into the SDF input. The output signal is collected by a multimode fiber, which is connected, to an optical spectrum analyzer (OSA). The resultant response is shown in Fig. 3.3.

*Wavelength division multiplexer (WDM)*-The light signal is treated by 4 WDMs where all of their device parameters are similar except the straight coupling length. The 3-dB splitter divides equally the signal into the 4 WDM inputs as shown in Fig. 3.4.

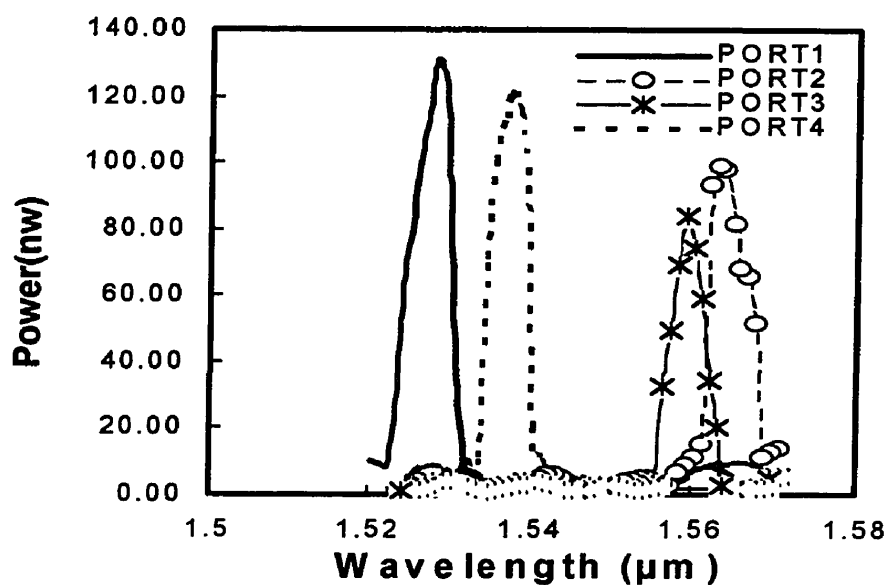


Figure 3.3 Response signal obtained from the four outputs of the MZI filter.

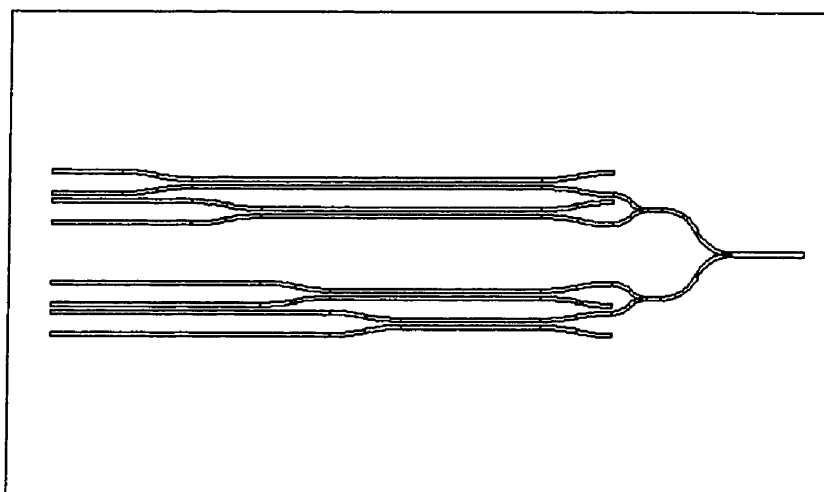


Figure 3.4 Mask pattern of directional coupler filter.

The waveguide configuration is identical to the previous one (see Fig. 3.2.).

Fig.3.5 shows that the surface of the fabricated device is pinhole and crack free.



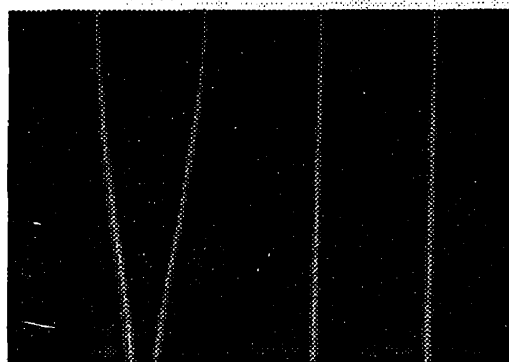
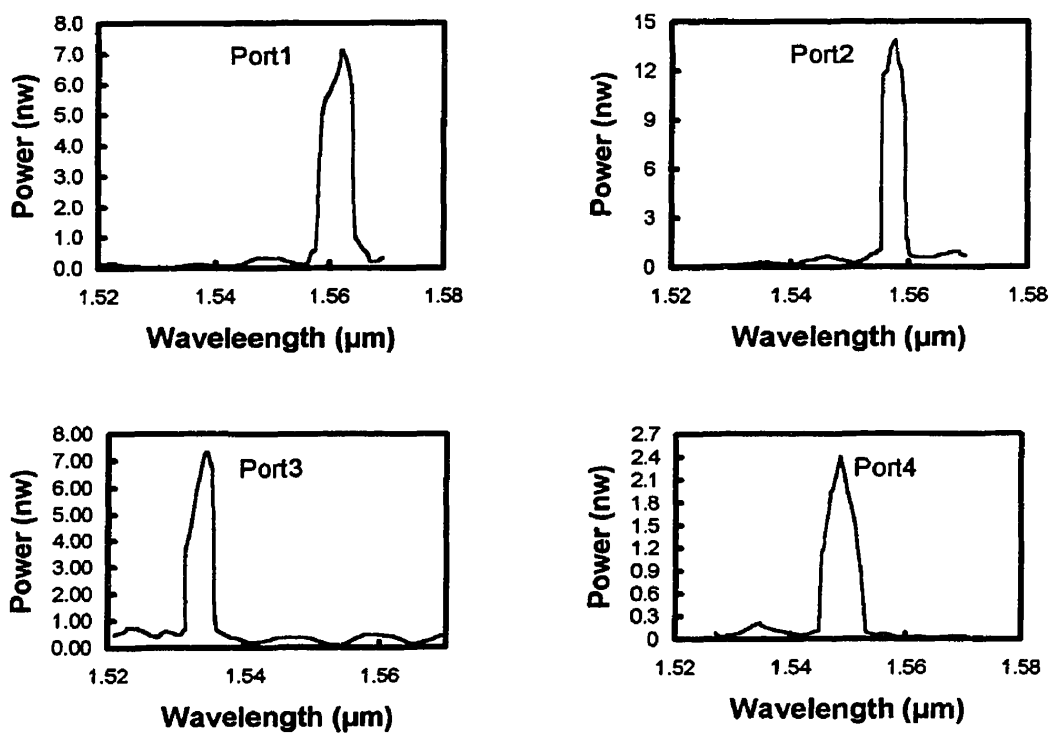


Figure 3.5 Optical micrograph of directional coupler.

Using the method described above the output signal spectrum from each channel is measured and is summarized in Fig. 3.6.



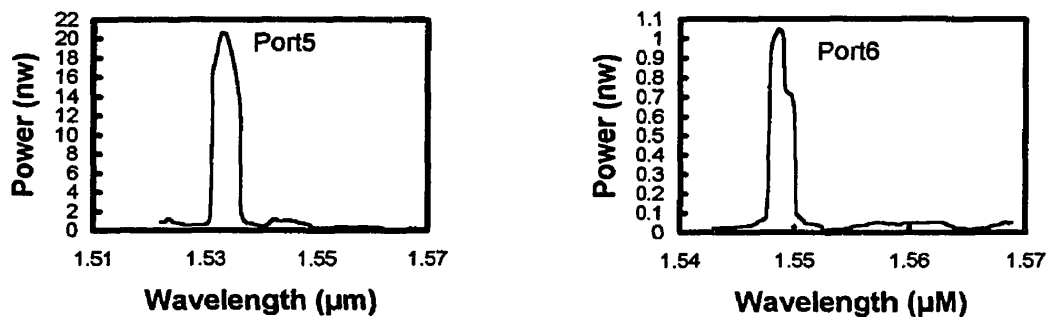


Figure 3.6. Output signal obtained from the six outputs of the directional coupler filter.

### 3.1.4. 1.55 $\mu\text{m}$ / 1.3 $\mu\text{m}$ and 1.55 $\mu\text{m}$ / 0.98 $\mu\text{m}$ WDM

Surface waveguides with dimensions and refractive indices closely matching that of single mode optical fiber are used to design and produce dual wavelength WDMs.<sup>9</sup>

Fig.3.7 depicts schematically the device structure. The 9.73  $\mu\text{m}$  thick *polyglass* film is deposited in a single step by spin coating on silicon substrate. The waveguides are 6  $\mu\text{m}$  high and 5  $\mu\text{m}$  wide.

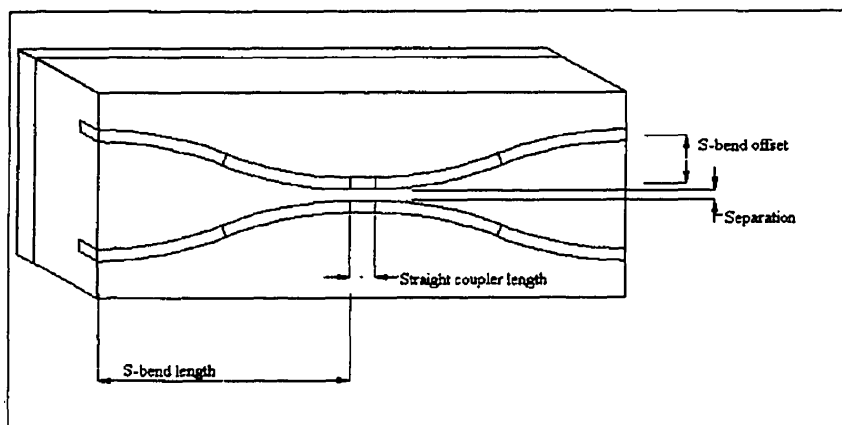


Figure 3.7 Schematic diagram of the WDM coupler and its waveguide structure.

Table 3.1 summarizes other parameters of the fabricated coupler WDMs. The calculated crosstalk is -13.34 dB for WDM2 and -32.93 dB for WDM3.<sup>6</sup>

Table 3.1: Parameters of dual wavelength coupler WDMs

WDM $\lambda_1/\lambda_2$ ( $\mu\text{m}$ )	Axial separa- tion ( $\mu\text{m}$ )	Straight coupler length ( $\mu\text{m}$ )	Calcula- ted crosstalk (dB)	Measured crosstalk (dB)
1 (1.55/0.98)	8	3900	-22.34	-13.78
2 (1.55/1.3)	9	2900	-13.34	-12.29
3 (1.55/1.3)	10	5450	-32.93	-17.19

WDM $\lambda_1/\lambda_2$ ( $\mu\text{m}$ )	S-bend length ( $\mu\text{m}$ )	S-bend offset ( $\mu\text{m}$ )
1 (1.55/0.98)	3000	125
2 (1.55/1.3)	3000	125
3 (1.55/1.3)	3000	125

### 3.3.4. Star Coupler

A 17x31 star coupler (see Fig. 3.8) is designed and produced using surface *polyglass* waveguides.<sup>10</sup> The total device length is 1.74 cm. The Rowland circle limiting slab waveguides are optimized to ensure that any element of the output array receive the same power when any of the input waveguides are excited.<sup>11</sup>

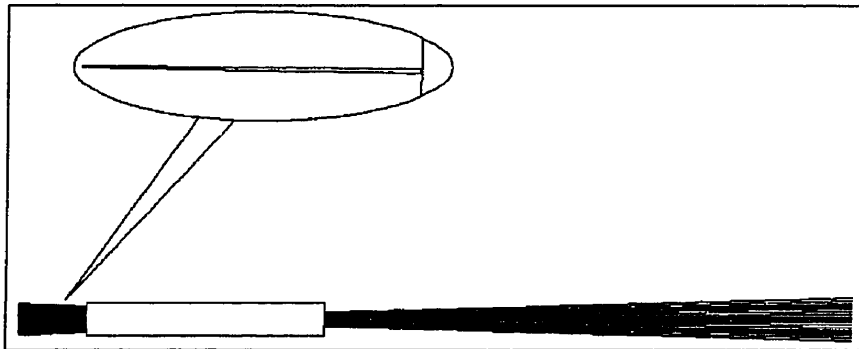


Figure 3.8 Mask pattern of the star coupler.

Figure 3.9 compares transmitted power from 31 output ports when input waveguide number 9 is excited.

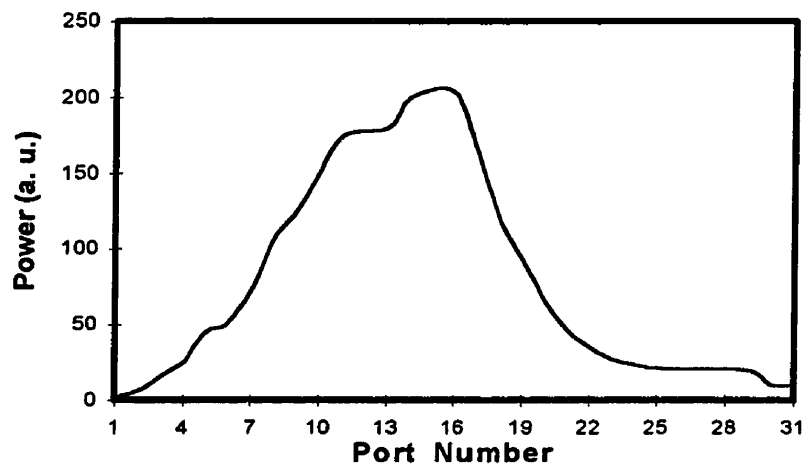


Figure 3.9 Star coupler output when light at  $\lambda=1.55 \mu\text{m}$  is coupled into the input waveguide number 9.

### 3.3.5. Acknowledgments

This work was funded in part by research grants from NSERC and NRC .

### 3.3.6. References

1. D. Barbier, M. Rattay, F. Sain Andre, G. Clauss, M. Trouillon, A. Kevorkain. J.-M. P. Delavaux, and E. Murphy, "Amplifying Four-Wavelength Combiner, Based on Erbium/Ytterbium-Doped Waveguide Amplifiers and Integrated Splitters", *IEEE Photonics Techn. Let.*, Vol. 9, No. 3, March 1997
2. Fardad, T. Touam, P. Meshkinfam, R. Sara, X.M. Du, M.P. Andrews and S.I. Najafi, "UV-light imprinted Bragg grating in sol-gel ridge glass waveguide with almost 100% reflectivity", *Electronics Letters*, Vol. 33, 11069-1070, February 1997.
3. X. M. Du, T. Touam, L. Degachi, J.L. Guilbault, M. P. Andrews, and S.I. Najafi, "Sol-gel waveguide fabrication parameters: an experimental investigation", *Optical Engineering*, Vol. 37 No. 4, April 1998.
4. S. I. Najafi, T. Touam, R. Sara, M. P. Andrews and M. A. Farded, "Sol-gel glass waveguide, and grating on silicon", submitted for publication to *Journal of Lightwave Technology*.
5. C. Y. Li, J. Chicham, M. P. Andrews, S. I. Najafi, J. D. Mackenzie, N. Peyghambarian, "Sol-Gel Integrated Optics Coupler by Ultra-Violet light Imprinting", *Electronics Let.*, Vol. 31, 271, February 1995.
6. A. Tervonen, S. Honkanen, S. I. Najafi, "Analysis of symmetric coupler and asymmetric Mach-Zehnder interferometers as 1.3- and 1.55-  $\mu\text{m}$  dual-wavelength demultiplexers/multiplexers", *Optical Engineering*, Vol. 32, No.9, 2083, September 1993.
7. Y. Yan, R. J. Deri, M. Seto and R. J. Hawkins, "GaAs/GaAlAs Asymmetric Mach-Zehnder Demultiplexer with Reduced Polarization Dependence", *IEEE Photonics Techn. Let.*, Vol. 1, No. 4, April 1989
8. Coudray, Y. Moreau, P. Etienne and J. Porque, "New developments in integrated optics using slo-gel process", invited paper, *International Conference SPIE*, Critical Review n° 68, Sol-gel and Polymer Photonics Devices San Diego, USA, July 1997

9. P. L. Auger, S. I. Najafi, "New method to design directional coupler dual wavelength multi/demultiplexers with bends at both extremities", *Optics Communications*, 111, 43-50, 1994.
10. D. Dragone, "Efficient NxN Star Coupler Using Fourier Optics", *Journal of Lightwave Techn.*, Vol. 7, No. 3, March 1989.
11. C. Dragone, C. H. Henry, I. P. Kaminow and R. C. Kistler, "Efficient Multichannel Integrated Optics Star Coupler on Silicon", *IEEE Photonics Techn. Let.*, Vol. 1, No. 8, August 1989.

### **3.4. Sol-gel glass Waveguide and Grating on Silicon**

#### **3.4.1. Abstract**

This paper reports on the fabrication and characterization of hybrid organic-inorganic glass sol-gel slab and channel waveguides by ultraviolet light imprinting in thin films deposited by a one-step dip-coating process. The adjustment of chemical composition of the materials provides precise selection of refractive index from 1.48 to 1.52 at the wavelength of 632.8 nm. The refractive index of the waveguides at 1.55  $\mu\text{m}$  is similar to that of optical fiber, thus reducing the reflection loss between the two to less than 0.01 dB. The effect of ultraviolet light exposure and heat treatment on waveguide refractive index is studied. Fabrication parameters to produce ridge waveguides are optimized to achieve very smooth side walls. Propagation losses in these waveguides are  $\sim 0.1$  dB/cm. Single mode buried waveguides, at 1.55  $\mu\text{m}$  wavelength, with circular mode profiles are demonstrated.

#### **3.4.2. Introduction and background**

Semiconductors, organic and inorganic dielectrics are the main material contenders for photonics.<sup>1</sup> Among these, glass integrated optics has attracted the attention of those materials scientists and photonics device engineers who seek to take advantage of its robustness, appealing optical properties, and compatibility with established silicon manufacturing protocols. The dominant techniques for fabricating glass integrated optics structures on silicon are flame hydrolysis deposition (FHD), chemical vapor deposition (CVD) and sol-gel processing.<sup>2</sup> At the present state-of-the-art, these are intrinsically high temperature methods because they invariably require a step to consolidate the glass (FHD, CVD, sol-gel) or to remove adventitious organic components (sol-gel). The sol-gel method is a compelling alternative to the first two because liquid solutions are coated rather simply onto surfaces by spinning or dipping. The capital costs are significantly lower for sol-gel processing, and the technique offers

an outstanding range of material properties and compositions that extend its capability to active devices for modulation, lasing and switching. This paper focuses on glasses and devices derived by *low temperature* sol-gel processing. The sol-gel method for integrated optics has been extensively reviewed,<sup>3,4</sup> where low temperature versions of the process have emerged with interesting potential by combining the attractive features of organic polymers with those of a silicate network. This organically modified glass fabric belongs to the class of hybrid organic-inorganic glasses known variously as “ormocers” (organically modified ceramics), “ormosils” (organically modified silicates), “ceramers”, “polycerams”, or simply hybrid sol-gel glasses (HSGG). We have investigated the HSGG approach to passive devices using direct photoinscription methods imported from the genre of techniques established for polymer lithography.<sup>5-13</sup> Our motivation has been to develop a rapid, direct photolithographic method to deposit planar, channel and ridge waveguides, gratings, power splitters and directional couplers at low temperatures (less than 200 °C), and to do so cheaply, with few steps and good reproducibility.

In our hands, optical devices can be rapidly prototyped with HSGG because 1) homogeneous thick films can be precision deposited, crack-free in a single step; 2) a large menu of organically modified materials can be synthesized in the laboratory to adapt quickly to specific device requirements; 3) HSGG materials can be strategically designed to take advantage of low cost alternatives to reactive ion etching, iterative rapid thermal annealing, reflow, and laser densification; and 4) HSGGs offer a singular advantage in being able to resolve conflicting material demands placed by device designers. The essence of this flexibility can be found in the coupling of the attractive features of organic polymers with those of inorganic glasses. In short, HSGG is a nimble material for photonics.

The present paper extends our investigations of photoinscribable hybrid sol-gel glasses to Bragg gratings in ridge waveguides on silicon. We examine several features related to the thermal and ultra-violet light processing of these glasses. The study



culminates in a demonstration and analysis of short length high reflectivity gratings imprinted by 193 nm radiation through a phase mask.

### 3.4.3. Hybrid sol-gel glass films

Sol-gel thin films were dip-coated on silicon substrates, which had a thermally grown SiO<sub>2</sub> layer on their surface. The refractive index of the sol-gel films was higher than that of SiO<sub>2</sub> and, therefore, the sol-gel films guided light as a slab waveguide. The guidance of light at HeNe laser wavelength, 0.6328 μm, was used to characterize the waveguides by prism coupling method<sup>14</sup>, and determine the refractive index and thickness of the films.

#### 3.4.3.1. Synthesis and fabrication

Two different sol compositions were prepared. In both cases, the photopolymerizable organosilicate framework was provided by methacryloxypropyltrimethoxysilane (MAPTMS). Composition A was based on the use of ZrO<sub>2</sub> as a refractive index modifier. The zirconium oxide was dispersed in the organosilicate matrix in the form of nanoscale inclusions much smaller than the wavelength of light. Homogeneous dispersion of ZrO<sub>2</sub> was assisted by hydrolyzing the Zr(OC<sub>3</sub>H<sub>7</sub>)<sub>4</sub> precursor with methacrylic acid in an 1:1 mole ratio. Composition B was prepared by co-hydrolysis of MAPTMS and isobutoxyaluminoxytriethoxysilane. Sols A and B were prepared as follows. MAPTMS was first hydrolyzed with 1.5 equivalents of H<sub>2</sub>O based on 0.1M HCl as the catalyst.

As required, either Zr(OC<sub>3</sub>H<sub>7</sub>)<sub>4</sub> or isobutoxyaluminoxytriethoxysilane in dried distilled isopropanol (1:1 volume ratio) was then added dropwise to the stirred solution of partially hydrolyzed MAPTMS. Sufficient equivalents of water were then added to hydrolyze the alkoxide substituents fully. Photoinitiator in the form of IRGACURE 184 (CIBA) was added to complete the preparation. Sols A and B were then aged at room temperature for 15 hours before films were precision dip-coated. Because

organically modified silicate glasses tolerate stress relaxation more effectively than do glasses derived from traditional silica sources, like tetraethoxyorthosilicate, slab waveguides could be fabricated in one step in thicknesses ranging from 2 to 10  $\mu\text{m}$ . After precision dip-coating, films derived from sol A were immediately heated (pre-baked) in air at 110  $^{\circ}\text{C}$  for 30 min., whereas those derived from sol B were heated to 95 $^{\circ}\text{C}$ . The pre-bake step is necessary to prevent gel contamination of the photomask used for ultra-violet light exposure.

The films were illuminated with uniform deep ultraviolet (UV) radiation (Oriel model 87000 system) through a fused silica photomask. This step induces free radical polymerization of the vinyl substituent on MAPTMS and promotes additional condensation and densification of the gel matrix, raising the refractive index of the host in those regions exposed to the radiation. A second heat treatment (post bake) at temperatures ranging from 130  $^{\circ}\text{C}$  to 160  $^{\circ}\text{C}$  was introduced to harden the films and further raise the refractive index.

#### 3.4.3.2. Characterization and results

The thicknesses of the thin films were selected such that the slab waveguides supported 2 to 5 modes at 0.6328  $\mu\text{m}$  wavelength. Film thickness,  $d$ , varies linearly with dip-coating speed<sup>13</sup>,  $V$ , and films with 2  $\mu\text{m}$  to 10  $\mu\text{m}$  thickness can be achieved in a single step. The thickness of the films used in the present work was 2  $\mu\text{m}$  to 2.5  $\mu\text{m}$ . Prism coupling method was employed to measure the precise thickness and refractive index of the films at  $\lambda=0.6328 \mu\text{m}$ .

Fig. 3.10a and 3.10b depict the dependence of the refractive index of the films with Zr and Al, respectively. In these experiments, 2  $\mu\text{m}$  thick films were exposed to UV-light for 2 min. and post baked at 150  $^{\circ}\text{C}$  for 5 h. The index of the hybrid organic-inorganic glass films are chemically and photochemically tunable from 1.485 to 1.520 for the A-type compositions (Fig. 3.10a) and from 1.485 and 1.497 for the aluminum containing composites (Fig. 3.10b). Curvature in the plots is not to be anticipated if the

refractive index changes were associated with the change in the Zr or Al content alone. Without UV-light exposure both films show the usual linear dependence of the refractive index on the concentration of the group 4 (Zr) and group 13 (Al) element

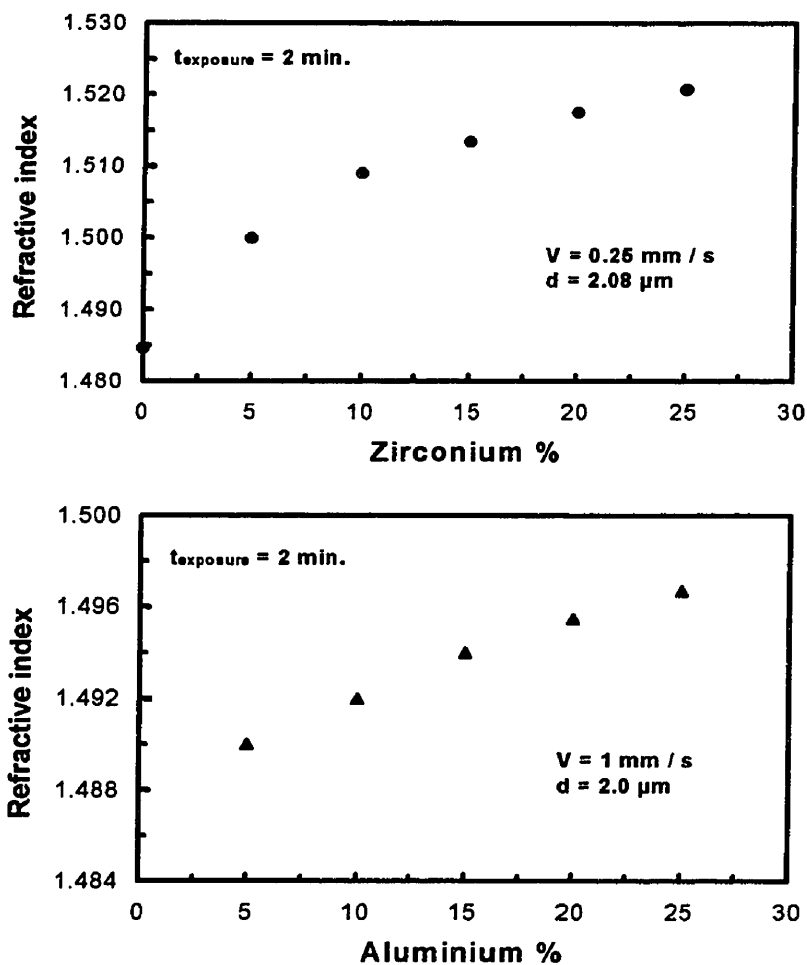


Figure 3.10 (a) Refractive index of zirconium-doped sol-gel glass films as a function of Zr concentration. Postbake temperature and time are 150 °C and 5 h respectively. UV-light exposure time is 2 min. (b) Same as (a) for aluminum-doped sol-gel.

On the other hand, the nonlinear dependence of  $n$  with transition or main group element content reflects the superposition of the refractive index change induced by UV-light polymerization.<sup>1</sup> The latter response is distinctly nonlinear.

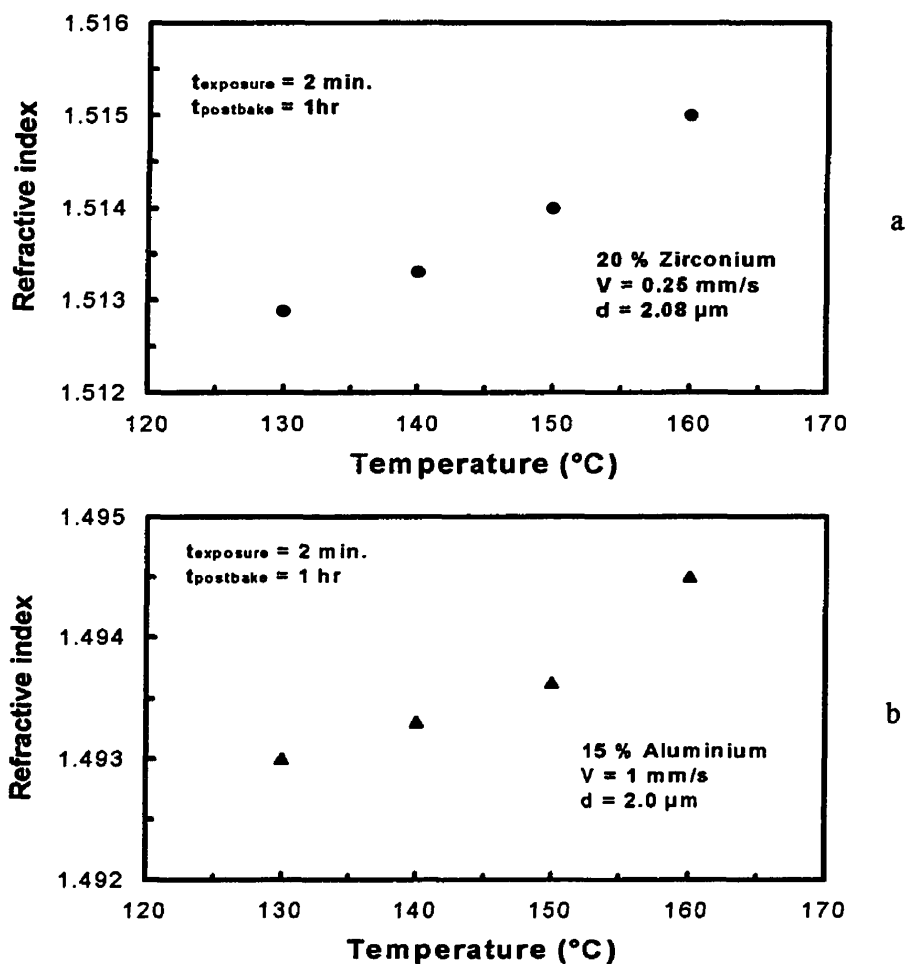


Figure 3.11 (a) refractive index of 20 mole% Zr sol-gel films as a function of postbake temperature. The films are exposed to UV-light for 2 min. (b) Similar to (a) for 15 mole% Al sol-gel films. Postbake time is 1h.

Figure 3.11 shows the variation in the refractive index for films of the two compositions. The films containing 20 mole %  $Zr^{4+}$  or 15 mole %  $Al^{3+}$  were exposed to

UV-light for 2 min and post baked at temperatures ranging from 130 °C to 160 °C for 1h

The refractive index of the  $Zr^{4+}$ -containing samples increased with temperature, reaching  $n = 1.150$  at 160 °C. For both compositions, the total change in refractive index with heating was almost the same, being approximately 0.002. This implies that heating causes additional densification of the gel films.

Figure 3.12a illustrates the variation of the sol-gel film refractive index with UV-light exposure time for films containing 20 mole %  $ZrO_2$ . Different UV-light exposure, post bake times and temperatures were used. A refractive index of 1.5105 was obtained for the type A film post baked at 130 °C for 1 h prior to UV-light exposure. After 20 min of UV exposure, the refractive index of the film increased by a net value of 0.006 (see Fig. 3.12b), and plateaued at 1.5111. Samples post baked at 150°C for 1 h had slightly higher refractive index, but  $\Delta n$  was unaffected by UV exposure.

Increasing the post bake time, increased the film refractive index, but decreased the refractive index difference  $\Delta n$  of UV-exposed compared with unexposed films deposited and processed under otherwise identical conditions. The maximum  $\Delta n$  for samples post baked at 150 °C for 5 h decreased to 0.003.

After 10 h post baking at this temperature,  $\Delta n$  dropped to zero, indicating that under certain conditions heating caused the films to evolve to the same final refractive index as did UV light exposure. The behavior of the type B compositions with  $Al^{3+}$  was qualitatively similar. In this case, the refractive index prior to irradiation was 1.4913. This value leveled off after about 10 min of irradiation (see Fig. 3.13).

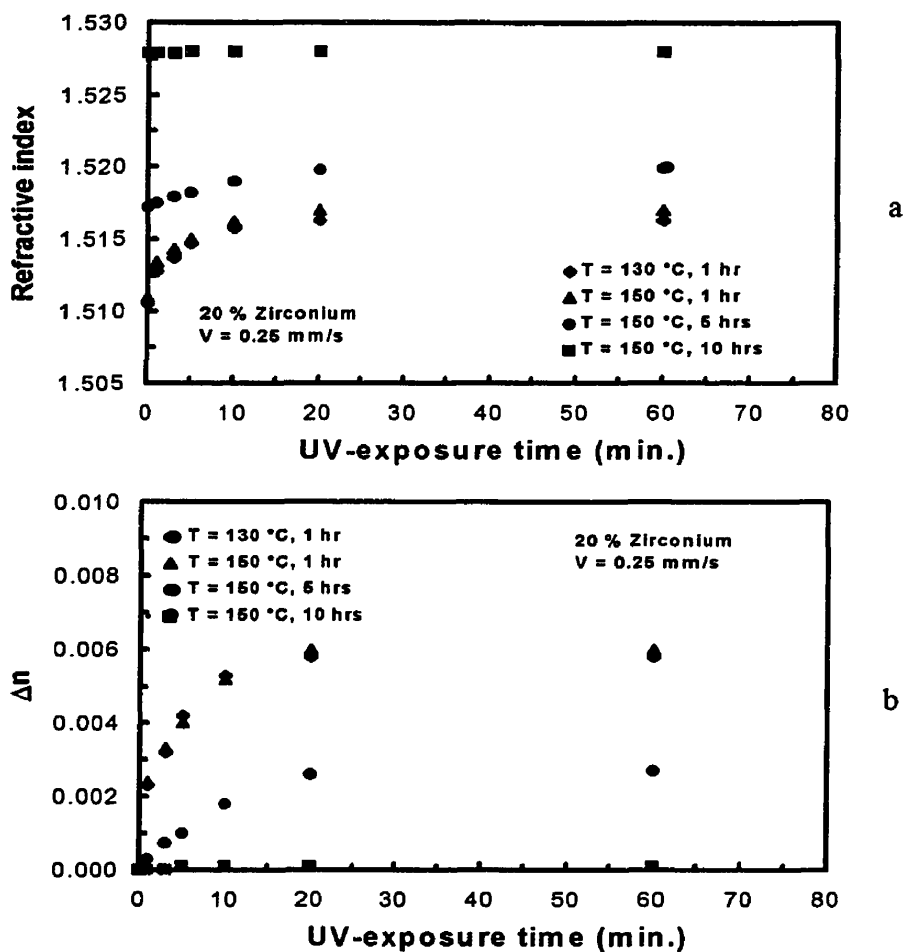


Figure 3.12 (a) Refractive index of 20 mole% Zr-doped sol-gel films as a function of UV-light exposure time for 130 and 150 °C postbake temperatures, and 1, 5 and 10 h postbake times. (b) Refractive index increase,  $\Delta n$ , as a function of UV-light exposure time for the same samples.

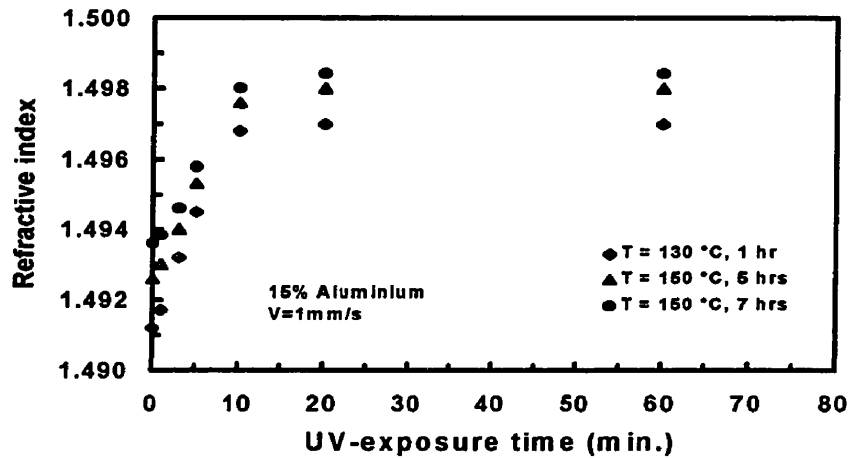


Figure 3.13 Similar to Fig. 3.12(a), but for 15 mole% Al-doped sol-gel films.

Refractive index of sol-gel waveguides were also measured at  $1.55 \mu\text{m}$  and will be discussed in section 4.

#### 3.4.4. Channel waveguides

A schematic of three different channel waveguides prepared by UV-light photoinscription is presented in Fig. 3.14. The (unclad) surface waveguide is made by UV-light photoinscription through a mask opening placed in direct contact with the gel film. The ridge waveguide is enunciated after UV exposure by an organic solvent wet etch process as described below. Overcoating the ridge waveguide with a hybrid organo-glass layer gives the buried waveguide. In Fig. 3.15 we show the  $1.55 \mu\text{m}$  mode profiles measured for the respective waveguides. As expected, the mode profiles of the surface and ridge waveguides in Figs. 3.15a and 3.15b are elliptical, whereas that of the buried waveguide is circular.

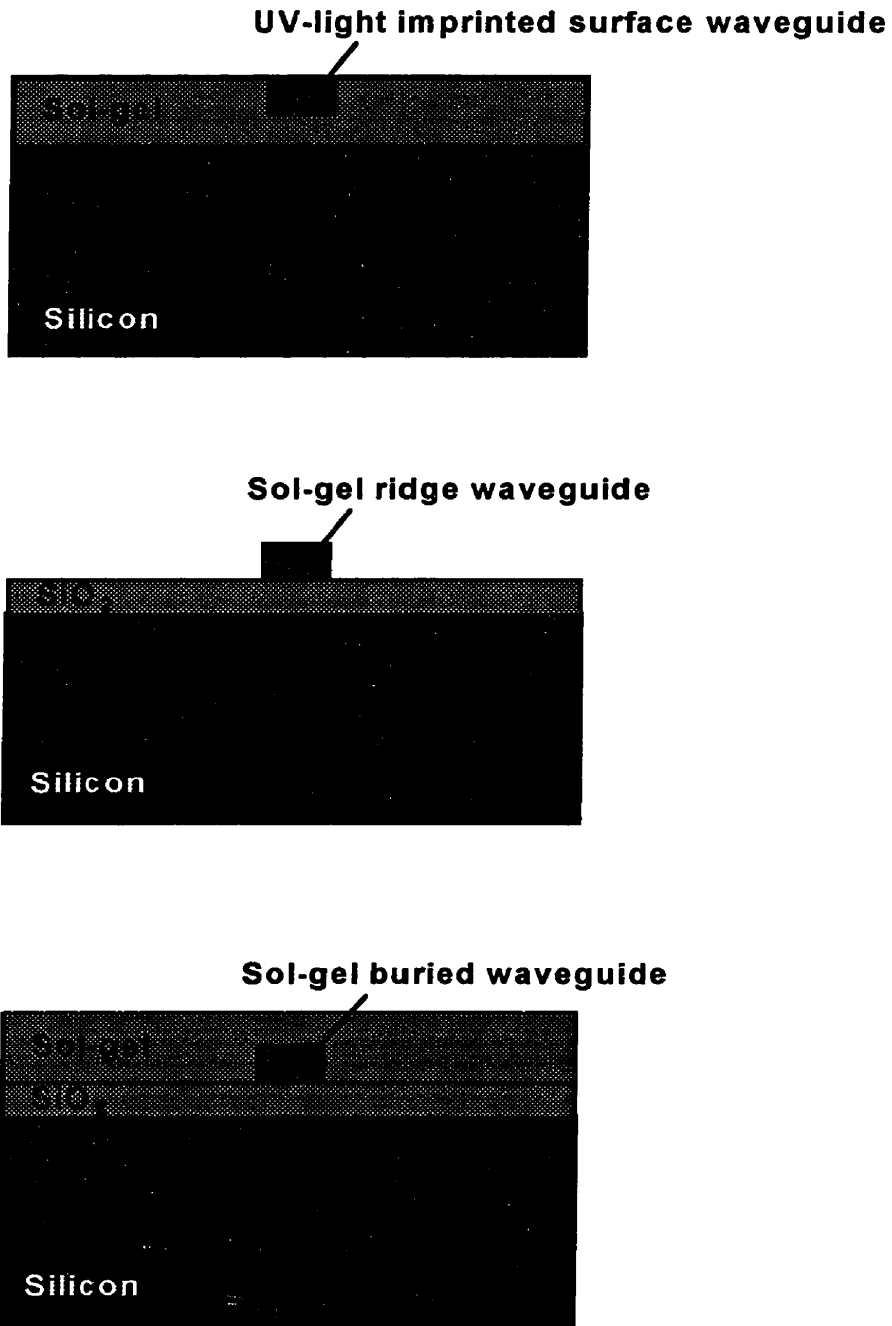


Figure 3.14 Schematic representation of different sol-gel glass channel waveguides on silicon. From top to bottom: surface, ridge and buried waveguides.



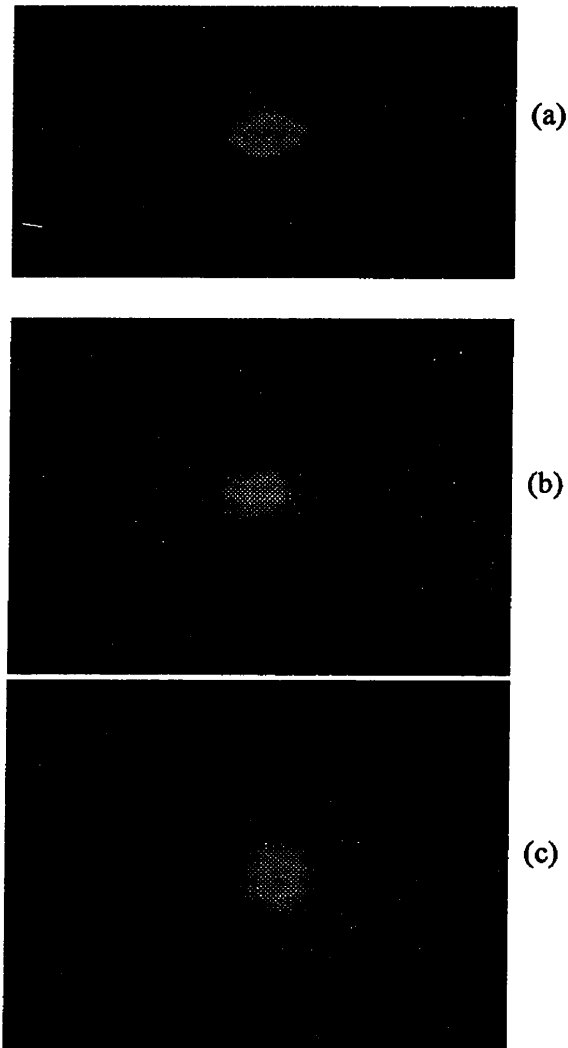


Figure 3.15 Measured mode profile of single mode, from top to bottom, surface, ridge and buried sol-gel glass waveguide.  $\lambda = 1.55 \mu\text{m}$ .

#### 3.4.4.1. Ridge channel waveguide fabrication

The prebaked sol-gel films were exposed to UV-light through a photolithography mask placed in contact with the film. The samples were then soaked in alcohol or

acetone to dissolve away the unexposed sol-gel film. A postbake at 150 °C for 5 hr was carried out to complete the densification of the hybrid sol-gel glass channel waveguides. The roughness of the side walls of the ridge waveguides is due to edge distortion associated with the lithographic process. The effect depends on several factors. These include the duration of the UV exposure (at fixed irradiance), thickness and absorptivity of the films, and the reflectivity of the substrate.<sup>15</sup> In contact printing, the resolution of the photolithographic process also depends on the gap between the photomask and the wafer. Some film thicknesses accentuate the interference diffraction effects and waveguide shape distortion. Diffraction along the surface normal is stronger for thick films than thin films. Long exposure times enhance the contributions due to diffraction and give rough edges. High-resolution optical microscopy and scanning electron microscopy (SEM) were utilized to examine the definition and quality of the ridge waveguides. Ridge waveguides in these examples were made using a 20-mole % ZrO<sub>2</sub> sol-gel with 1 to 4 min UV irradiation times. Decreasing the exposure time improved the smoothness of the sidewalls of the ridge waveguides. Figure 3.16 compares top views of optical micrographs of two waveguides made by 1 and 4 min exposure to UV radiation. Cross-section SEM images of these waveguides are also shown in Figure 3.16. Note that the waveguide made using 1 min exposure has straight and smooth side walls. Propagation losses of these ridge waveguides were measured as explained elsewhere.<sup>14</sup> On average, the waveguides exhibit ~0.1 dB/cm loss at 1.55 μm wavelength.

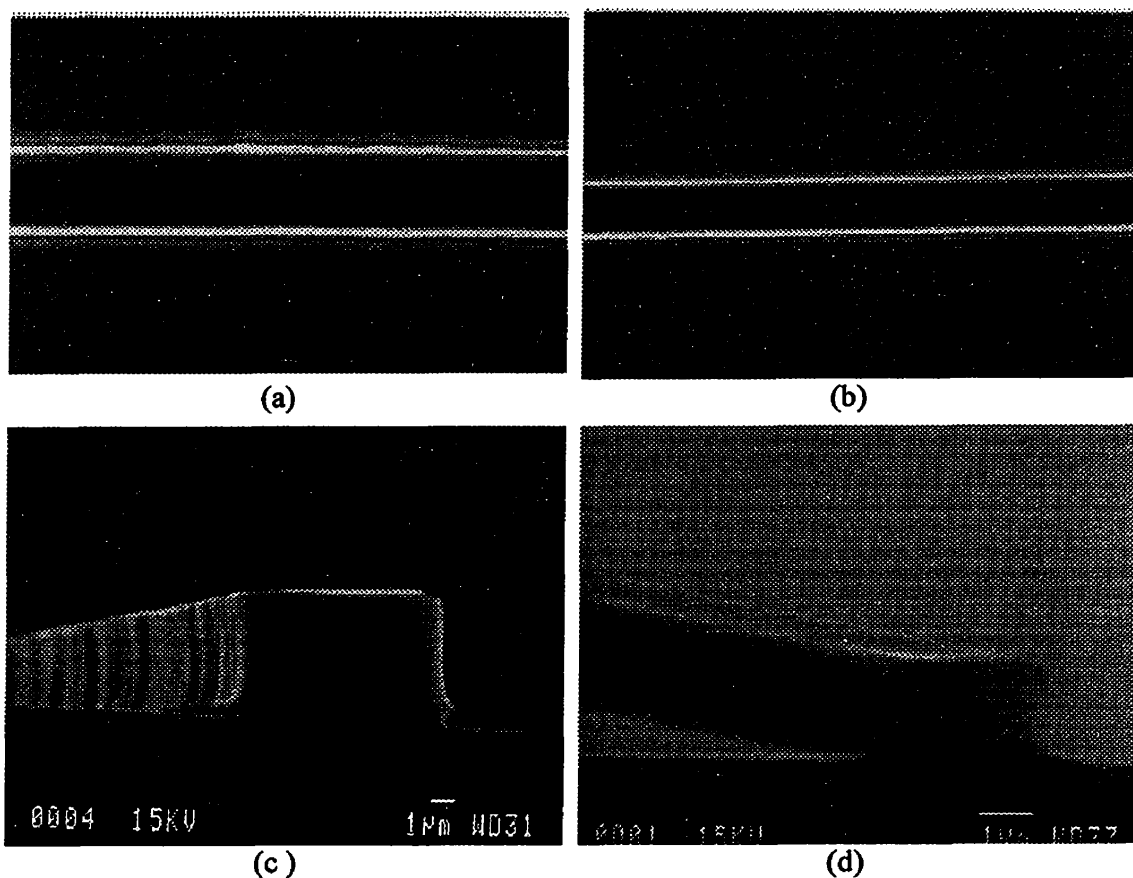


Figure 3.16 (a) and (b) Optical microscope photograph of Zr-doped ridge waveguides exposed to UV-light for (a) and (c) 4 min and (b) and (d) 1 min. Waveguide widths are, respectively, 8  $\mu\text{m}$  and 6  $\mu\text{m}$ . (c) and (d) Scanning electron micrograph of the waveguides.

### 3.4.5. Ridge waveguide with grating

#### 3.4.5.1. Grating fabrication

Gratings were made by inscription into ridge waveguides through a phase mask with 193 nm (ArF excimer) radiation. Fig. 3.17(a) shows a top view optical micrograph of such a grating. The photograph which is taken using a phase contrast microscope illustrates the refractive index modulation of the grating. The exposure to UV-light through the phase mask also produces a surface modulation, but, as seen in Fig.3.17(b),

this modulation is very small (less than 50 nm in our waveguides with grating). We have neglected the surface modulation in our calculation described in Section 3.2.5.2. The ridge waveguide was made as described in Section 3.2.4 using 2 min UV-light exposure. It was postbaked at 150 °C for 5 h prior to writing the grating.

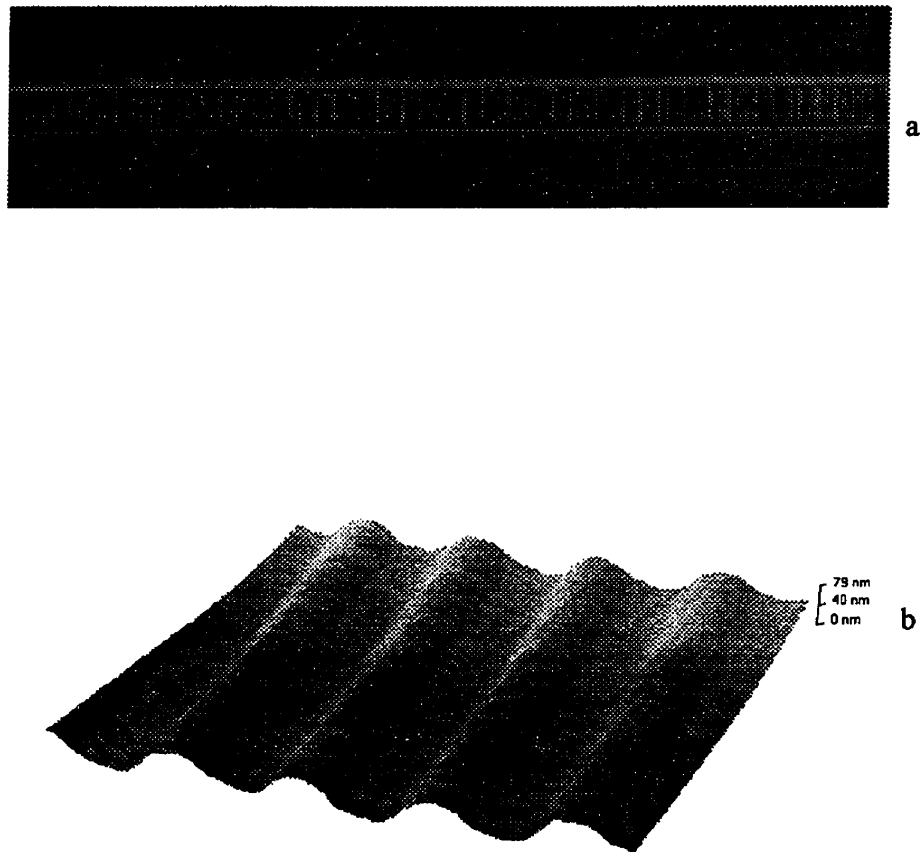


Figure 3.17 (a) Optical microscope photograph of a grating imprinted in sol-gel ridge waveguides. Grating period in  $0.5025 \mu\text{m}$ . (b) Atomic force microscope picture of grating.

### 3.4.5.2. Grating properties

As we have described in detail in Ref. 13, coupled mode theory was used to model the behavior of the waveguide/Bragg grating (see Fig. 3.18). In this theory, a mode incident from one direction excites a counter-propagating mode as it progresses. Coupled mode theory is used to account for the interaction of the incoming and excited modes by treating the grating as a perturbation of an ideal waveguide, i.e. a waveguide without a grating. Our analysis of the ridge waveguide/Bragg grating assembly leads to the following formula for the periodic modulation of the refractive index:

$$\Delta n(x, z) = \sum_{m \geq 0} \Delta n_m(x) \cos(m\gamma z + \phi_m) \quad (3.1)$$

where  $\phi_0 = 0$ ,  $\gamma = 2\pi/\Lambda$ , and  $\Lambda$  is the period of the grating. The reflectivity of the grating for TE and TM polarization states is calculated as described in Ref. 13. Figure 3.19 illustrates the calculated response of a single mode ridge waveguide with a 1.5 mm long grating.

Light from an erbium-doped tunable fiber laser was coupled into the waveguide and the output focused on a detector. The laser was tuned to achieve maximum and minimum transmission, allowing the TE and TM state reflectivity of the grating to be determined with appropriate polarizing optics. The laser was not sufficiently stable to acquire the full reflectivity curve as a function of wavelength. Nevertheless, the respective TE and TM reflectivities were 97% and 95%. Figure 3.19 compares the measured reflectivity with the calculated from theory for the TE mode. As can be seen, the agreement between the two is excellent.

From the Bragg relation,  $\Lambda = \lambda/2N_{\text{eff}}$ , we determined the effective index ( $N_{\text{eff}}$ ) of the ridge waveguides with their gratings. These data were inverted to calculate the refractive index of the waveguides at 1.55  $\mu\text{m}$ , assuming a step index profile for the ridge structures. The refractive index of the type A hybrid glass containing zirconium

oxide was 1.5035. Analysis of the organoaluminosilicate ridge waveguide yielded a value of 1.4810.

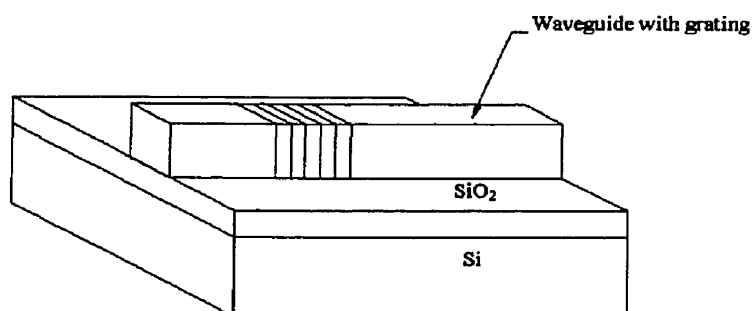


Figure 3.18 Waveguide configuration employed in the analysis of sol-gel ridge waveguides with grating.

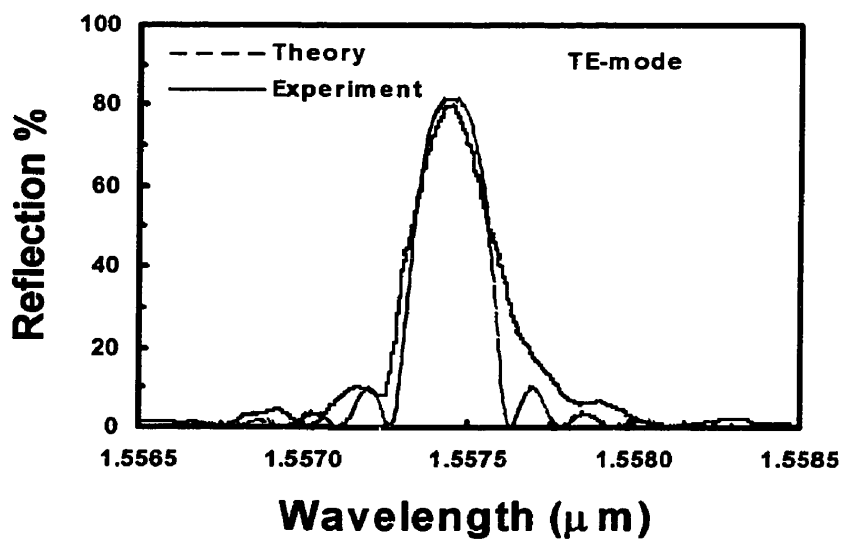


Figure 3.19 Calculated and measured response of a 4.5- $\mu\text{m}$  thick, 6- $\mu\text{m}$  wide, sol-gel ridge waveguide with Bragg grating. Grating length = 5 mm.

### 3.4.6. Conclusion

We have developed a new process for fabrication of high quality sol-gel glass waveguides on silicon. This low-temperature process can be used to produce surface, ridge and buried integrated optics devices. The waveguides are reproducible, are made in a few steps without using costly equipment.

An in-depth study is carried out to select fabrication parameters for production of hybrid organic-inorganic ridge waveguides by sol-gel process. It is shown that both UV-light exposure and heat-treatment (postbake) increase the refractive index of sol-gel films. Rather large refractive index differences between waveguide and substrate can be achieved. In a ridge waveguide built on a SiO<sub>2</sub> buffer layer, the difference between the waveguide and the substrate refractive indices is ~0.05. The same  $\Delta n$  can be achieved when the ridge is buried under a low refractive index sol-gel cladding. This allows production of short devices. In a surface waveguide the maximum  $\Delta n$  is 0.006. Therefore, sol-gel ridge (and buried ridge) waveguides may be more suitable for integrated optics circuit production.

It is shown that the refractive index of Zr- and Al- sol-gels permits continuous tailoring of the waveguide refractive index in the range of interest (1.485 - 1.520 and 1.485 - 1.495 at 632.8 nm wavelength, respectively) in optical telecommunication. Long exposure time and high post-baking temperature increase waveguide refractive index to reach a constant saturated value.

Ridge waveguides with smooth side walls are obtained by 1 min UV-light exposure indicating that high resolution microstructures can be patterned by this process. Once these waveguides are buried using a low refractive index sol-gel cladding, the mode profile of the single mode waveguide becomes circular and similar to that of optical fiber.

The refractive index of both sol-gel systems developed in this work are close to that of optical fiber. The reflection loss between our sol-gel waveguides and conventional silica fiber, at  $\lambda=1.55 \mu\text{m}$ , is less than 0.01 dB.

The simplicity of the process and the possibility of controlling accurately the device parameters suggest that the materials described in this paper are promising for low-cost and large scale production of integrated photonic circuits.

### 3.4.7. Acknowledgment

We acknowledge gratefully research grants from Natural Sciences and Engineering Research Council of Canada, and National Research Council of Canada.

### 3.4.8. References

1. M.P. Andrews and S.I. Najafi, "Passive and active sol-gel materials and devices", Critical Review Conf. On Sol-Gel and Polymer Photonic Devices, San Diego, Aug. 1997, SPIE Vol. CR68, pp. 253-285.
2. Advances in Integrated Optics, S. Martelucci, A.N. Chester and M. Bertolotti (Eds.), Plenum, New York, 1994, pp. 121-150.
3. (a) B. Novak, "Hybrid nanocomposite materials - between inorganic glasses and organic polymers", *Advanced Materials* 5 (1993) 422-432. (b) P. Judenstein and C. Sanchez, "Hybrid organic - inorganic materials: a land of multidisciplinary", *J. Mater. Chem.* 6 (1996) 53111-525. (c) U. Schubert, N. Husing, and A. Lorenz, "Hybrid inorganic - organic materials by sol-gel processing of organo-functional metal alkoxides", *Chem. Mater.* 7 (1995)2010 - 2027.
4. Critical Review Conference on Sol-Gel and Polymer Photonics Devices, San Diego, July 1997, SPIE Vol. CR68, editors: M.P. Andrews and S.I. Najafi.
5. "Sol-gel deposits active devices for optical circuits", *Opto & Laser Europe*, Feb. 1997, page 12.
6. "Bragg gratings written in sol-gel waveguides achieve near 100% reflectivity", *Laser Focus World*, Aug. 1997.
7. "Nanoparticles form glass layers free from cracks", *Opto & Laser Europe*, July 1997, page 25.



8. P. Coudray, J. Chisham, A. Malek-Tabrizi, C.Y. Li, M.P. Andrews, N. Peyghambarian and S.I. Najafi, "Ultraviolet light imprinted sol-gel silica glass devices on silicon", *Opt. Commun.* **128** (1996) 19-22.
9. C.Y. Li, J. Chisham, M.P. Andrews, S.I. Najafi, J.D. Mackenzie and N. Peyghambarian, "Sol-gel integrated optical coupler by ultraviolet light imprinting", *Electron. Lett.* **31** (1995) 271-272.
10. S.I. Najafi, M.P. Andrews, M.A. Fardad, G. Milova, T. Touam and P. Coudray, "UV-light imprinted surface, ridge and buried sol-gel glass waveguides and devices on silicon", invited paper, *Proc. Conf. Integrated Optics for Signal Processing*, Berlin, October 1996, pp. 10-15.
11. P. Coudray, J. Chisham, M.P. Andrews and S.I. Najafi, "Ultraviolet light imprinted sol-gel silica glass low-loss waveguides for use at 1.55  $\mu\text{m}$ ", *Opt. Eng.* **36** (1997) 1234-1240.
12. A. Fardad, M. P. Andrews and S. I. Najafi, "Novel sol-gel fabrication of integrated optical waveguides", *Conf. On Integrated Optics Devices: Potential for Commercialization*, SPIE, San Jose, Feb. 1997, SPIE Vol. 2997, pp.7278.
13. Touam, G. Milova, Z. Saddiki, M.A. Fardad, M.P. Andrews, J. Chrostowski and S.I. Najafi, "Organoaluminophosphate sol-gel silica glass thin films for integrated optics", *Thin Solid Films*, in press.
14. Najafi, *Introduction to Glass Integrated Optics*, Artech House, Boston, 1992.
15. Moreau, *Semiconductor Lithography, Principles, Practices and Materials*, Plenum Press, New York, 1988, 355-403.
16. T. Touam and S. I. Najafi, "Accurate analysis of reflective and diffractive gratings for integrated optics", *Conference on Integrated Optics Devices: Potential for Commercialization*, San Jose, Feb. 1997, SPIE Vol. 2695, 1996, pp. 57-70.

### 3.3. Sol-gel Integrated Optics Devices: Star Coupler and Dense WDM

A broad range of integrated optics components and devices can be produced from organic polymer modified hybrid silicate glasses via the solution sol-gel process. Indeed, these hybrid glass material platforms and fabrication processes have attracted significant attention.<sup>1,2</sup> We have recently developed a simple method to produce very compact high reflectivity waveguide Bragg gratings for hybrid glass photonic chip technologies.<sup>3</sup> This paper extends our work in this area to the design and fabrication of sol-gel glass integrated optics star couplers and dense wavelength division multiplexers. Our research builds on a growing library of materials and protocols that can be used to manufacture channel waveguides by resist-free UV-light photolithography.<sup>4,5</sup> For example, Fig. 3.20 shows a scanning electron micrograph of a sol-gel glass ridge waveguide. The structure was developed by a simple alcohol solvent wet etch step to replace reactive ion etch processing. Our photoinscription techniques have now been extended to more complex device structures like star couplers.

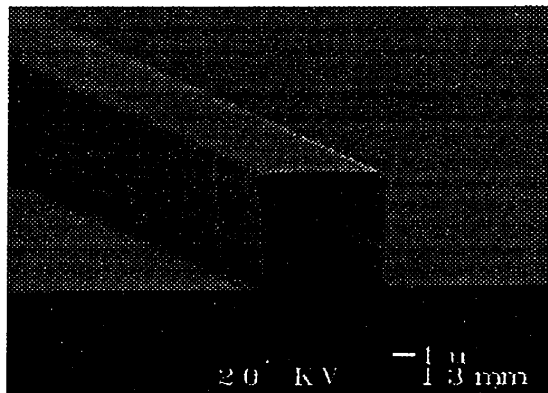


Figure 3.20 Scanning electron micrograph of sol-gel glass ridge waveguide.

Two-dimensional diffraction theory<sup>6</sup> was used to design a compact  $8 \times 31$  star coupler. The total length and the Rowland circle limiting slab waveguides were optimized to ensure that any of the output arrays received the same power when any of the input waveguides were excited. Star couplers were then produced in sol-gel glass in

both surface and ridge waveguide formats. Figure 3.21 shows a schematic of the device configuration. Figure 3.22 compares the transmitted power from 31 output ports when the central waveguide was excited. For experimental verification, the inset of Fig.3.22 depicts a photograph of 1.55  $\mu\text{m}$  wavelength light focused from the output ports of the star coupler.

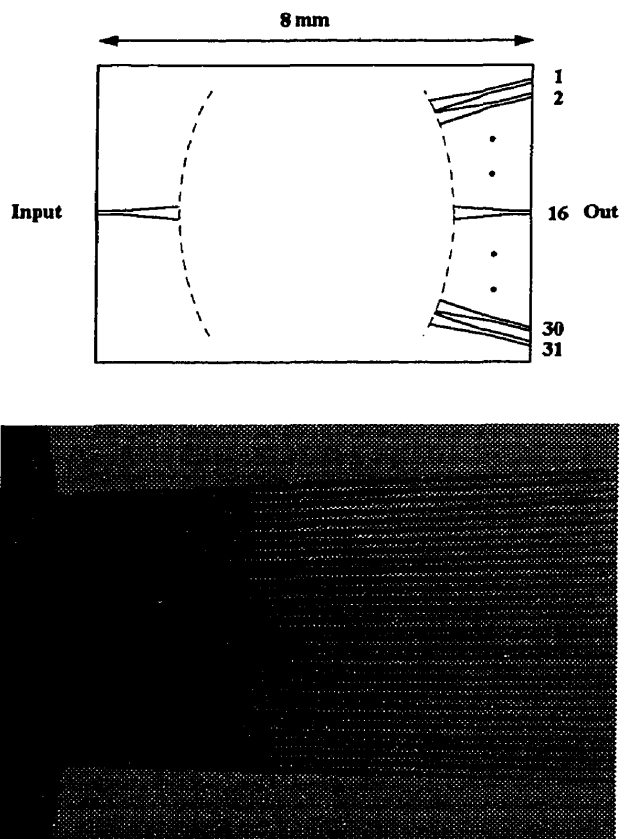


Figure 3.21 Top) Schematic representation and dimensions of 8x31 star couple  
Bottom) Optical micrograph of output side of the coupler.

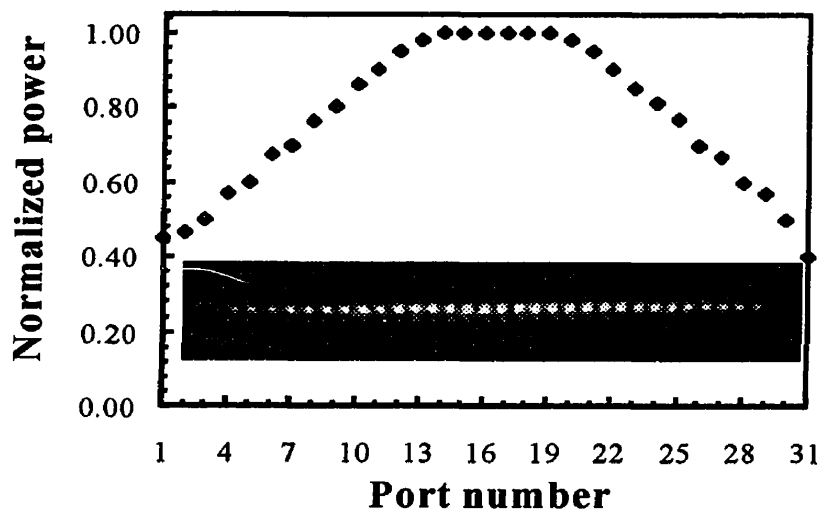


Figure 3.22 Star coupler output when light at  $1.55 \mu\text{m}$  is coupled into the central waveguide. Inset is a photograph of light from the output ports of the star coupler, at  $1.55 \mu\text{m}$ , focused on a camera.

A phase arrayed waveguide configuration was selected for dense wavelength division multiplexing (dense WDM). We have designed 4, 8, 16, 32, 64 and 128 channel dense WDMs with channel spacing from 100 GHz to 1000 GHz. These have been conceived for 800 nm and  $1.55 \mu\text{m}$  applications in data and computer networks and in telecommunication architectures. Figure 3.23 depicts a computed optical response of a dense WDM. The measured response of dense WDMs will be presented.

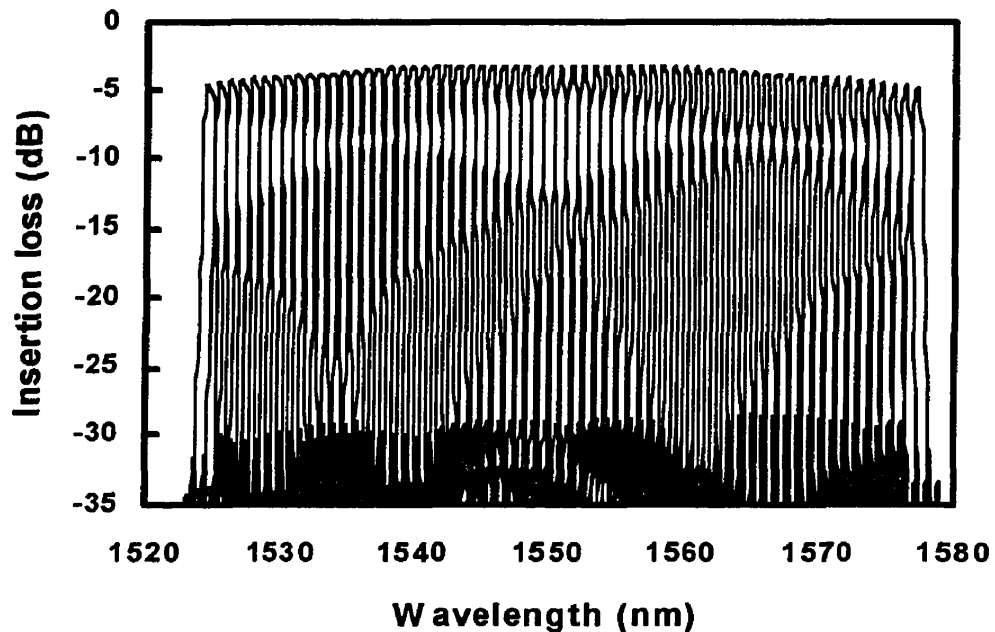


Figure 3.23 Optical response of 64 channels dense WDM.

### 3.3.1. References

1. M. P. Andrews and S. I. Najafi, "Passive and active sol-gel materials and devices," in *Critical Reviews Conference on Sol-Gel and Polymer Photonic Devices*, San Diego, CA, SPIE, Aug. 1997, Vol. CR68, pp. 253-285.
2. *Sol-Gel for Photonics*, editor: S I. Najafi, SPIE vol. MS148, 1998.
3. S. I. Najafi, T. Touam, R. Sara, M. P. Andrews and M. A. Fardad, "Sol-gel glass waveguide and grating on silicon", *Journal of Lightwave Technology*. Vol. 16, No. 9, Sept. 1998 1640-1646.
4. T. Touam, G. Milova, Z. Siddiki, M. A. Fardad, M. P. Andrews , J. Chrostowski and S. I. Najafi, "Organoaluminophosphate sol-gel silica glass thin films for integrated optics", *Thin Solid Films* 307 (1997) 203-207.
5. X. M. Du, T. Touam, L. Degachi, J. L. Guilbault, M. P. Andrews and S. I. Najafi,

- “Sol-gel waveguide fabrication parameters: an experimental investigation”, *Optical Engineering* 37 (1998) 1101-1104.
6. C. Dragone, “ An NxN optical multiplexer using a planar arrangement of two star couplers”, *IEEE Photon. Tech. Lett.* 3 (1991) 812-819.

### **3.3.2. Acknowledgment**

We acknowledge gratefully research grants from Natural Sciences and Engineering Research Council of Canada, and National Research Council of Canada.

## CHAPITRE IV: CONCLUSION ET PERSPECTIVE

### 4.1. Conclusion

La technologie de fabrication des guides d'ondes par voie sol-gel a atteint actuellement un niveau très avancé qui lui permet de produire des circuits photoniques intégrés extrêmement performants. Dans ce travail, nous avons voulu contribuer dans une modeste part à la compréhension fondamentale des mécanismes d'hydrolyse, de polycondensation, de gélification et de condensation. Cette compréhension est rendue nécessaire pour mieux contrôler la structure, l'homogénéité et la pureté du verre hybride. Ainsi, plusieurs variantes de verre hybride ont été réalisées selon un protocole chimique bien défini, ceci pour modifier l'indice de réfraction afin d'améliorer la résolution photolithographique de sa composante photoactive. En effet, nous sommes arrivés à ajuster l'indice de réfraction du verre hybride à celui de la fibre monomode standard de télécommunication en éliminant à la fois les pertes de couplage dues à la réflexion Fresnel et la discordance modale (*mode-field mismatch*).

Nous avons élaboré des courbes d'étalonnage (abaques) relatives au changement d'indice de réfraction en fonction de la dose ultraviolet et de la température, ainsi que les abaques de revêtement et de contraste photolithographique. Désormais, il est possible d'obtenir la structure autant macroscopique que microscopique, du guide requis en moyennant ces abaques et le protocole chimique choisi.

De plus, nous avons utilisé la méthode vectorielle des modes couplés pour concevoir un réseau de Bragg sur un guide en relief. Le protocole chimique, les abaques et le modèle ont produit une excellente concordance entre la théorie et l'expérimentation. En effet, le protocole chimique prévoit un indice effectif qui répond aux exigences de la relation de Bragg et les abaques ont permis l'obtention d'un guide à section rectangulaire.

Quant aux multi/démultiplexeurs à deux longueurs d'ondes et les filtres spectraux que nous avons caractérisés, ils ont été conçus en moyennant une méthode numérique BPM (*Beam Propagation Method*). Lors des simulations, nous avons

introduit comme paramètres de la structure du guide (différence d'indice de réfraction et dimensions du coeur) les données obtenues graphiquement via les abaques. Après réalisation, ces composants, dont la fonctionnalité est incontestable, ont manifesté des caractéristiques très proches des prédictions numériques.

Finalement, nous nous sommes basés sur la théorie de diffraction bidimensionnelle pour concevoir un coupleur en étoile. Encore une fois, les abaques ont été d'une grande utilité pour accorder les caractéristiques physiques aux exigences des lois de la physique. Le dispositif d'une longueur de moins de 2 cm est hautement compact et sa fonctionnalité est exactement celle prévue puisqu'il permet de diviser la puissance optique entre 31 portes.

#### 4.2. Perspectives

Lors de l'établissement des différents protocoles chimiques conduisant à des verres hybrides de structure amorphe, la structure de gel de départ ainsi que la façon de la traiter thermiquement conditionnent largement la possibilité d'obtenir un verre hybride dense compte tenu de l'évolution chimique résumée tout au début de ce mémoire. Il est donc important de choisir le traitement thermique de façon à éviter la cristallisation, les microfractures et le moussage. À cet effet, il nous paraît essentiel de recommander la détermination de la température de transition vitreuse  $T_g$  (*Glass Transition Temperature*). Nous suggérons alors des verres hybrides fabriqués au-dessous de  $T_g$  car selon les études antérieurement citées, il n'y a aucune différence avec les verres obtenus par les procédés conventionnels en matière d'indice de réfraction, de densité et de coefficient d'expansion thermique.

Le réseau de Bragg que nous avons fabriqué est un réseau à modulation d'indice sur un guide en relief. Les conditions de fabrication, spécialement la température, font en sorte que ce procédé serait particulièrement indiqué pour incorporer l'assemblage réseau/guide en relief à un laser semi-conducteur dans le but de constituer un laser à réflexion distribuée de Bragg (*DBR Distributed Bragg Reflector Laser*) ou simplement



de réaliser le laser DBR complètement par verre hybride. Il faut savoir que l'amplificateur à base de guides dopés à l'Erbium a été réalisé par voie sol-gel bien que le recuit ait été opéré à de hautes températures (900 °C), ce qui peut toujours être amélioré.

**BIBLIOGRAPHIE**

ANDREWS M. P., SARAVANAMUTTU K., TOUAM T., SARA R., DU X. M., NAJAFI S. I., "Collateral Densification Associated with the Photoresponse of Hybrid Sol-gel Glasses for Depositing Bragg Gratings on Ridge Waveguide", Proc. SPIE, Vol. 3290, (1998).

ANDREWS Mark P., NAJAFI S. Iraj, "Passive and Active Sol-Gel Materials and Devices", Critical Review Conference Sol-gel Polymer Photonic Devices, SPIE, San Diego, Vol. CR68, (1997), 253-285.

BARBIER D., RATTAY M., SAIN ANDRE F., CLAUSS G., TROUILLON M., KEVORKAIN A., DELAVALUX J.-M. P., and MURPHY E., "Amplifying Four-Wavelength Combiner, Based on Erbium/Ytterbium-Doped Waveguide Amplifiers and Integrated Splitters", *IEEE Photonics Techn. Let.*, Vol. 9, No. 3, March 1997

BENNETT M. J., HOULTON M., PRICE J. B., "New Ceramic Coatings for High Temperature Gas-cooled Reactor Materials Protection", Oesterr. Forschunszent. Seibersdorf. Number OEFZS BER 4086, (1981), N1-N14.

BRADLEY D. C., MEHROTRA R. C., GAUR P. D., "Metal Alkoxides", Academic Press, London, (1978), 150-160.

BRINKER C. Jeffrey, SHERER G. W., "Sol-gel Science", Academic Press, San Diego, (1990), 113.

BRINKER C. J., HARRINGTON M. S., "Sol-gel Derived Antireflective Coating for Silicon", *Solar Energy Mat.* 5, (1981), 159-172.

DISLICH H., "Glassy and Crystalline Systems from Gel: Chemical Basis and Technical Application", *Journal of Non-crystal. Solid.* 57, (1983), 371-388.

DISLISH H., HINZ P., "History and Principles of the Sol-gel Process and Some New Multicomponent Oxide Coatings", *Journal of Non-crystalline Solids* 48, (1982), 11-16.

DRAGONE C., "An NxN Optical Multiplexer Using Planar Arrangement of Two Star Couplers", *IEEE Photonics Technology Letters*, Vol. 3, No. 9, (1991), 812-814

DRAGONE D., "Efficient NxN Star Coupler Using Fourier Optics", *Journal of Lightwave Techn.*, Vol. 7, No. 3, March 1989.

DRAGONE C., HENRY C. H., KAMINOW I. P. and KISTLER R. C., "Efficient Multichannel Integrated Optics Star Coupler on Silicon", *IEEE Photonics Techn. Let.*, Vol. 1, No. 8, August 1989.

ELMOR W. C., "Ferromagnetic Colloid for Studying Magnetic Structures", *Physic Revue* 54, (1938), 309-310.

FLORY P. J., "Molecular Size Distribution in Three-Dimensional Polymers", *Journal of Am. Chemi. Society* 63, (1941), 3083-3100.

FREIDEL C., CRAFTS J. M., "Synthesis of Tetraethylsilane from Diethylzinc and Silicon Tetrachloride", *Ann.*, 1865, 136-203.

HAMMERSLEY J. M., "Percolation Theory: II The Connective Constant", *Proceeding Cambridge Philosophia Society* 53, (1957), 642-645.

HUNTER J. Robert, "Introduction to Modern Colloid Science", Oxford University Press, New York, (1993), 1-93.

IMAI H., HIROSHIMA H., K. Awazu, and H. Onuki, "Structural Change in Sol-Gel Derived SiO<sub>2</sub> Films Using Ultraviolet Irradiation", Proc. SPIE, Vol. 2288, (1994), 71-76.

LANUTTI J. J., CLARK D. E., "(a) Sol-gel Derived Ceramic-ceramic Composites using Short Fibers, (b) Long Fiber Reinforced Sol-gel Al<sub>2</sub>O<sub>3</sub> Composites", Mat. Res. Soc. Sympo. Proceeding 32, (1984), 369-381.

LI C.-Y., ANDREWS M. P., NAJAFI S. I., MACKENZIE J. D., PEYGHAMBARIAN N., "Sol-gel Integrated Optics Coupler by Ultraviolet Light Imprinting", Electronics Letters 31, (1995), 271-272.

MADDIYASNI K. S., LYNCH C. I., SMITH J. S., "Preparation of Ultra-high-purity Submicron Reflectory Oxides", Journal of Am. Ceramic Society 48, (1965), 372-375.

MARTELUCCI S., CHESTER A.N. and BERTOLOTTI M., Edition Plenum, New York, 1994, pp. 121-150.

MATIJEVIC E., "The Role of Chemical Complexing in the Formation and Stability of Colloidal Dispersion", Academic Press, New York, Edt. M. Kerker, A. C. Zettlemayer, R. L. Rowell, Vol. I, (1977), 397-412.

MURAWSKI L., CHUNG C. H., MACKENZIE J. D., "Electrical Properties of Semiconducting Oxide Glasses", Journal of Non-crystal. Solid. 32, (1979), 91-104.

NAJAFI S. Iraj et WU C., "Potassium Glass Waveguide Directional Couplers at 0.6328 and 1.3  $\mu\text{m}$ ", Applied Optics, Vol. 28, No. 13, pp. 2459-2460, juillet 1989.

NAJAFI S. I., TOUAM T., SARA R., ANDREWS M. P. and FARDED M. A., "Sol-gel glass waveguide, and grating on silicon", *Journal of Lightwave Technology*, Vol. 16, No. 9, September 1998, 1640-1646.

RAI-CHOUDHURY P., Handbook of Microlithography, Micromachining, and Microfabrication, vol. 1: Microlithography, *SPIE Optical Engineering Press*, 1997, 17-45.

RAMAN G., GNANAM F. D., RAMASAMY P., "The Growth of SbSBr, SbSCl, and SbSF Single Crystals in Gels", *Journal of Crystal Growth* 75, (1986), 466-470.

ROY R., "Aids in Hydrothermal Experimentation Methods of Making Mixtures for both 'Dry' and 'Wet' Phase Equilibrium Studies", *Journal of Am. Ceramic Society* 39, (1956), 145-148.

SARA R., SADDIKI Z., TOUAM T., CHROSTOWSKI J., ANDREWS M. P. and NAJAFI S. Iraj, "SEM and AFM Studies of Polyglass Ridge Waveguides", Proceedings of SPIE, *Conference on Integrated Optics Devices III*, Vol. 3620, San Jose, January 1999.

SARA R., TOUAM T., BLANCHETIERE C., SADDIKI Z., SARAVANAMUTTU K., DU X. M., CHROSTOWSKI J., ANDREWS M. P. and NAJAFI S. Iraj, "Photolithography fabrication of Sol-Gel Ridge Waveguide", Proceedings of SPIE, *Conference on Organic-Inorganic Hybrid Materials for Photonics*, Vol. 3469, San Diego, July 1998, 118-123.

SARA R., TOUAM T., ANDREWS M. P. and NAJAFI S. Iraj, " Polyglass Integrated Photonics Devices", Proceedings of SPIE, *Conference on Organic-Inorganic Hybrid Materials for Photonics*, Vol. 3469, San Diego, July 1998, 51-53.

SARA R., TOUAM T., COUDRAY P., ANDREWS M. P., NAJAFI S. Iraj, "Polyglass Integrated Optics Devices for Lightwave Communication", Proceedings of SPIE, *Conference on Organic-Inorganic Hybrid Materials for Photonics*, Vol. 3469, San Diego, July 1998, 44-50.

SCHROEDER H., "Oxide Layers Deposited from Organic Solutions", Physics of Thin Films, Academic Press, New York, Edt. G. Hass, R. E. Thun, Vol. 5, (1969), 87-141.

SHMIDT K. Hellmut, "Chances and Limitations of Sol-gel Derived Metal Oxide and Chalcogenide Nanocomposites for Optic and Photonic Application", Proceedings of SPIE, Vol. 2288, (1994).

SZE S. M., "Semiconductor Devices Physics and Technology", Murray Hill, New Jersey, (1985), 382-427.

TERVONEN A., HONKANEN S., NAJAFI S. I., "Analysis of symmetric coupler and asymmetric Mach-Zehnder interferometers as 1.3- and 1.55-  $\mu\text{m}$  dual-wavelength demultiplexers/multiplexers", *Optical Engineering*, Vol. 32, No.9, 2083, September 1993.

TOUAM T., MILOVA G., SADDIKI Z., FARDAD M. A., ANDREWS M. P., CHROSTOWSKI J., NAJAFI S. I., "Organoaluminophosphate Sol-gel Silica Glass Thin Films for Integrated Optics", *Thin Solids Films* 307, (1997), 203-207.

TOUAM T. and NAJAFI S. I., "Accurate analysis of reflective and diffractive gratings for integrated optics", Conference on Integrated Optics Devices: Potential for Commercialization, San Jose, Feb. 1997, SPIE Vol. 2695, 1996, pp. 57-70.

VAN DE VEN T. G. M., "Colloidal Hydrodynamics", Academic Press, Colloid Science, Edit. R. H. Ottewil, and R. L. Rowell, (1989), 563-579.

VERBEEK B. H., HENRY C. H., OLSON N. A., ORLOWSKI K. J., KAZAINOV R. R. and JOHNSON B. H., "Integrated Four-Chanel Mach-Zehnder Multi/Demultiplexer Fabricated with Phosphorous Doped SiO<sub>2</sub> Waveguide on Si", Journal of Lightwave Technology, Vol. 6, No. 6, (1988), 1011-1015.

WAGNIER T, PHALIPPON J., ZARZYCKI J., "Monolithic Aerogels in the Systems SiO<sub>2</sub>-B<sub>2</sub>O<sub>3</sub>, SiO<sub>2</sub>-P<sub>2</sub>O<sub>5</sub> and SiO<sub>2</sub>-B<sub>2</sub>O<sub>3</sub>-P<sub>2</sub>O<sub>5</sub>", Journal of Non-crystall. Solid. 63, (1984), 117-130.

WATANABE T., Ooba N., HAYASHIDA S., KURIHARA T. and IMAMURA S., "Polymeric Optical Waveguide Circuits Formed Using Silicon Resin", Journal of Lightwave Technology, Vol. 16, No. 6, (1998), 1049-1055.

YOLDAS B. E., "Introduction and Effect of Structural Variation in Inorganic Polymers and Glass Network", Journal of Non-crystall. Solid. 51, (1982), 105-121.